AMP-Activated Protein Kinase (AMPK) Activation for the Treatment of Mitochondrial Disease

Alexander E. Green

A Thesis submitted to the Faculty of Graduate studies in Partial Fulfillment of the Requirements for the Degree of

Master of Science

Graduate Program in Kinesiology and Health Science

York University

Toronto, Ontario, Canada

October 2013

Abstract

There are multiple copies of mtDNA per cell and each mtDNA molecule contains the information to encode 13 electron transport chain (ETC) proteins. When mtDNA is depleted, there is a decrease in ETC activity. 5' AMP-activated protein kinase (AMPK) is a kinase that can initiate mitochondrial biogenesis and mitophagy. We hypothesized that treating cells harbouring low numbers of mtDNA with an AMPK activator (5-Aminoimidazole-4-carboxamide ribonucleoside; AICAR) would ameliorate the decrease in ETC activity and improve mtDNA copy number. We developed myoblasts (C2C12 cells) depleted of mtDNA with long-term ethidium bromide treatment. We treated selected clones for 24 hours with 1 mM AICAR to activate AMPK. AICAR treatment decreased markers of mitochondrial biogenesis, mitochondrial function (e.g. maximal cellular respiration), and mitochondrial degradation. Thus, failing to increase the energy producing capacity of the cell, activation of AMPK may have induced an energy sparing mechanism.

Acknowledgements

Completing this dissertation has been one of the most challenging experiences of my life. It would not be possible without the support of my friends and family. All of you have helped me through the worst of times and been there at the best of times. I am truly lucky for having you in my life.

Thank you to my parents, Al and Mary, and my step-parents, Shelley and David. You have always encouraged me to strive for success and provided thoughtful advice.

Thank you to all of my lab mates and fellow graduate students. There are so many to mention and I apologize if I miss one along the way. To Keir, I thank you for the endless patience and guidance you showed me during my training. Thank you to Mike and Sobia, you two always provided great advice and often a laugh or two. Ayesha, Anna and Heather, you three have been a source of comedy, exercise (e.g. cricket and snowboarding) and of course knowledge. Michael, thank you for your continued advice and endless reality checks. Donna and Bunty, thank you for immediately welcoming me to York University in my first week. To Yuan, thank you for the companionship during the many weekend hours. Chris and Alexa, thank you for the many stimulating conversations we shared. Aviva, I will never forget the hours sweating in 308 together. To Steve and Olga, thank you for being awesome friends and fans of the Canucks and rock music, respectively. To Liam, we started together on the east and west coasts and it's been great memories ever since. Always remember to keep your refrigerator stocked. To the rest of the "bros" - Sammy, Carlo, Matt, Jon, and Eric - keep it real. Finally, to Kathryn, thank you for your patience and dedication in helping me collect the data for this thesis. It truly could not have been done without you.

I would also like to thank my friends from outside of our academic niche. To all the members of the York Track and Field Team, meeting with you has truly been one of the most enjoyable experiences I have had at York. I only wish I could have overcome my injuries and competed alongside you. To the members of the Queen's Track Team, my four years as a member will forever remain a part of me wherever I go. Even now as an alumnus, you still welcome me as one of your own and help me to relax, without you I may not have made it to where I am.

To the past and current professors that have helped me in my research, I would like to thank you for your time and effort. Particularly, I would like to thank Dr. Brendon Gurd of Queen's University. If you had not given me the opportunity to start my research career with you, I surely would not be where I am today. I would also like to thank my committee members for their time and consideration. Finally and especially, I would like to thank my supervisor Dr. David Hood. Your knowledge and guidance have truly influenced how I do research and made me a better researcher for it. Thank you again, for all your time, patience, effort, and other innumerable traits.

Table of Contents

List of Figures

Review Of Literature

Manuscript

Appendix B: Additional Data

List of Abbreviations

ADK	Adenosine Kinase
ADP	Adenosine Diphosphate
adPEO	Autosomal Dominant Progressive External Opthalmoplegia
AICAR/AR	5-Aminoimidazole-4-carboxamide ribonucleoside
AK	Adenylate Kinase
Ambra1	Activating Molecule In Beclin-1-Regulated Autophagy
AMP	Adenosine Monophosphate
AMPK	AMP Activated Protein Kinase
ANOVA	Analysis of Variance
ATG	Autophagy Related Gene
ATP	Adenosine Triphosphate
$BafA_1$	Bafilomycin A_1
Bcl-2	B-Cell CLL/Lymphoma 2
Bif1	Bax-Interacting Factor 1
CaMK	Ca^{2+}/Calmodulin-dependent Protein Kinase
CaMKK	Calcium/Calmodulin-Dependent Protein Kinase Kinase
CL	Cardiolipin
COX	Cytochrome C Oxidase
CQ	Chloroquine
CSB	Conserved Sequence Blocks
D-Loop	Displacement Loop
DMEM	Dulbecco's Modification of Eagle's Medium
DNA	Deoxyribonucleic Acid
DPBS	Dulbecco's Phosphate Buffered Saline
Drp1	Dynamin-Related Protein 1
EDL	Extensor Digitorum Longus
EndoG	Endonuclease G
ER	Endoplasmic Reticulum
ERRα	Estrogen-Related Receptor alpha
EtBr	Ethidium Bromide
ETC	Electron Transport Chain
FIP200	RB1-Inducible Coiled-Coil 1
Fis1	Mitochondrial Fission Protein 1
GβL	G-Protein Beta-Subunit-Like Protein
GPx	Glutathione peroxidase
H-Strand	Heavy Strand
H_2DCFDA	2',7'-Dichlorodihydrofluorescein Diacetate
HSP_1	Heavy Strand Promoter 1
HSP_2	Heavy Strand Promoter 2

IMM	Inner Mitochondrial Membrane
IP3R	Inositol 1,4,5-Trisphosphate Receptor Type 1
kb	Kilobases
KSS	Kearns-Sayre Syndrome
L-Strand	Light Strand
LC3	Microtubule-Associated light Chain 3
LC3	Microtubule-associated Protein Light Chain 3
LHON	Leber's Hereditary Optic Neuropathy
LKB1	Liver Kinase B1
LS	Leigh's Syndrome
LTR	LysoTracker Red
MDS	Mitochondrial Depletion Syndrome
MELAS	Mitochondrial Encephalomyopathhy with lactic Acidosis and Stroke-Like Episodes
MERRF	Myoclonic Epilepsy with Ragged Red Fibers
Mfn1	Mitofusin-1
Mfn2	Mitofusin-2
MMR	Mismatch Repair
MnSOD	Manganese Superoxide Dismutase
MRPS12	Mitochondrial Ribosomal Protein S12
mtDNA	Mitochondrial DNA
MTERF	Mitochondrial Transcription Terminal Factor
MTGFM	MitoTracker Green FM
mTOR	Mammalian Target of Rapamycin
mTORC1	mTOR Complex I
MTS	Mitochondrial Targeting Sequence
mtSSB	Mitochondrial Single Stranded Binding Protein
NAF-1	Nuclear Assembly Factor 1
NARP	Neuropathy Ataxia with Retinitis Pigmentosa
NCR	Non-Coding Region
nDNA	Nuclear DNA
NER	Nucleotide Excision Repair
NRF-1	Nuclear Receptor Factor-1
NRF-2	Nuclear Receptor Factor-2
NUGEMPs	Nuclear Genes Encoding Mitochondrial Proteins
O_H	Heavy Strand Replication Origin
oh^{8}dG	8-hydroxydeoxyguanosine
O_L	Light Strand Replication Origin
OMM	Outer Mitochondrial Membrane
Opa1	Optic Atrophy 1
Ori_b	Bidirectional Replication Origin
PARL	Presenilins-Associated Rhomboid-Like Protein

PC	Phosphatidylcholine
PE	Phosphatidylethanolamine
PGC-1α	Peroxisome Proliferator-Activated Receptor Gamma Coactivator 1-alpha
PGC-1β	Peroxisome Proliferator-Activated Receptor Gamma Coactivator 1-beta
PI	Phosphatidylinositol
PI3K	Phosphoinositide 3-Kinase
PINK1	PTEN-Induced Putative Kinase 1
POLMRT	Mitochondrial RNA Polymerase
POLγ	Polymerase Gamma
PRC	PGC-1α Related Co-Activator
Rab5	Rab-Protein 5
RITOLS	Ribonucleotide Incorporation Throughout the Lagging Strand
ROS	Reactive Oxygen Species
SDM	Strand-Displacement Mechanism
SirT1	Silent Mating Type Information Regulation 2 Homolog 1
Tak1	TGF-beta Activated Kinase 1
TEFM	Mitochondrial Transcription Elongation Factor
TFAM	Mitochondrial Transcription Factor A
TFB2M	Mitochondrial Transcription Factor B2
TIM	Translocase of the Inner Mitochondrial Membrane
TMRE	Tetramethylrhodamine Ethyl Ester
TOM	Translocase of the Outer Mitochondrial Membrane
TSC2	Tuberous Sclerosis 2
Ulk1	Serine/Threonine-Protein Kinase 1
UTR	Untranslated Region
UVRAG	UV Radiation Resistance-Associated Gene Protein
Vps34	Phosphoinositide 3-Kinase Class III
ZMP	AICAR Monophosphate
ΔΨmt	Mitochondrial Membrane Potential

Review of Literature

1. Mitochondrial DNA

Among mammalian organelles, mitochondria are distinct because, other than the nucleus, they are the only organelle to contain genetic material. According to the endosymbiotic theory, mitochondrial DNA (mtDNA) is a remnant of DNA contained within prokaryotic organisms that were engulfed by early eukaryotic cells (*1*). Mitochondria are the main source of energy for mammalian cells. Within mitochondria, the tricarboxylic acid (TCA) cycle and the electron transport chain (ETC) coordinately produce adenosine triphosphate (ATP) – the cellular form of energy. The presence of mtDNA remains necessary to mitochondria, as it encodes gene products essential for the production of the ETC and ATP Synthase.

Akin to the nuclear genome, mutagens and free radicals can manipulate the mitochondrial genome. Directly and indirectly, these mutations are associated with common diseases, such as Parkinson's disease, Alzheimer's disease, and diabetes mellitus (*2*). In the late 1980s, mutations in mtDNA were identified as the origin of unique metabolic diseases (*3*). For these reasons, mtDNA is a source of great mystery and interest both at the basic and applied research levels.

1.1. Characteristics and Structure

In mammals, mtDNA is a circular, double-stranded DNA molecule. Human mtDNA is 16.6 kb long with a large non-coding region (NCR) and genes encoding 13 peptides, 22 tRNAs and 2 rRNAs (Fig. 1a; *4-6*). These peptides include 7 subunits of NADH Dehydrogenase, 1 subunit of Cytochrome bc_1, 3 subunits of Cytochrome C Oxidase (COX), and 2 subunits of ATP Synthase. No subunits of Succinate Dehydrogenase (i.e. Complex II of the ETC) are encoded by mtDNA. Each strand of mtDNA contains unique characteristics. The heavy strand (H-Strand) encodes the majority of mtDNA genes, including 12 peptides, 16 tRNAs and 2 rRNAs. It is named the heavy strand because it is relatively guanine-rich and consequently has a greater molecular weight. The light strand (L-strand) encodes 1 peptide and 8 tRNAs and comprises the relatively lighter strand abundant with cytosine nucleotides. The Non-Coding Region (NCR) contains important regulatory sequences and DNA structures including 3 hypervariable regions, the H-strand replication origin (O_H), the bidirectional replication origin (Ori_b), 3 conserved sequence blocks (CSB), the heavy-strand promoter 1 (HSP_1), the light-strand promoter (LSP) and the displacement loop (D-Loop; Fig. 1a; (*6*). The D-Loop is a unique triple-stranded region within the NCR. The majority of variability in the human mtDNA genome is within the NCR and is primarily focused within the hypervariable regions (*6*).

Multiple mtDNA molecules are contained in each mitochondrion and an estimated $10^3 – 10^4$ copies of mtDNA exist in each somatic mammalian cell (*7*). These mtDNA

molecules are organized into structures, called nucleoids, by accessory proteins (*8*). Mitochondrial transcription factor A (TFAM) is the most abundant nucleoid protein. High-resolution microscopy has revealed that TFAM induces U-turns in mtDNA (*9*). Unfolded mtDNA has a diameter of 5 μm. Each nucleoid compacts the 5 μm diameter mtDNA into an estimated 100 nm diameter complex (*8*). Originally, it was estimated that 2-10 mtDNA molecules were contained within each nucleoid. However, recent studies suggest each nucleoid contains an average of 1.45 mtDNA molecules (*10*).

It is important to note that the size and shape of mtDNA and the distribution of mtDNA genes vary between species. Many organisms, such as *Tetrahymena pyriformis* and *Saccharomyces cerevisiae*, contain linear mtDNA (*11*). Even within the mammalian class, mtDNA can vary in length. For example, bovine mtDNA is only 16.3 kb long (*12*).

1.2. Mitochondrial DNA Replication and Transcription

The replication and transcription processes of mtDNA are inherently intertwined. Traditionally, it is believed that before replication can occur, transcription must begin and provide the primers required for the subsequent replication.

1.2.1. Mitochondrial DNA Replication

Many aspects of mtDNA replication remain greatly debated or poorly understood (*6*). These aspects include the components of the mtDNA copying machinery, the overall mechanism of mtDNA duplication, and the origin of mtDNA replication.

The prevailing dogma among mitochondrial research is that the main mtDNA replisome comprises of Twinkle, mitochondrial single stranded binding protein (mtSSB) and polymerase gamma (POLγ; Fig. 1b). This is a result of *in vitro* studies that have demonstrated these as the minimum required proteins for mtDNA duplication (*13*). POLγ is a heterotrimeric protein composed of an α and 2 β subunits. Currently, POLγ is the only mitochondrial DNA polymerase known in humans. Although others have suggested other DNA polymerases likely exist, none have yet to be identified (*6*). POLγ is unable to replicate double stranded mtDNA (*6*). Therefore double stranded mtDNA must be unraveled by the DNA helicase, Twinkle. This produces single stranded mtDNA for POLγ to replicate (*14*). Overexpression of Twinkle has been shown to increase novel mtDNA synthesis (*15*). mtSSB binds and stabilizes the newly synthesized single stranded DNA. Its presence extends the maximum length of double stranded DNA replicated by POLγ and Twinkle to ~16 kb from 2 kb (*16*) and thus suggests its crucial role in DNA replication. Another protein important for mtDNA replication is Mitochondrial Transcription Termination Factor (MTERF1). MTERF1 binds mtDNA and slows mtDNA synthesis (*17*). This is believed to reduce the rate of misincorporated nucleotides. Overall, *in vitro* with only POLγ, Twinkle and mtSSB, mtDNA synthesis occurs at rate of 180 BP/min. *In vivo,* mtDNA is estimated to synthesize at 270 BP/min (*16*).

Currently, there are two major competing theories of mtDNA replication (*6*, *18*). It is believed both are accurate and do occur. Both share initiation through binding of RNA primers to either the O_H or Ori_b sites. For a thorough review of mtDNA replication

theories and evidence, the reader is directed to (Holt et al. 2012; *6*). Briefly, mtDNA replication was originally believed to occur in a strand-displacement mechanism (SDM; Fig. 1b). In this theory, the replication of the heavy-strand originates at the O_H producing a long single-stranded DNA molecule, termed the leading-strand. Concurrently, multiple mitochondrial single-stranded DNA binding proteins (mtSSB) bind the displaced light-strand or lagging-strand. Replication continues until the machinery reaches the O_L. Upon reaching the O_L, replication of the light-strand begins in the opposite direction, replicating the light-strand and producing the complement to the lagging-strand.

The major competing theory to the SDM is the Ribonucleotide Incorporation Throughout the Lagging Strand (RITOLS) theory (Fig. 1b; *19*). According to the RITOLS theory, mtDNA replication initiates at either the O_H or the Ori_b. However, as the leading-strand is generated, RNA intermediates are produced and stabilize the displaced L-strand. These RNA intermediates are then either replaced or converted to DNA to create a nascent mtDNA molecule. Also, there is some evidence for a nuclear DNA-(nDNA) like strand-coupled mechanism for replicating mtDNA (*6*, *20*).

Research has demonstrated multiple origins of replication. The most recognized is the O_H site at nucleotide 191 of human mtDNA (*6*). Replication of the H-strand continues in a clockwise direction from this point. Approximately two-thirds of the way around the mtDNA molecule lays the second origin of replication (O_L). A second origin of replication has been identified in the NCR. This replication origin (Ori_b) is able to initiate replication bi-directionally (*21*). The reasons for 2 origins in the NCR are unknown.

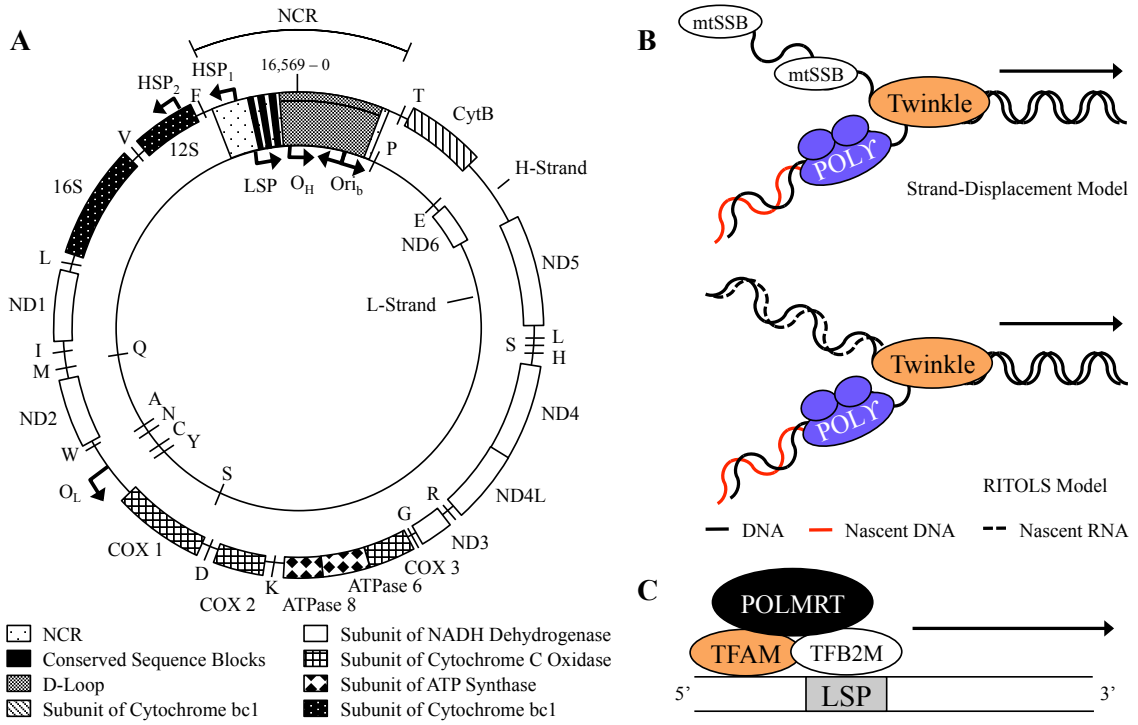

Figure 1. *mtDNA replication and transcription***.** A) Representation of a single mtDNA molecule with the genes for the 13 peptides, 22 tRNAs, and 2 rRNAs labeled. Also included are the three origins of replication – OH, Orib, and OL, the light strand promoter (LSP), the heavy strand promoter (HSP), conserved sequence blocks (CSBs), Non-Coding Region (NCR), and the displacement loop (D-Loop). B) Depiction of two models of mtDNA replication. In both models Twinkle unravels mtDNA and POL γ binds to one strand and begins to create a complimentary strand. The non-template strand is stabilized by mtSSB in the strand-displacement model or by temporary RNA strands in the RITOLS model. C) The 3-component transcriptional machinery model consists of TFAM, TFB2M, and POLMRT. Transcription proceeds from a promoter (e.g. LSP) and proceeds in a 5' to 3' direction.

1.2.2. Mitochondrial DNA Transcription

Similar to mtDNA replication, mtDNA transcription has been extensively studied but remains poorly understood. mtDNA transcription has been reproduced *in vitro*, albeit not without difficulty (*22*). A reported 6-12 liters of KB (derivatives of HeLa cells) cells were required to reproduce mtDNA transcription and likely limited early research into the topic.

There remains a debate about the required machinery for transcription (*23*). A prevailing mechanism suggests that mtDNA transcription only requires mitochondrial transcription factor B2 (TFB2M) and mitochondrial RNA polymerase (POLMRT; *24*). Alone TFB2M and PLMRT are able to initiate mtDNA transcription at all three of the identified mtDNA promoter regions (LSP, HSP_1 and HSP_2; *23*). The competing theory suggests that mitochondrial transcription factor A (TFAM) is also required. Studies show that the presence of TFAM increases the rate of transcription initiating at LSP and HSP_1, in a concentration-dependent manner (*24*). However, TFAM appears to decrease the rate of transcription at HSP_2 (*25*). Some evidence suggests that transcription at HSP_1 preferentially produces transcripts coding only the rRNA and acts to maintain the higher amount of rRNA versus mRNA required for translation (*26*). Other proteins that regulate mtDNA transcription include the MTERF family (MTERF1-4), the mitochondrial Leucine-Rich Pentatricopeptide Repeat Containing protein, the Mitochondrial Ribosomal Protein 12, and the Mitochondrial Transcription Elongation Factor (TEFM; *23*).

Promoters for mtDNA have been long predicted to exist within the NCR (*23*). Indeed, the LSP and HSP_1 are within the NCR. However, the more recently identified HSP_2 is located within the coding region for 12S rRNA (*26*). As mentioned above, TFAM appears to regulate which promoters are actively transcribed.

Conventionally, mtDNA transcription is believed to generate polycistronic transcripts of the entire H-strand and L-strand coding regions (*23*). These long transcripts are then post-transcriptionally processed to generate individual mRNAs, tRNAs, and rRNAs. Current research has suggested that this may not be the case. Transcription initiating at HSP_2 and LSP produce the long polycistronic transcripts previously observed. However, transcription initiated at the HSP_1 appears to terminate just past the rRNA coding regions (*26*).

1.3. Fidelity Regulation

The maintenance of mtDNA is critical to cellular function. Mutations and deletions of mtDNA result in severe cellular dysfunction and disease. In 2005, Kujoth et al. created a mouse model of mtDNA dysfunction (*27*). This mouse, hereafter denoted as the POLγ Mutator mouse, has a mutation in the *Polg1* gene that disables the exonuclease activity of POLγ. This impairs POLγ's proofreading ability and results in the accumulation of mtDNA mutations throughout the decreased life span of the organism. The dysfunctional POLγ results in increased levels of apoptosis, kyphosis, and many other symptoms. This emphasizes the importance of maintaining mtDNA fidelity to the survival and function of organisms.

The maintenance of mtDNA fidelity begins with proper the replication of mtDNA. POLγ incorporates the wrong nucleotide an estimated 1 in every 250,000 base pairs (*28*). This low rate of errors may be a result of the inherent proofreading ability of POLγ and the MTERF family of proteins. MTERFs are believed to slow mtDNA replication to enable accurate nucleotide sequence polymerization (*17*). However, if POLγ makes a mistake, other processes can be invoked to maintain the genome's integrity.

DNA repair mechanisms in mitochondria were believed to be far less extensive than those of the nucleus. Early evidence demonstrated that mitochondria are capable of nucleotide excision repair. This process occurs in 4 steps (*29*): (1) removal of the damaged DNA base and DNA cleavage, (2) processing of the cleaved DNA, (3) gap filling, and (4) ligation. The first two steps of this pathway are performed by monofunctional glycosylases with AP endonuclease 1 (APE1) and bifunctional glycocsylases, such as 8-oxoguanine-DNA glycosylase 1 (OGG1; *29*, *30*). POLγ then completes the gap filling process by inserting the appropriate nucleotide (*31*). Finally, DNA ligase 3 (LIG3) connects the DNA fragments (*29*). Evidence suggests that p53, a tumor suppressor protein, can translocate to the mitochondria of a cell and assist in mtDNA repair under certain conditions (*29*).

Recently, proteins of nuclear DNA repair pathways have been observed in mitochondrial fractions and suggest that mtDNA repair may be much more extensive than previously thought (*29*). Mismatch repair (MMR) was originally identified in rat liver mitochondrial lysate (*32*). Not much is known about MMR in the mitochondrion,

but it is believed that it does not share the same protein machinery as nuclear MMR (*29*). Single-stranded and double-stranded DNA break repair have also been observed (*29*). It is suggested the mechanism may be similar to homologous recombination observed in nDNA. Another unique aspect of mitochondrial DNA maintenance is the ability to degrade mtDNA. Unlike nDNA, mtDNA exists in multiple copies and, if catastrophic damage occurs, a single copy of mtDNA could be degraded without a significant effect on cell homeostasis. Additionally, other work has also suggested that a "bottleneck" exists, where mtDNA mutations can be selected against during embryonic development (*33*). Furthermore, there is evidence that mtDNA containing large deletions and specific mutations actually provide a replicative advantage, so that the degradation of these mtDNA molecules could indeed be necessary, to prevent accumulation of incomplete or error filled mtDNA (*6*). The main endonuclease in mitochondria is Endonuclease G (EndoG; *29*). EndoG is also released from the mitochondria to fragment nDNA during apoptosis (*34*).

Novel evidence has added another disconnect in our understanding of mtDNA fidelity regulation. Mitochondria are dynamic organelles that continually undergo fission and fusion to maintain a reticular network. Mitofusin proteins (mitofusin 1 – Mfn1 and mitofusin 2 – Mfn2) regulate outer mitochondrial membrane fusion (*35*, *36*). In skeletal muscle, genetic ablation of these proteins results in an increase in the number of mtDNA mutations observed and a decrease in mitochondrial DNA copy number (*37*, *38*). Thus, there may be a connection between organelle dynamics and the genomic stability.

1.4. Mitochondrial DNA Copy Number

Numerous copies of mitochondrial DNA exist per cell, and this number is highly regulated. In humans, Mitochondrial Depletion Syndrome (MDS) is the result of a lower than normal number of mtDNA molecules. Furthermore, a study has identified that as much as 18% of electron transport chain deficiencies observed in children are associated with MDS (*39*). Additionally, Durham et al. found that the average mtDNA density was 0.0039 mtDNA/um^3 in skeletal muscle from patients with MDS versus 0.0825 - 0.220 mtDNA/um^3 healthy controls (*40*). This corresponded to COX deficient fibers in the patients, although some fibers with 0.01 – 0.015 mtDNA/um^3 still maintained some COX activity. Thus, there may be a critical threshold for mtDNA required maintenance of ETC enzyme activity and mtDNA copy number is critical to oxidative phosphorylation and cellular homeostasis. However, the mechanism regulating mitochondrial DNA copy number is not known.

It has been long known that mtDNA copy number can be manipulated by the use of DNA intercalating agents, particularly Ethidium Bromide (EtBr; *41*). This has been an invaluable tool in mitochondrial and mtDNA research. Because it is positively charged, EtBr preferentially accumulates in the negatively charged matrix of mitochondria. Thus, at low levels EtBr is believed to specifically affect mtDNA (*42*). Acute treatment (less than 15 days) with DNA intercalating agents produces cells partially depleted of mtDNA (ρ^- cells; *41*). In 143B.TK^- cells, chronic treatment can completely abolish mtDNA, resulting in ρ^0 cells (*43*). Innoue et al. suggested C2C12 cells have a resistance to

mtDNA depletion by EtBr and that another intercalating agent, ditercalinium, is more effective (*44*). However, many researchers have successfully employed longer treatments of EtBr (greater than 6 weeks) to create ρ^- C2C12 cells (*45*). This might suggest that mtDNA is so critical to C2C12 survival that this cell line expresses factors that make it particularly resistant to mtDNA depletion.

Studies have investigated the role specific proteins have on mtDNA copy number. In humans, mtDNA depletion can result from mutations in genes essential for mtDNA replication (e.g. *Polg1, Polg2* and *C10orf2* – Twinkle) and mitochondrial dNTP supply (e.g. Mitochondrial Deoxyguanosine Kinase; *DGUOK,* Thymidine Kinase 2; *TK2*, and Thymidine Phosphorylase; *TYMP*; *46*). Transgenic mice with a homozygous ablation of *TFAM*, *C10orf2*, *Polg1*, and *Polg2* (the accessory subunit of POLγ) all die during embryonic development between ~E8.5 and 10.5 (*47-50*). Analysis revealed no or very little (approximately < 5% of wildtype levels) mtDNA in $TFAM^{-/-}$, $Polg1^{-/-}$, and $Polg2^{-/-}$ animals. In contrast, transgenic mice overexpressing Twinkle and TFAM protein maintain higher levels of mtDNA (*14*, *51*). The levels of Twinkle protein in these mice directly correlated with the mtDNA copy number (*14*). When Twinkle and TFAM were simultaneously overexpressed an additional increase in mtDNA copy number occurred, suggesting independent regulation of mtDNA copy number (*15*). This effect was suggested to be a result of Twinkle's role in *de novo* synthesis of mtDNA and TFAM's role in mtDNA stabilization. However, the authors suggested that too much mtDNA could also be detrimental to the organism. They observed increases in mtDNA caused the

appearance of cytochrome c oxidase (COX) deficient muscle fibers (*15*). Surprisingly, ablating TFB1M results in an increase in mtDNA, perhaps through a compensatory increase in TFAM expression (*52*). This evidence all indicates the critical role these proteins play in mtDNA copy number regulation.

1.5. Mitochondrial DNA Disorders

Approximately 1 in 7,200 individuals are diagnosed with a mitochondrial disease due to mtDNA mutations (*53*). It has been suggested that this prevalence is underestimated due to the difficulty in diagnosing these disorders. This is supported by a study that found 1 in 200 newborns have a detectable level of pathological mtDNA in their umbilical cord blood (*54*). These diseases result in a wide array of phenotypes that can include hearing impairment, stroke-like episodes, ataxia, and exercise intolerance (*55*). Complicating the matter further, there are stark differences between tissues and even between patients with the same disease origin (*56*). This contributes to the difficulty in diagnosing these diseases and furthers the requirement for individual treatment of these diseases.

1.5.1. Types and Origins

mtDNA disease arises from alterations in many proteins that directly or indirectly affect mitochondria. These include mutations in both the nuclear and mitochondrial genome.

1.5.1.1. Nuclear Genes Causing mtDNA Diseases

Nuclear DNA is acquired through Mendelian inheritance. It also possesses numerous repair pathways to prevent accumulation of potentially hazardous DNA damage. However, damage does occur and diseases such as cancer are a result. In the case of mtDNA disease, mutations in nuclear proteins required for the replication, transcription, and translation of mtDNA all cause mitochondrial disease. This can cause a loss of mtDNA, or mutations and deletions of mtDNA (27, 46, 57; Fig. 2). Mutations in many genes required for mtDNA replication (such as *Polg1* and *C10orf2*) can produce diseases such as Autosomal Dominant Progressive External Opthalmoplegia (adPEO), where there is progressive weakening of external eye muscles (46, 57).

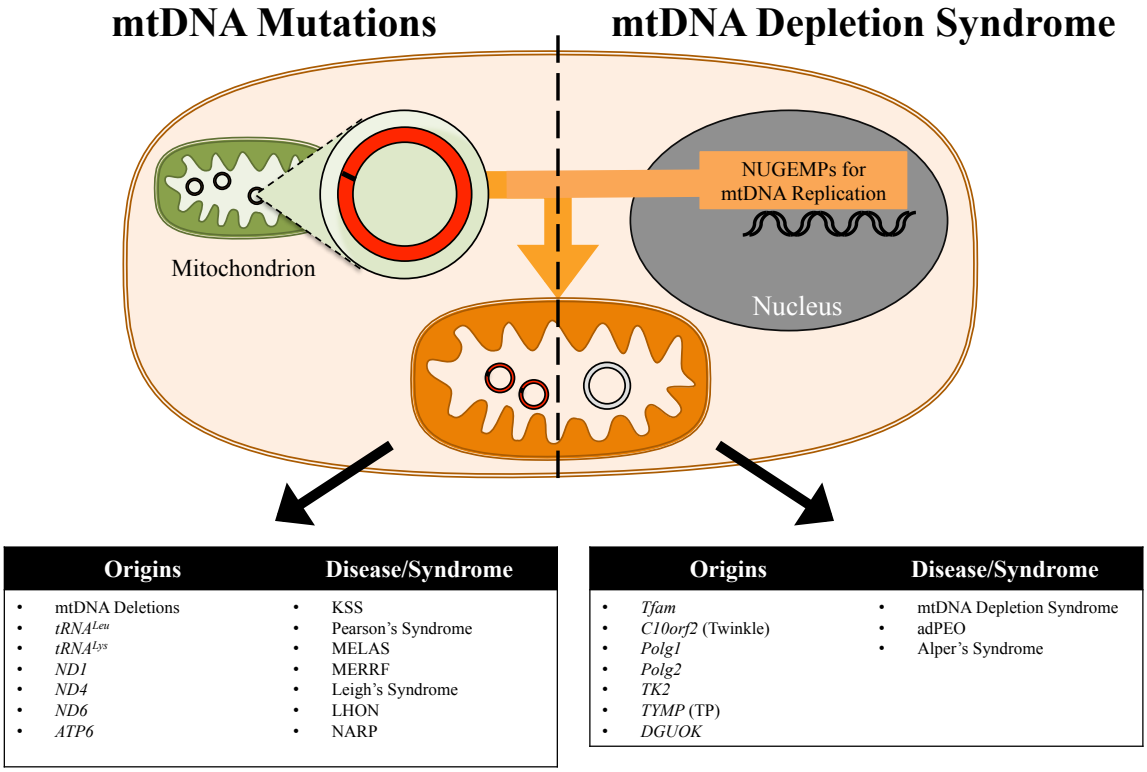

Origins	Disease/Syndrome
• mtDNA Deletions • *tRNA*^{Leu} • *tRNA*^{Lys} • *ND1* • *ND4* • *ND6* • *ATP6*	• KSS • Pearson's Syndrome • MELAS • MERRF • Leigh's Syndrome • LHON • NARP

Origins	Disease/Syndrome
• *Tfam* • *C10orf2* (Twinkle) • *Polg1* • *Polg2* • *TK2* • *TYMP* (TP) • *DGUOK*	• mtDNA Depletion Syndrome • adPEO • Alper's Syndrome

Figure 2. *mtDNA disease origins*. Mitochondrial DNA diseases can originate from both the mitochondrial and nuclear genome. mtDNA deletions can result in diseases including KSS and Pearson's Syndrome. mtDNA mutations result in inherent diseases originating from the specific mutations, such as MELAS, MERRF, and LHON. Mutations in nDNA can cause defects in mtDNA replication resulting in a lack of mtDNA. This is called mtDNA Depletion Syndrome (MDS) and can also result in adPEO and Alper's Syndrome.

1.5.1.2. Mitochondrial Sources of mtDNA mutations

Mutations in mtDNA accumulate from exposure to oxidative stress, UV irradiation, and mutagens. The ETC is a significant source of cellular reactive oxygen species (ROS). During maximal respiration as much as 3% of total cellular oxygen is converted to ROS (*58*). Because of its proximity to the ETC, mtDNA is susceptible to oxidation by ROS. Early studies showed that the oxidized nucleic acid base, 8-hydroxydeoxyguanosine (oh^8dG), was present once every 800 bases in mtDNA and only once every 130,000 bases in the nuclear genome (*59*). These oxidized bases can then cause improper incorporation of the wrong nucleic acids during mtDNA transcription and replication (*31*). The effect of ROS on mtDNA is the core of the mitochondrial theory of aging, whereby ROS from the ETC causes mutations in the mtDNA and these mutations consequently cause creation of dysfunctional gene products from mtDNA leading to more ROS being produced and more oxidative damage to cellular components, such as cell membranes, proteins, and DNA (*60*).

Specific diseases due to mutations or deletions of mtDNA have only been known for 25 years. In 1988, two laboratories simultaneously discovered the first mtDNA diseases – deletions of mtDNA present in patients with mitochondrial myopathies (*61*) and a point mutation causing Leber's Hereditary Optic Neuropathy (LHON; *3*). Identification of these diseases was facilitated by identification of a maternally inherited pedigree of morbidity. There are many mitochondrial myopathies currently recognized as originating from mutations or deletions in mtDNA. These include Leigh's Syndrome

(LS), Kearns-Sayre Syndrome (KSS), Mitochondrial Encephalomyopathy with Lactic Acidosis and Stroke-Like Episodes (MELAS), Myoclonic Epilepsy with Ragged Red Fibers (MERRF), and Neuropathy Ataxia with Retinitis Pigmentosa (NARP; *62*; Fig. 2).

1.5.2. Effects

The symptoms of mitochondrial myopathies are extremely tissue-dependent and patient-specific. These diseases are progressive in nature and result in a shortened lifespan. Since numerous copies of mtDNA exist, both wildtype and pathological mtDNA molecules can coexist in a cell in a state called heteroplasmy (62). Before symptoms present, pathological mtDNA must be expressed at a high enough level. The tolerable amount of mutated mtDNA before symptoms present is known to be tissue-specific. For example, the A3243G mutation in mtDNA causes diabetes at low levels (40-50%), but can also cause PEO and MELAS with higher mutation loads, 60-70% and 80-95%, respectively (*63*). Highly metabolic tissues, such as the heart, liver, skeletal muscle, and neurons, are particularly affected (*62*). For example, in skeletal muscle, massive dysfunctional mitochondria proliferate, accumulate at the sarcolemmal membrane, and produce ragged red fibers. In patients, these disorders can present with conditions such as extreme exercise intolerance, diabetes mellitus, ataxia, and hearing loss (*62*).

1.5.3. Potential Cures and Treatments

To date, there are no cures for mitochondrial diseases. Clinical approaches mostly attend to secondary disorders caused by these diseases. Many theoretical therapies and cures have been demonstrated in cell culture and animal models. Only recently have studies investigated some of these treatments in patients.

The genetic and pharmaceutical remedies in cell culture and animal models can be categorized into a) treatments that improve cellular function through compensatory mechanisms and b) those that replace or correct the mutant genetic material. Because of the importance of PGC-1α pathway to mitochondrial biogenesis (reviewed in section 2.1), many research groups have used overexpression of PGC-1α to improve mitochondrial function in models of mitochondrial disease. In fibroblasts from patients with mtDNA diseases, Srivastava et al. showed partial improvements in basal respiration when transduced with viruses overexpressing PGC-1α and PGC-1β (*64*). Although not directly affecting mtDNA, ablations of COX assembly factors – including COX10, Surf1, COX15 and Sco2 – are common models of mitochondrial disease. Skeletal muscle overexpression of PGC-1α slowed the onset of COX enzyme activity dysfunction in mice lacking COX10 (*65*), and improved COX enzyme activity in mice not expressing Surf1 (*66*). Furthermore, researchers have investigated the use of drugs targeting the PGC-1α-AMPK pathway. In cell culture, a study by Golubitzky et al., treated cells harbouring mutations in nuclear genes encoding NADH Dehydrogenase subunits with drugs shown to increase mitochondrial biogenesis, including resveratrol and 5-Aminoimidazole-4-

carboxamide ribonucleoside (AICAR; *67*). They identified AICAR, an AMPK agonist, as the most beneficial small compound to cellular ATP and ROS levels. Other studies found that the PPAR panagonist, bezafibrate, elicited similar effects as PGC-1α overexpression on *COX10*$^{-/-}$ mice (*65*), but induced weight loss and massive amounts of apoptosis in *Surf1*$^{-/-}$ and *COX15*$^{-/-}$ mice respectively (*66*). However, AICAR was found to ameliorate the COX enzyme activity deficit in *Surf1*$^{-/-}$ mice, *COX15*$^{-/-}$ mice, and mice expressing a mutant form of *Sco2*$^{ko/ki}$ (*66*). This suggests that transgenic PGC-1α overexpression may assist in compensating for defects observed in mitochondrial disease, but drugs targeting this pathway are not a panacea for mitochondrial disease.

Studies have shown that genetically targeting nuclear encoded RNAs to the mitochondria can compensate for mutated mtDNA encoded RNAs. Kolesnikova et al. first demonstrated that transducing a derivative of the yeast $tRNA^{Lys}$ into transmitochondrial cybrids, with the A8344G mutation, results in the import of the $tRNA^{Lys}$ into mitochondria (*68*). Furthermore, the $tRNA^{Lys}$ was able to improve mitochondrial respiration, mitochondrial membrane potential, and activities of the ETC complexes. More recently, laboratories have demonstrated that by attaching a sequence from the 3' untranslated region (UTR) of human Mitochondrial Ribosomal Protein S12 (MRPS12) mRNA, nuclear encoded tRNAs and larger mRNAs can be imported into mitochondria (*69*). In cybrids harbouring the A8344G and A3243G mutations, targeting of the $tRNA^{Lys}$ and $tRNA^{Leu}$, respectively, partially rescues cellular respiration (*69*). Thus,

targeting of nuclear tRNAs and mRNAs to the mitochondria may provide a method to essentially replace the mutated tRNAs and mRNAs in mtDNA diseases.

Alternatively, a study has used exercise to improve mitochondrial dysfunction in a mouse model with mtDNA mutations. The POLγ mutator mouse has a mutation in the proofreading region of *Polg1* gene that results in an accumulation of mtDNA mutations (*27*). With exercise, the pathologies, including increased levels of apoptosis, increased mtDNA mutations, and decreased mtDNA copy number, are reversed (*70*). This suggests that exercise is a potential therapy for diseases related to mutations in *Polg1* and mtDNA mutations.

A recent Cochrane review emphasized our dearth of knowledge of mitochondrial disease treatments. They found only 12 randomized-control trials of sufficient integrity to be considered (*71*). These studies supplemented patients with creatine (*72*-*74*); coenzyme Q10, creatine, and lipoic acid in combination (*75*); dichloroacetate (*76*-*80*); dimethylglycine (*81*), and cysteine (*82*). The reviewers found insufficient evidence to conclude that any of these treatments were beneficial.

Other studies have investigated the use of exercise in patients with mitochondrial disorders. Improvements in VO_{2max}, endurance performance, and muscle strength have all been observed (*83*, *84*). Furthermore, mitochondrial proteins, such as cytochrome c, appear to increase similarly between patient and control individuals with training (*85*). However, no changes in mtDNA copy number were observed in patients with mtDNA deletions, suggesting the underlying cause of the disease remains present (*84*). Basic

scientific evidence suggests there are many potential therapies and cures for mitochondrial disease. However, more human studies must be completed before a resolution to mitochondrial disease can be found.

2. Mitochondrial Content Regulation

Mitochondria play a pivotal role in cell homeostasis. They are generators of intracellular energy but also regulators of cell death. Thus, maintaining a healthy mitochondrial pool is absolutely vital. Their function is mediated by either the growth of new mitochondria, or by the degradation of old and defective mitochondria.

2.1. Mitochondrial Biogenesis

Mitochondrial biogenesis is the process by which a cell attains more mitochondrial content. Unlike traditional textbook depictions of the organelle, mitochondria actually form a dynamic reticulum reaching throughout the cell. Therefore mitochondrial biogenesis is more than the growth of new discrete mitochondria, but rather the expansion of this organelle network. This process requires expansion of both the inner and outer mitochondrial membranes (IMM and OMM, respectively), and the creation and import of proteins (Fig. 3).

2.1.1. Mitochondrial Membrane Synthesis

Mitochondrial membranes play a critical role in mitochondrial homeostasis. The OMM defines the outer border of a mitochondrion. The OMM can undergo fission, via the action of Drp1 and Fis1, and fusion with other mitochondria, through Mfn1 and Mfn2 (*86*). The IMM houses the key components of the ETC and thus plays a vital role in oxidative energy production. Mitochondrial membranes have unique lipid composition profiles that are different between the IMM and OMM. For example, rat liver IMMs

contain 14-23% cardiolipin (CL), 32-39% phosphatidylethanolamine (PE), 28-45% phosphatidylcholine (PC), and 2-7% phosphatidylinositol (PI), versus rat liver OMMs that contain 3-10% CL, 20-35% PE, 38-45% PC, and 5-20% PI (*87*, *88*). However, the synthesis, import, and localization mechanisms for these lipids are poorly understood. Many phospholipids are synthesized in the mitochondria, including CL and PE, but PC and PI are primarily synthesized in the ER (*87*, *88*). CL is a key phospholipid for mitochondrial function. It comprises 18% of phospholipids in rat liver mitochondria (*88*, *89*). Mutations in the gene encoding Taffazin, a key protein in CL synthesis, cause Barth syndrome (*89*, *90*). Barth syndrome is characterized by dilated cardiomyopathy, skeletal myopathy, and infantile death in males (*90-92*). The severity of this disease may be due to the diverse role of CL in mitochondrial homeostasis. CL is known to assist in the stabilization and activity of Complex III and IV of the ETC (*87*, *91*, *92*). Also, CL participates in mitochondrial protein import (*87*, *93*, *94*) and regulates mitochondrial-mediated apoptosis by binding cytochrome c (*93-95*). Although the mechanisms of mitochondrial phospholipid synthesis are poorly understood, it appears they are critical for the organelle's function.

2.1.2. Mitochondrial Protein Synthesis

There are an estimated 1,100-1,400 proteins in human mitochondria and mtDNA, as described previously (section 1), encodes only 13 of these peptides (*95*). Nuclear genes encoding mitochondrial destined proteins are called nuclear genes encoding mitochondrial proteins (NUGEMPs). Despite the mitochondrion's enormous proteome,

Peroxisome Proliferator-Activated Receptor Gamma Co-Activator 1-alpha (PGC-1α) appears to regulate much of the NUGEMP expression and is thus called the "master regulator of mitochondrial biogenesis" (*97*). PGC-1α is a transcriptional co-activator. It binds transcription factors containing a LXXLL motif, promoting their activity, and remodels chromatin to increase transcription of genes related to mitochondrial biogenesis. PGC-1α is upregulated under many conditions, including cold-exposure and exercise training – a common stimulus to increase mitochondrial content (Fig. 3). However, mice that lack PGC-1α are viable and do contain mitochondria. Although, these mitochondria are less functional, and the mice experience attenuated mitochondrial biogenesis (*98*). Some of this may be explained through compensatory increases in other PGC-1α family members, including PGC-1β (*99*) and PGC-1α Related Co-Activator (PRC; *100*), which share some of PGC-1α's activity.

PGC-1α is able to induce a transcriptional cascade leading to mitochondrial protein synthesis. Specifically, PGC-1α induces the transcription of Nuclear Receptor Factors-1 and -2 (NRF-1 and NRF-2) and Estrogen-Related Receptor alpha (ERRα; *97*). NRF-1 is able to consequently increase the expression of TFAM and thus, PGC-1α coordinates the transcription of both the nuclear and mitochondrial genome for mitochondrial biogenesis (Fig. 3).

2.1.3. Protein Import Into the Mitochondria

After NUGEMPs are transcribed and translated into mitochondrial-destined proteins, they must be imported into the mitochondria (Fig. 3). Proteins are targeted for

import by a mitochondrial targeting sequence (MTS), which is most commonly found at the N-terminus (*101*). However, there is no consensus on the MTS sequence, although, an algorithm exists that can use the amino acid sequence of a protein to predict the likelihood of mitochondrial localization (*102*). When entering a mitochondrion, proteins must be channeled to the appropriate compartment, such as the matrix, IMM, intermembrane space, or OMM (*101*). This import is achieved through a variety of protein import machineries (*101*). Protein transfer through the OMM is achieved by the Translocase of the Outer Mitochondrial Membrane (TOM) complex, and respectively through the IMM by the Translocase of the Inner Mitochondrial Membrane (TIM) complex. Once imported, the MTS is cleaved and chaperone proteins assist in protein refolding (*101*).

2.1.4. Mitochondrial Biogenesis Stimuli

Mitochondrial biogenesis is an extremely regulated process. Generally, it can occur in response to cellular energy deprivation as is indicated by calcium transients, an increase in the AMP to ATP ratio, and excess ROS production (Fig. 3). A traditional adaptation to exercise is increased mitochondrial content (*103*) and this adaptation is mediated by the aforementioned stress signals.

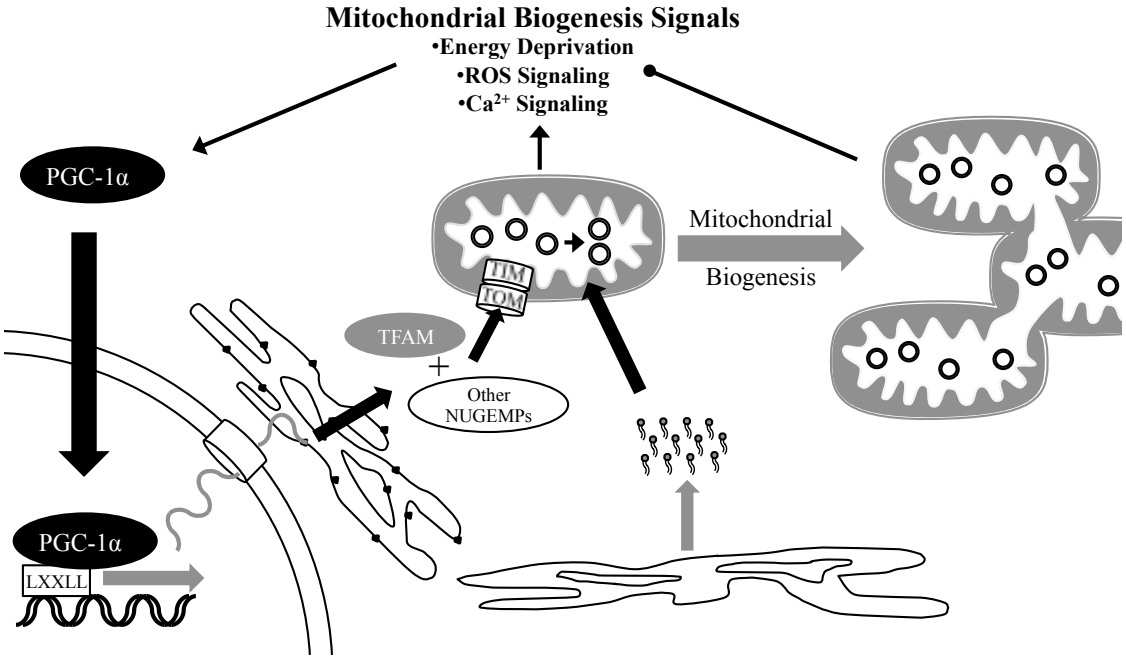

Figure 3. *Mitochondrial biogenesis.* Mitochondrial biogenesis occurs in response to numerous cellular signals such as energy deprivation, ROS or Ca^{2+}. The master regulator of mitochondrial biogenesis, PGC-1α, coordinates the expression of nuclear genes encoding mitochondrial proteins (NUGEMPS), such as TFAM. Mature TFAM protein and other NUGEMPs can then enter the mitochondria through the protein import machinery (e.g. TOM and TIM complexes). These proteins increase the replication and transcription of mtDNA, and increase ETC capacity. Concurrently, new phospholipids are integrated from the endoplasmic reticulum to expand the mitochondrial membrane. Collectively, these processes result in an expanded mitochondrial network.

2.2. Mitochondrial Dynamics

The fusion and fission of mitochondria is an intermediate regulatory loop that lies between biogenesis and degradation. When mitochondria are part of a network they share their contents and are able to maintain function. In 2001, two COX activity deficient cybrid lines, containing homoplasmic mtDNA for the A3243G and A4269G mutations, were fused using electric pulses (*37*, *96*). The authors found that 10-14 days after fusion, the fused cells regained COX activity. This is evidence of "functional complementarity," whereby mtDNA from different mitochondria can share their contents. OMM fusion and IMM fusion is mediated by the mitofusin proteins (Mfn1 and Mfn2) and Opa1, respectively (*86*). In mice deficient of Mfn1 and Mfn2, there was a loss of mtDNA stability and progressive loss of COX enzyme activity in skeletal muscle (*37*, *104*). This emphasizes the requirement of functional, reticular organelles.

Lastly, mitochondrial fission is the process of mitochondria budding off from the reticulum. The proteins, Drp1 and Fis1, regulate mitochondrial fission (*86*). Dysfunctional mitochondria undergo fission from the mitochondrial network upon loss of membrane potential. These punctate mitochondria can then be engulfed by autophagosomes and degraded, through mitochondrial autophagy.

2.3. Mitochondrial Degradation

The removal of dysfunctional mitochondria is critical to cellular function. Accumulation of oxidative damage to mitochondrial proteins, lipids and DNA can lead to

cellular dysfunction. Proteolytic pathways involved in mitochondrial quality control include innate mitochondrial proteases and the ubiquitin-proteasome degradation of OMM proteins. Whole organelle degradation is achieved by mitochondrial autophagy (mitophagy).

2.3.1. Mitochondrial Proteases

Mitochondrial proteins can be degraded by intrinsic proteases. These enzymes are important to the regulation and function of the organelle because they degrade oxidized proteins and facilitate targeting of mitochondria for mitophagy. For example, Lon protease degrades phosphorylated TFAM to regulate mtDNA copy number (*104*, *105*) and preferentially degrades oxidized proteins, such as Aconitase (*105*, *106*). An important protease for organelle quality control is PARL. Under normal conditions, PARL cleaves PINK1 and prevents its stabilization on the OMM (*106*, *107*). However, when mitochondria lose their membrane potential, PINK1 accumulates on the OMM and signals for the degradation of mitochondria through mitophagy (*106*-*108*).

2.3.2. Ubiquitin-Proteasome Degradation of OMM Proteins

The ubqiquitin-proteaseome system dismantles cytosolic proteins tagged for degradation by E3 ubiquitin ligases (*108*, *109*). The proteasome is known to degrade proteins of the endoplasmic reticulum (ER) membrane, and recently has been identified to play a similar role in degrading OMM proteins (*109*, *110*). Tanaka et al. showed that Mfn1 and Mfn2 are ubiquitinated and can be selectively degraded by the proteasome in a

p97 AAA^+ protease dependent manner (*110*, *111*). Furthermore, this was suggested to prevent mitochondrial fusion and enabled subsequent mitophagy to occur.

2.3.3. Mitophagy

Autophagy or "self-eating" is a highly conserved cellular process. Originally, macroautopagy (henceforth referred to as "autophagy") was thought to be an imprecise degradation process. Recent literature dictates that autophagic substrates can be very specific. Of particular note, whole mitochondria can be processed through mitochondrial autophagy or mitophagy. Our understanding of the mitophagy pathway is incomplete. However, it has been suggested that mitophagy is essential to the health of many tissues, including skeletal muscle where it appears to be critical to the maintenance of muscle mass (*111-113*).

2.3.3.1. Autophagy Induction and Autophagosome Maturation

Mitophagy and general autophagy induction share similar pathways. The processes can be initiated by many disturbances, such as serum starvation, glucose starvation, amino acid starvation, and exercise (*112-114*). Mammalian Target of Rapamycin Complex 1 (mTORC1) and AMPK are nutrient sensitive complexes that regulate the autophagy initiation signal cascade. Briefly, mTORC1 activity is reduced in the absence of free amino acids and AMPK is activated under conditions of energy depletion by an increase in the AMP/ATP ratio, and other signals (reviewed in section 3.3). mTORC1 is a multi-protein complex, comprised of mTOR, raptor, GβL, and PRAS40. mTORC1 is

the major negative regulator of autophagy, that is to say, when active, mTORC1 inhibits the induction of autophagy. mTORC1 decreases the activity of the Ulk1-Atg13-FIP200 complex by phosphorylating Ulk1 on Ser757 (*114-116*). Contrasting the role of mTORC1, AMPK can initiate autophagy by two mechanisms. AMPK can bind and phosphorylate Ulk1 at Ser317 and Ser777, thus activating the protein complex (*112*, *114-116*). Also, AMPK can inactivate mTORC1 by phosphorylating TSC2, a protein upstream of mTORC1. This alleviates the inhibition on Ulk1. Ulk1 then phosphorylates Atg13, FIP200 and itself, activating the complex (*112*, *117*). An active Ulk1-Atg13-FIP200 phosphorylates Ambra1, activating it (*112*, *117*), and initiating the maturation of the autophagosome.

The maturation of the autophagosome requires the sequestering of a lipid membrane and, sequentially, its elongation and maturation. The origin of the autophagosomal membrane is unknown (*112*). However, the protein complexes required for its maturation are well characterized. The core of PI3K Class III complex is Beclin-1, Vps34, and p150 (*112*). Its role in the creation of autophagosomal membrane is positively regulated by Ambra1 (activated by the Ulk1-Atg13-FIP200 complex), Atg14, Rab5, UVRAG, and Bif1 binding, and negatively regulated by Rubicon, IP3R, NAF-1 and Bcl-2 binding (*112*). Concurrently, autophagy related genes (ATGs) covalently attach PE to Microtubule-Associated Light Chain 3 (LC3) to create LC3-II (*112*, *118*), in a series of sequential conjugation steps. ROS, produced during starvation, is essential to activation of Atg4, the initial enzyme in this process (*118*, *119*). Consequently, LC3-II

integrates into the autophagosomal membrane and serves as an anchor protein to attach the autophagosome to its target. Critical to conversion of LC3-I to LC3-II is Atg7. Atg7 conjugates to LC3-I and serves as an intermediate prior to the attachment of PE. Elimination of Atg7 in reticulocytes and skeletal muscle animals yields delayed mitophagy initiation (*119*, *120*) and accumulate dysmorphic and respiratory-deficient mitochondria (*120*, *121*).

2.3.3.2. Cargo Selection

Although general autophagy and mitophagy share many mechanisms, the distinguishing characteristic of mitophagy is that it selectively degrades mitochondria. For a mitochondrion to be degraded, it must be segregated from the mitochondrial network, targeted, and consequently enveloped by an autophagosome.

Segregation occurs when a fission event occurs that results in two mitochondria of unequal membrane potentials (*106*, *107*, *121*). The depolarized mitochondrion is prevented from fusing back into the mitochondrial network when PINK1 selectively accumulates on depolarized mitochondria (refer to section 2.3.1; *106*, *107*, *122*). The ubiquitin E3 ligase, Parkin, is then attracted to the mitochondria and will ubiquitinate OMM proteins, such as Mfn1 and Mfn2 (*110*, *122*). This leads to proteolytic degradation of Mfn1 and Mfn2 (see section 2.3.2; *110*, *123*), preventing the fusion of the depolarized mitochondrial back into the organelle network. The autophagosome is then tethered to other ubiquitinated OMM proteins by p62, which has binding motifs for both LC3-II and ubiquitin (*123*). This allows for the autophagosome to envelope the mitochondrion and

consequently shuttle it to a lysosome for fusion and degradation. Also, Parkin has been suggested to interact with Ambra1 and facilitate the induction of mitophagy in response to mitochondrial depolarization, thus providing a connection between mitochondrial dysfunction and mitophagy induction (*123*, *124*).

Nix is an OMM protein and has many roles in mitophagy. It is involved in the recruitment of Parkin to depolarized mitochondria (*124*, *125*), and independently can induce autophagy and bind the autophagosome. Nix can dissociate the Bcl-2–Beclin1 complex (*125*, *126*), thus alleviating the inhibition of Beclin1 and inducing autophagy. Furthermore, it can directly bind LC3-II to initiate envelopment of a mitochondrion (*126*).

2.3.3.3. Degradation by the Lysosome

Upon maturation and envelopment of target complexes, the autophagosome fuses with the lysosome to produce an autolysosome (*88*, *112*). Upon fusion, pH-dependent enzymes, such as Cathepsin-D, degrade the contents (*127*). To measure autophagic flux, fusion can be inhibited by lysosomal inhibitors, such as Bafilomycin A_1 ($BafA_1$) and Chloroquine (CQ). These chemicals raise the pH of the lysosome and prevent its fusion and/or decrease the activity of the proteolytic enzymes (*128*).

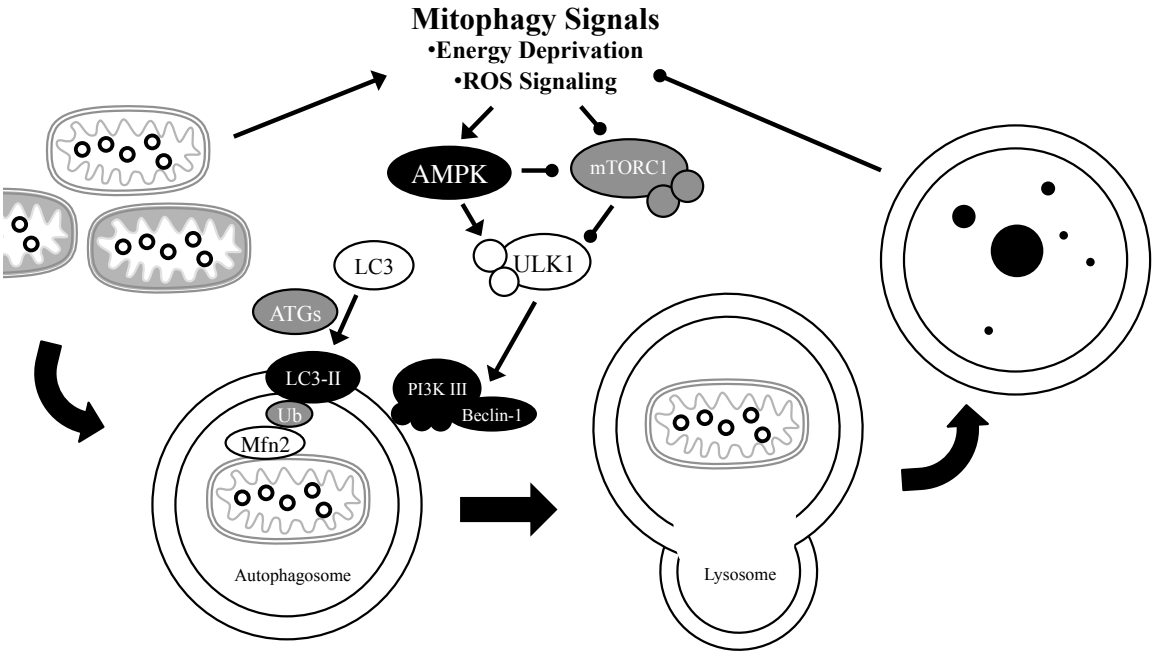

Figure 4. *Mitophagy.* Entire mitochondria can be degraded through a specialized form of autophagy, termed mitophagy. Energy deprivation and aberrant ROS signaling from dysfunctional organelles can activate AMPK and inhibit mTORC1 leading to the creation of an autophagosome by ATG proteins and the Vps34 complex. These autohagosomes contain LC3-II that can bind ubiquitinated outer mitochondrial membrane proteins. This allows the autophagosome to form around mitochondria targeted for degradation. The autophagosome then fuses with a lysosome and the contents are degraded and released back into the cell.

3. AMP-Activated Protein Kinase

3.1. Structure

AMPK is a heterotrimeric protein. The complete complex consists of a catalytic (α) and 2 regulatory subunits (β and γ). There are 2 isoforms of the α subunit (α_1 and α_2), 2 isoforms of the β subunit (β_1 and β_2), and 3 isoforms of the γ subunit (γ_1, γ_2, and γ_3; *129*). The α subunit contains the kinase activity of the AMPK enzyme. Phosphorylation at Thr172 of the α subunit, by upstream kinases, increases AMPK activity 100-fold (*130*). Immediately, after the kinase domain is an Autoinhibitory Domain (AID), which when removed or mutated renders the α subunit constitutively active (*131*). The γ subunit contains four bindings sites for adenine nucleotides (*129*). Under basal conditions, 2 ATP molecules and 1 AMP molecule occupy two sites (*130*). Upon energy depletion or cellular stress, 2 AMP molecules and 1 ADP molecule replace these and prevent the dephosphorylation of the α subunit. The binding of AMP to these sites increases the activity of AMPK by an additional order of magnitude.

Many of these isoforms have multiple versions due to alternative initiation or splice variants (*129*). Also, these subunits and their different isoforms are expressed in a tissue-specific manner. Early studies identified general AMPK mRNA and protein levels to be highest in rat skeletal muscle versus other tissues, including the heart and liver (*132*). However, AMPK activity was much lower in skeletal muscle versus liver (*132*, *133*). With respect to subunit isoform expression, northern and western blotting revealed that

α_1 is found ubiquitously in all tissues and α_2 is primarily present in the heart, liver, and skeletal muscle (*134*). Similar to the α subunits, the β_1 subunit protein is located in liver, heart, brain, lung and testes, and the β_2 subunit is expressed primarily in skeletal muscle, heart, brain and lung (*135*). Furthermore, the β_1 subunit appears to be only expressed in the soleus (a predominantly slow-twitch muscle). Where as, the extensor digitorum longus (EDL; a primarily fast-twitch muscle), contains both β_1 and β_2 isoforms (*136*). Likewise, the γ subunits also have tissue-specific presence. With regards to mRNA content, γ_1 mRNA is transcribed in all tissues, albeit at different levels, γ_2 mRNA is present in all tissues except the lung, and γ_3 mRNA is found almost exclusively in skeletal muscle (*137*). Furthermore, there is also a fiber-type specific distribution of γ subunit protein formation. The γ_3 subunit is highly expressed in fast-twitch glycolytic muscle (e.g. white gastrocnemius), followed by fast-twitch oxidative muscle (e.g. red gastrocnemius), and is undetectable in slow-twitch muscle (e.g. soleus; *138*, *139*). Furthermore, throughout the differentiation of C2C12 myoblasts, there is a shift in AMPK subunit expression and activity (*140*). At Day 0 of differentiation, the α_2 and γ_2 subunits were predominant. As differentiation progressed until day 7, there was a gradual increase in α_1, β_1, β_2, and γ_3 subunits expression, and this resulted in a greater AMPK activation. All of this data emphasizes the importance and highly regulated tissue- and fiber-type specific expression of the AMPK subunits.

3.2. Purpose and Role

Fundamentally, AMPK may be considered a nutrient and energy sensing protein. It regulates the activation and inhibition of cellular processes depending on the energy-status of the cell. When active, AMPK has been shown to inhibit energy-dependent pathways, including protein-synthesis, lipid-synthesis, and glycogen-synthesis (*130*). In contrast, active AMPK can increase energy production through glycolysis, fatty acid oxidation, autophagy, and mitochondrial biogenesis (*130*). The following paragraphs focus on its role in mitochondrial biogenesis and autophagy (Fig. 5).

Since mitochondria are the site of oxidative phosphorylation and provide most of the energy to the cell, maintenance of mitochondrial quantity and quality is fundamental to proper energy homeostasis. In the absence of AMPK, mice have lower mitochondrial content and ambulate less (*141*), indicating an important role for AMPK in mitochondrial biogenesis. PGC-1α is the "master regulator of mitochondrial biogenesis." AMPK has been shown to directly phosphorylate PGC-1α (*142*). This may allow PGC-1α to translocate to the nucleus and promote its own transcription, resulting in a transcriptional cascade leading to the expansion of mitochondrial reticulum (Fig. 4). AICAR has also been shown to cause increased binding of the USF-1 and GATA transcription factors to the promotor of PGC-1α and PGC-1α mRNA expression (*143*). Also, AMPK activation has been shown to act as a prerequisite for other post-translational modifications to PGC-1α, such as deacetylation by SirT1 (*144*). This demonstrates the importance of AMPK to maintaining mitochondrial content.

Mitophagy is crucial to the maintenance of a functional mitochondrial pool. AMPK triggers upstream events that are shared between general autophagy and mitophagy. AMPK phosphorylates TSC2 and raptor, resulting in mTORC1 inhibition (*145*, *146*). As well, AMPK can phosphorylate and activate Ulk1 (*114*; Fig. 4). These modifications result in increased autophagic induction (*114*). When Ulk1 or AMPK is absent, accumulation of dysfunctional mitochondria occurs (*116*). Thus, AMPK is crucial to maintaining a healthy and productive mitochondrial pool.

3.3. Activation and Regulation

The energy status or AMP/ATP ratio of the cell, directly regulates AMPK. However, AMPK is also susceptible to regulation by other signals through the phosphorylation of Thr172 of the AMPK α subunit (*129*). There are many known physiological regulators of AMPK, and additionally, pharmacological activators of AMPK are being discovered continuously and implemented in medical practice.

Physiologically, changes in the AMP/ATP ratio and the activity of upstream kinases regulate the activity of AMPK. Adenylate kinase (AK) is an enzyme that converts 2 ADP molecules to 1 ATP molecule and 1 AMP molecule. Because of a high rate of activity, AK induces large changes in AMP levels, and thus it is logical that AMPK is more sensitive to AMP levels than ADP (*147*). Furthermore, the kinases that

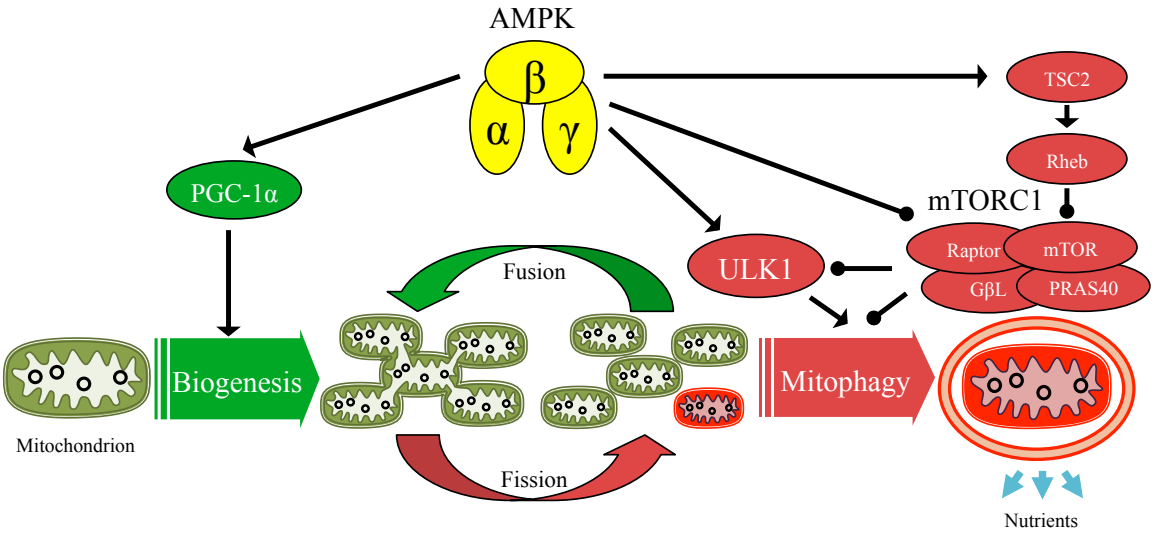

Figure 5. *AMPK regulation of mitochondrial biogenesis and mitophagy*. The AMPK protein complex can phosphorylate PGC-1 α. This facilitates the translocation of PGC-1 α to the nucleus where it can stimulate the transcription of genes required for mitochondrial biogenesis. AMPK can also activate mitophagy. Phosphorylation of TSC2, Raptor, and ULK1 by AMPK activates mitophagy. TSC2 activates mitophagy by phosphorylating Rheb, which can then inhibit mTORC1. AMPK can also directly inhibit mTORC1 by phosphorylating Raptor. Inhibition of mTORC1 results in mitophagy induction.

activate AMPK at Thr172 are LKB1, CaMKK, and Tak1 (*129*). These enzymes are responsive to many stimuli. LKB1's activity can increase in response to increased ROS production and Ca^{2+} elevation (*129*). CaMKK is highly sensitive to Ca^{2+} levels and is activated often in response to transient Ca^{2+} changes. The role of Tak1 in AMPK activation is still to be determined (*129*). These proteins and the pathways leading to their activation are considered the primary regulators of AMPK and its actions.

Pharmacologically, AMPK has many activators. Metformin is an AMPK agonist used in the treatment of diabetes (*148*). Recent research shows that salicylate (the origin of Aspirin®) can directly activate AMPK (*149*). In laboratory research, AICAR is used as an AMPK agonist (*150*). AICAR is cell permeable and is phosphorylated by adenosine kinase to produce ZMP, an AMP analog. ZMP is then able to bind AMPK and increase its activation and prevent its dephosphorylation. Groups have shown that repeated treatment with AICAR results in increased mitochondrial biogenesis, both in cell culture and animal models (*151*, *152*). A-769662, another AMPK agonist was identified recently. It activates AMPK through binding of the β subunit and is thought to be more specific than AICAR (*129*). Furthermore, Compound C is used experimentally as an inhibitor of AMPK (*148*). Thus, many drugs directly or indirectly activate AMPK and could prove vital for potential therapies relating to metabolic and other diseases.

4. References

1. M. W. Gray, Mitochondrial evolution, *Cold Spring Harb Perspect Biol* **4**, a011403 (2012).

2. L. Cavelier *et al.*, MtDNA mutations in maternally inherited diabetes: presence of the 3397 ND1 mutation previously associated with Alzheimer's and Parkinson's disease, *Hereditas* **135**, 65–70 (2001).

3. D. C. Wallace *et al.*, Mitochondrial DNA mutation associated with Leber's hereditary optic neuropathy, *Science* **242**, 1427–1430 (1988).

4. S. Anderson *et al.*, Sequence and organization of the human mitochondrial genome, *Nature* **290**, 457–465 (1981).

5. G. Attardi, The elucidation of the human mitochondrial genome: a historical perspective, *Bioessays* **5**, 34–39 (1986).

6. I. J. Holt, A. Reyes, Human mitochondrial DNA replication, *Cold Spring Harb Perspect Biol* **4** (2012).

7. N. Larsson, D. A. Clayton, Molecular genetic aspects of human mitochondrial disorders, *Annu. Rev. Genet.* (1995).

8. C. Kukat, N.-G. Larsson, mtDNA makes a U-turn for the mitochondrial nucleoid, *Trends Cell Biol.* (2013).

9. H. B. Ngo, J. T. Kaiser, D. C. Chan, The mitochondrial transcription and packaging factor TFAM imposes a U-turn on mitochondrial DNA, *Nat. Struct. Mol. Biol.* **18**, 1290–1296 (2011).

10. C. Kukat *et al.*, Super-resolution microscopy reveals that mammalian mitochondrial nucleoids have a uniform size and frequently contain a single copy of mtDNA, *Proceedings of the National Academy of Sciences* **108**, 13534–13539 (2011).

11. J. Nosek, L. Tomáska, H. Fukuhara, Y. Suyama, L. Kovác, Linear mitochondrial genomes: 30 years down the line, *Trends Genet.* **14**, 184–188 (1998).

12. S. Anderson *et al.*, Complete sequence of bovine mitochondrial DNA. Conserved features of the mammalian mitochondrial genome, *Journal of Molecular Biology* **156**, 683–717 (1982).

13. J. A. Korhonen, X. H. Pham, M. Pellegrini, M. Falkenberg, Reconstitution of a minimal mtDNA replisome in vitro, *EMBO J.* **23**, 2423–2429 (2004).

14. H. Tyynismaa *et al.*, Twinkle helicase is essential for mtDNA maintenance and regulates mtDNA copy number, *Human Molecular Genetics* **13**, 3219–3227 (2004).

15. E. Ylikallio, H. Tyynismaa, H. Tsutsui, T. Ide, A. Suomalainen, High mitochondrial DNA copy number has detrimental effects in mice, *Human Molecular Genetics* **19**, 2695–2705 (2010).

16. M. Falkenberg, N.-G. Larsson, C. M. Gustafsson, DNA Replication and Transcription in Mammalian Mitochondria, *Annu. Rev. Biochem.* **76**, 679–699 (2007).

17. A. K. Hyvärinen *et al.*, The mitochondrial transcription termination factor mTERF modulates replication pausing in human mitochondrial DNA, *Nucleic Acids Research* **35**, 6458–6474 (2007).

18. R. H. Willott *et al.*, Mutations in Troponin that cause HCM, DCM AND RCM: what can we learn about thin filament function? *Journal of Molecular and Cellular Cardiology* **48**, 882–892 (2010).

19. T. Yasukawa *et al.*, Replication of vertebrate mitochondrial DNA entails transient ribonucleotide incorporation throughout the lagging strand, *EMBO J.* **25**, 5358–5371 (2006).

20. A. Reyes, M. Y. Yang, M. Bowmaker, I. J. Holt, Bidirectional replication initiates at sites throughout the mitochondrial genome of birds, *J. Biol. Chem.* **280**, 3242–3250 (2005).

21. T. Yasukawa, M. Y. Yang, H. T. Jacobs, I. J. Holt, A bidirectional origin of replication maps to the major noncoding region of human mitochondrial DNA, *Molecular Cell* **18**, 651–662 (2005).

22. M. W. Walberg, D. A. Clayton, In vitro transcription of human mitochondrial DNA. Identification of specific light strand transcripts from the displacement loop region, *J. Biol. Chem.* **258**, 1268–1275 (1983).

23. M. L. Bestwick, G. S. Shadel, Accessorizing the human mitochondrial transcription machinery, *Trends Biochem. Sci.* **38**, 283–291 (2013).

24. T. E. Shutt, M. F. Lodeiro, J. Cotney, C. E. Cameron, G. S. Shadel, Core human mitochondrial transcription apparatus is a regulated two-component system in vitro, *Proceedings of the National Academy of Sciences* **107**, 12133–12138 (2010).

25. M. F. Lodeiro *et al.*, Transcription from the second heavy-strand promoter of human mtDNA is repressed by transcription factor A in vitro, *Proceedings of the National Academy of Sciences* **109**, 6513–6518 (2012).

26. J. Montoya, G. L. Gaines, G. Attardi, The pattern of transcription of the human mitochondrial rRNA genes reveals two overlapping transcription units, *Cell* **34**, 151–159 (1983).

27. G. C. Kujoth *et al.*, Mitochondrial DNA Mutations, Oxidative Stress, and Apoptosis in Mammalian Aging, *Science* **309**, 481–484 (2005).

28. M. J. Longley, D. Nguyen, T. A. Kunkel, W. C. Copeland, The fidelity of human DNA polymerase gamma with and without exonucleolytic proofreading and the p55 accessory subunit, *J. Biol. Chem.* **276**, 38555–38562 (2001).

29. L. Kazak, A. Reyes, I. J. Holt, Minimizing the damage: repair pathways keep mitochondrial DNA intact, *Nature reviews Molecular Cell Biology* **13**, 659–671 (2012).

30. N. C. de Souza-Pinto *et al.*, Repair of 8-oxodeoxyguanosine lesions in mitochondrial DNA depends on the oxoguanine DNA glycosylase (OGG1) gene and 8-oxoguanine accumulates in the mitochondrial DNA of OGG1-defective mice, *Cancer Res.* **61**, 5378–5381 (2001).

31. K. G. Pinz, S. Shibutani, D. F. Bogenhagen, Action of mitochondrial DNA polymerase gamma at sites of base loss or oxidative damage, *J. Biol. Chem.* **270**, 9202–9206 (1995).

32. P. A. Mason, E. C. Matheson, A. G. Hall, R. N. Lightowlers, Mismatch repair activity in mammalian mitochondria, *Nucleic Acids Research* **31**, 1052–1058 (2003).

33. W. Fan *et al.*, A mouse model of mitochondrial disease reveals germline selection against severe mtDNA mutations, *Science* **319**, 958–962 (2008).

34. G. van Loo *et al.*, Endonuclease G: a mitochondrial protein released in apoptosis and involved in caspase-independent DNA degradation, *Cell Death Differ* **8**, 1136–1142 (2001).

35. A. Santel, M. T. Fuller, Control of mitochondrial morphology by a human mitofusin, *Journal of Cell Science* **114**, 867–874 (2001).

36. Y. Eura, N. Ishihara, S. Yokota, K. Mihara, Two mitofusin proteins, mammalian homologues of FZO, with distinct functions are both required for mitochondrial fusion, *J. Biochem.* **134**, 333–344 (2003).

37. H. Chen *et al.*, Mitochondrial fusion is required for mtDNA stability in skeletal muscle and tolerance of mtDNA mutations, *Cell* **141**, 280–289 (2010).

38. S. Vielhaber *et al.*, Mitofusin 2 mutations affect mitochondrial function by mitochondrial DNA depletion, *Acta Neuropathol* **125**, 245–256 (2013).

39. E. Sarzi *et al.*, Mitochondrial DNA depletion is a prevalent cause of multiple respiratory chain deficiency in childhood, *J. Pediatr.* **150**, 531–4, 534.e1–6 (2007).

40. S. E. Durham, E. Bonilla, D. C. Samuels, S. DiMauro, P. F. Chinnery, Mitochondrial DNA copy number threshold in mtDNA depletion myopathy, *Neurology* **65**, 453–455 (2005).

41. P. Desjardins, E. Frost, R. Morais, Ethidium bromide-induced loss of mitochondrial DNA from primary chicken embryo fibroblasts, *Molecular and Cellular Biology* (1985).

42. M. M. NASS, Differential effects of ethidium bromide on mitochondrial and nuclear DNA synthesis in vivo in cultured mammalian cells, *Experimental Cell Research* **72**, 211–222 (1972).

43. M. P. King, G. Attardi, Human cells lacking mtDNA: repopulation with exogenous mitochondria by complementation, *Science* **246**, 500–503 (1989).

44. K. Inoue *et al.*, Isolation of mitochondrial DNA-less mouse cell lines and their application for trapping mouse synaptosomal mitochondrial DNA with deletion mutations, *J. Biol. Chem.* **272**, 15510–15515 (1997).

45. A.-M. Joseph, A. A. Rungi, B. H. Robinson, D. A. Hood, Compensatory responses of protein import and transcription factor expression in mitochondrial DNA defects, *Am. J. Physiol., Cell Physiol.* **286**, C867–75 (2004).

46. W. C. Copeland, Defects in mitochondrial DNA replication and human disease, *Crit. Rev. Biochem. Mol. Biol.* **47**, 64–74 (2012).

47. N. G. Larsson *et al.*, Mitochondrial transcription factor A is necessary for mtDNA maintenance and embryogenesis in mice, *Nat. Genet.* **18**, 231–236 (1998).

48. D. Milenkovic *et al.*, TWINKLE is an essential mitochondrial helicase required for synthesis of nascent D-loop strands and complete mtDNA replication, *Human Molecular Genetics* **22**, 1983–1993 (2013).

49. N. Hance, M. I. Ekstrand, A. Trifunovic, Mitochondrial DNA polymerase gamma is essential for mammalian embryogenesis, *Human Molecular Genetics* **14**, 1775–1783 (2005).

50. M. M. Humble *et al.*, Polg2 is essential for mammalian embryogenesis and is required for mtDNA maintenance, *Human Molecular Genetics* **22**, 1017–1025 (2013).

51. M. I. Ekstrand *et al.*, Mitochondrial transcription factor A regulates mtDNA copy number in mammals, *Human Molecular Genetics* **13**, 935–944 (2004).

52. M. D. Metodiev *et al.*, Methylation of 12S rRNA is necessary for in vivo stability of the small subunit of the mammalian mitochondrial ribosome, *Cell Metabolism* **9**, 386–397 (2009).

53. D. Skladal, J. Halliday, D. R. Thorburn, Minimum birth prevalence of mitochondrial respiratory chain disorders in children, *Brain* **126**, 1905–1912 (2003).

54. H. R. Elliott, D. C. Samuels, J. A. Eden, C. L. Relton, P. F. Chinnery, Pathogenic mitochondrial DNA mutations are common in the general population, *Am. J. Hum. Genet.* **83**, 254–260 (2008).

55. R. H. Haas *et al.*, The in-depth evaluation of suspected mitochondrial disease, *Molecular Genetics and Metabolism* **94**, 16–37 (2008).

56. D. R. Thorburn, Mitochondrial disorders: prevalence, myths and advances, *J Inherit Metab Dis* **27**, 349–362 (2004).

57. J. N. Spelbrink *et al.*, Human mitochondrial DNA deletions associated with mutations in the gene encoding Twinkle, a phage T7 gene 4-like protein localized in mitochondria, *Nat. Genet.* **28**, 223–231 (2001).

58. G. C. Brown, V. Borutaite, There is no evidence that mitochondria are the main source of reactive oxygen species in mammalian cells, *Mitochondrion* **12**, 1–4 (2012).

59. C. Richter, J. W. Park, B. N. Ames, Normal oxidative damage to mitochondrial and nuclear DNA is extensive, *Proc. Natl. Acad. Sci. U.S.A.* **85**, 6465–6467 (1988).

60. A. Trifunovic, Mitochondrial DNA and ageing, *Biochim. Biophys. Acta* **1757**, 611–617 (2006).

61. I. J. Holt, A. E. Harding, J. A. Morgan-Hughes, Deletions of muscle mitochondrial DNA in patients with mitochondrial myopathies, *Nature* **331**, 717–719 (1988).

62. R. W. Taylor, D. M. Turnbull, Mitochondrial DNA mutations in human disease, *Nat Rev Genet* **6**, 389–402 (2005).

63. E. A. Schon, E. Bonilla, S. DiMauro, Mitochondrial DNA mutations and pathogenesis, *J. Bioenerg. Biomembr.* **29**, 131–149 (1997).

64. S. Srivastava *et al.*, PGC-1alpha/beta induced expression partially compensates for respiratory chain defects in cells from patients with mitochondrial disorders, *Human Molecular Genetics* **18**, 1805–1812 (2009).

65. T. Wenz, F. Diaz, B. M. Spiegelman, C. T. Moraes, Activation of the PPAR/PGC-1α Pathway Prevents a Bioenergetic Deficit and Effectively Improves a Mitochondrial Myopathy Phenotype, *Cell Metabolism* **8**, 249–256 (2008).

66. C. Viscomi *et al.*, In vivo correction of COX deficiency by activation of the AMPK/PGC-1α axis, *Cell Metabolism* **14**, 80–90 (2011).

67. A. Golubitzky *et al.*, O. S. Shirihai, Ed. Screening for Active Small Molecules in Mitochondrial Complex I Deficient Patient's Fibroblasts, Reveals AICAR as the Most Beneficial Compound, *PLoS ONE* **6**, e26883 (2011).

68. O. A. Kolesnikova *et al.*, Nuclear DNA-encoded tRNAs targeted into mitochondria can rescue a mitochondrial DNA mutation associated with the MERRF syndrome in cultured human cells, *Human Molecular Genetics* **13**, 2519–2534 (2004).

69. G. Wang *et al.*, Correcting human mitochondrial mutations with targeted RNA import, *Proceedings of the National Academy of Sciences* **109**, 4840–4845 (2012).

70. A. Safdar *et al.*, Endurance exercise rescues progeroid aging and induces systemic mitochondrial rejuvenation in mtDNA mutator mice, *Proceedings of the National Academy of Sciences* **108**, 4135–4140 (2011).

71. G. Pfeffer, K. Majamaa, D. M. Turnbull, D. Thorburn, P. F. Chinnery, Treatment for mitochondrial disorders, *Cochrane Database Syst Rev* **4**, CD004426 (2012).

72. M. A. Tarnopolsky, B. D. Roy, J. R. MacDonald, A randomized, controlled trial of creatine monohydrate in patients with mitochondrial cytopathies, *Muscle Nerve* **20**, 1502–1509 (1997).

73. T. Klopstock *et al.*, A placebo-controlled crossover trial of creatine in mitochondrial diseases, *Neurology* **55**, 1748–1751 (2000).

74. C. Kornblum *et al.*, Creatine has no beneficial effect on skeletal muscle energy metabolism in patients with single mitochondrial DNA deletions: a placebo-controlled, double-blind 31P-MRS crossover study, *Eur. J. Neurol.* **12**, 300–309 (2005).

75. M. C. Rodriguez *et al.*, Beneficial effects of creatine, CoQ10, and lipoic acid in mitochondrial disorders, *Muscle Nerve* **35**, 235–242 (2007).

76. N. De Stefano *et al.*, Short-term dichloroacetate treatment improves indices of cerebral metabolism in patients with mitochondrial disorders, *Neurology* **45**, 1193–1198 (1995).

77. J. Vissing, U. Gansted, B. R. Quistorff, Exercise intolerance in mitochondrial myopathy is not related to lactic acidosis, *Ann Neurol.* **49**, 672–676 (2001).

78. G. E. Duncan, L. A. Perkins, D. W. Theriaque, R. E. Neiberger, P. W. Stacpoole, Dichloroacetate therapy attenuates the blood lactate response to submaximal exercise in patients with defects in mitochondrial energy metabolism, *J. Clin. Endocrinol. Metab.* **89**, 1733–1738 (2004).

79. P. Kaufmann *et al.*, Dichloroacetate causes toxic neuropathy in MELAS: A randomized, controlled clinical trial, *Neurology* **66**, 324–330 (2006).

80. P. W. Stacpoole *et al.*, Controlled clinical trial of dichloroacetate for treatment of congenital lactic acidosis in children, *Pediatrics* **117**, 1519–1531 (2006).

81. J.-M. Liet *et al.*, The effect of short-term dimethylglycine treatment on oxygen consumption in cytochrome oxidase deficiency: a double-blind randomized crossover clinical trial, *J. Pediatr.* **142**, 62–66 (2003).

82. M. Mancuso *et al.*, Oxidative stress biomarkers in mitochondrial myopathies, basally and after cysteine donor supplementation, *J. Neurol.* **257**, 774–781 (2010).

83. P. Cejudo *et al.*, Exercise training in mitochondrial myopathy: A randomized controlled trial, *Muscle Nerve* **32**, 342–350 (2005).

84. T. Taivassalo *et al.*, Endurance training and detraining in mitochondrial myopathies due to single large-scale mtDNA deletions, *Brain* **129**, 3391–3401 (2006).

85. P. J. Adhihetty, T. Taivassalo, R. G. Haller, D. R. Walkinshaw, D. A. Hood, The effect of training on the expression of mitochondrial biogenesis- and apoptosis-related proteins in skeletal muscle of patients with mtDNA defects, *AJP: Endocrinology and Metabolism* **293**, E672–E680 (2007).

86. H. Otera, N. Ishihara, K. Mihara, New insights into the function and regulation of mitochondrial fission, *Biochim. Biophys. Acta* **1833**, 1256–1268 (2013).

87. C. Osman, D. R. Voelker, T. Langer, Making heads or tails of phospholipids in mitochondria, *The Journal of Cell Biology* **192**, 7–16 (2011).

88. G. Daum, Lipids of mitochondria, *Biochim. Biophys. Acta* **822**, 1–42 (1985).

89. S. Bione *et al.*, A novel X-linked gene, G4.5. is responsible for Barth syndrome, *Nat. Genet.* **12**, 385–389 (1996).

90. P. G. Barth *et al.*, An X-linked mitochondrial disease affecting cardiac muscle, skeletal muscle and neutrophil leucocytes, *J. Neurol. Sci.* **62**, 327–355 (1983).

91. K. Shinzawa-Itoh *et al.*, Structures and physiological roles of 13 integral lipids of bovine heart cytochrome c oxidase, *EMBO J.* **26**, 1713–1725 (2007).

92. B. Gomez, N. C. Robinson, Phospholipase digestion of bound cardiolipin reversibly inactivates bovine cytochrome bc1, *Biochemistry* **38**, 9031–9038 (1999).

93. S.-Y. Choi *et al.*, Cardiolipin deficiency releases cytochrome c from the inner mitochondrial membrane and accelerates stimuli-elicited apoptosis, *Cell Death Differ* **14**, 597–606 (2007).

94. F. Sinibaldi *et al.*, Insights into cytochrome c-cardiolipin interaction. Role played by ionic strength, *Biochemistry* **47**, 6928–6935 (2008).

95. S. E. Calvo, V. K. Mootha, The mitochondrial proteome and human disease, *Annu Rev Genomics Hum Genet* **11**, 25–44 (2010).

96. T. Ono, K. Isobe, K. Nakada, J. I. Hayashi, Human cells are protected from mitochondrial dysfunction by complementation of DNA products in fused mitochondria, *Nat. Genet.* **28**, 272–275 (2001).

97. J. Lin, C. Handschin, B. M. Spiegelman, Metabolic control through the PGC-1 family of transcription coactivators, *Cell Metabolism* **1**, 361–370 (2005).

98. P. J. Adhihetty *et al.*, The role of PGC-1 on mitochondrial function and apoptotic susceptibility in muscle, *AJP: Cell Physiology* **297**, C217–C225 (2009).

99. J. Lin, P. Puigserver, J. Donovan, P. Tarr, B. M. Spiegelman, Peroxisome proliferator-activated receptor gamma coactivator 1beta (PGC-1beta), a novel PGC-1-related transcription coactivator associated with host cell factor, *J. Biol. Chem.* **277**, 1645–1648 (2002).

100. U. Andersson, R. C. Scarpulla, Pgc-1-related coactivator, a novel, serum-inducible coactivator of nuclear respiratory factor 1-dependent transcription in mammalian cells, *Molecular and Cellular Biology* **21**, 3738–3749 (2001).

101. B. Kulawiak *et al.*, The mitochondrial protein import machinery has multiple connections to the respiratory chain, *Biochim. Biophys. Acta* **1827**, 612–626 (2013).

102. M. G. Claros, P. Vincens, Computational method to predict mitochondrially imported proteins and their targeting sequences, *Eur. J. Biochem.* **241**, 779–786 (1996).

103. J. O. Holloszy, Biochemical adaptations in muscle. Effects of exercise on mitochondrial oxygen uptake and respiratory enzyme activity in skeletal muscle, *J. Biol. Chem.* **242**, 2278–2282 (1967).

104. B. Lu *et al.*, Phosphorylation of human TFAM in mitochondria impairs DNA binding and promotes degradation by the AAA+ Lon protease, *Molecular Cell* **49**, 121–132 (2013).

105. D. A. Bota, K. J. A. Davies, Lon protease preferentially degrades oxidized mitochondrial aconitase by an ATP-stimulated mechanism, *Nature Cell Biology* **4**, 674–680 (2002).

106. S. M. Jin *et al.*, Mitochondrial membrane potential regulates PINK1 import and proteolytic destabilization by PARL, *The Journal of Cell Biology* **191**, 933–942 (2010).

107. D. P. Narendra *et al.*, D. R. Green, Ed. PINK1 Is Selectively Stabilized on Impaired Mitochondria to Activate Parkin, *PLoS Biol* **8**, e1000298 (2010).

108. D. Finley, Recognition and Processing of Ubiquitin-Protein Conjugates by the Proteasome, *Annu. Rev. Biochem.* **78**, 477–513 (2009).

109. M. J. Baker, T. Tatsuta, T. Langer, Quality control of mitochondrial proteostasis, *Cold Spring Harb Perspect Biol* **3** (2011).

110. A. Tanaka *et al.*, Proteasome and p97 mediate mitophagy and degradation of mitofusins induced by Parkin, *The Journal of Cell Biology* **191**, 1367–1380 (2010).

111. E. Masiero *et al.*, Autophagy Is Required to Maintain Muscle Mass, *Cell Metabolism* **10**, 507–515 (2009).

112. B. Ravikumar *et al.*, Regulation of Mammalian Autophagy in Physiology and Pathophysiology, *Physiological Reviews* **90**, 1383–1435 (2010).

113. C. He *et al.*, Exercise-induced BCL2-regulated autophagy is required for muscle glucose homeostasis, *Nature* **481**, 511–515 (2012).

114. J. Kim, M. Kundu, B. Viollet, K.-L. Guan, AMPK and mTOR regulate autophagy through direct phosphorylation of Ulk1, *Nature Cell Biology* **13**, 132–141 (2011).

115. J. W. Lee, S. Park, Y. Takahashi, H.-G. Wang, The association of AMPK with ULK1 regulates autophagy, *PLoS ONE* **5**, e15394 (2010).

116. D. F. Egan *et al.*, Phosphorylation of ULK1 (hATG1) by AMP-activated protein kinase connects energy sensing to mitophagy, *Science* **331**, 456–461 (2011).

117. S. Alers, A. S. Löffler, S. Wesselborg, B. Stork, Role of AMPK-mTOR-Ulk1/2 in the regulation of autophagy: cross talk, shortcuts, and feedbacks, *Molecular and Cellular Biology* **32**, 2–11 (2012).

118. R. Scherz-Shouval *et al.*, Reactive oxygen species are essential for autophagy and specifically regulate the activity of Atg4, *EMBO J.* **26**, 1749–1760 (2007).

119. J. Zhang *et al.*, Mitochondrial clearance is regulated by Atg7-dependent and -independent mechanisms during reticulocyte maturation, *Blood* **114**, 157–164 (2009).

120. J. J. Wu *et al.*, Mitochondrial dysfunction and oxidative stress mediate the physiological impairment induced by the disruption of autophagy, *Aging (Albany NY)* **1**, 425–437 (2009).

121. G. Twig *et al.*, Fission and selective fusion govern mitochondrial segregation and elimination by autophagy, *EMBO J.* **27**, 433–446 (2008).

122. D. Narendra, A. Tanaka, D. F. Suen, R. J. Youle, Parkin is recruited selectively to impaired mitochondria and promotes their autophagy, *The Journal of Cell Biology* **183**, 795–803 (2008).

123. W.-X. Ding, X.-M. Yin, Mitophagy: mechanisms, pathophysiological roles, and analysis, *Biological Chemistry* **393**, 547–564 (2012).

124. W. X. Ding *et al.*, Nix Is Critical to Two Distinct Phases of Mitophagy, Reactive Oxygen Species-mediated Autophagy Induction and Parkin-Ubiquitin-p62-mediated Mitochondrial Priming, *Journal of Biological Chemistry* **285**, 27879–27890 (2010).

125. G. Bellot *et al.*, Hypoxia-Induced Autophagy Is Mediated through Hypoxia-Inducible Factor Induction of BNIP3 and BNIP3L via Their BH3 Domains, *Molecular and Cellular Biology* **29**, 2570–2581 (2009).

126. I. Novak *et al.*, Nix is a selective autophagy receptor for mitochondrial clearance, *EMBO Rep.* **11**, 45–51 (2010).

127. X.-D. Zhang, L. Qi, J.-C. Wu, Z.-H. Qin, DRAM1 regulates autophagy flux through lysosomes, *PLoS ONE* **8**, e63245 (2013).

128. D. J. Klionsky *et al.*, Guidelines for the use and interpretation of assays for monitoring autophagy. *Autophagy* **8**, 445–544 (2012).

129. G. R. Steinberg, B. E. Kemp, AMPK in Health and Disease, *Physiological Reviews* **89**, 1025–1078 (2009).

130. D. G. Hardie, F. A. Ross, S. A. Hawley, AMPK: a nutrient and energy sensor that maintains energy homeostasis, *Nat. Rev. Mol. Cell Biol.* **13**, 251–262 (2012).

131. T. Pang *et al.*, Conserved alpha-helix acts as autoinhibitory sequence in AMP-activated protein kinase alpha subunits, *J. Biol. Chem.* **282**, 495–506 (2007).

132. A. J. Verhoeven *et al.*, The AMP-activated protein kinase gene is highly expressed in rat skeletal muscle. Alternative splicing and tissue distribution of the mRNA, *Eur. J. Biochem.* **228**, 236–243 (1995).

133. S. P. Davies, D. Carling, D. G. Hardie, Tissue distribution of the AMP-activated protein kinase, and lack of activation by cyclic-AMP-dependent protein kinase, studied using a specific and sensitive peptide assay, *Eur. J. Biochem.* **186**, 123–128 (1989).

134. D. Stapleton *et al.*, Mammalian AMP-activated protein kinase subfamily, *J. Biol. Chem.* **271**, 611–614 (1996).

135. C. Thornton, M. A. Snowden, D. Carling, Identification of a novel AMP-activated protein kinase beta subunit isoform that is highly expressed in skeletal muscle, *J. Biol. Chem.* **273**, 12443–12450 (1998).

136. Z. Chen *et al.*, Expression of the AMP-activated protein kinase beta1 and beta2 subunits in skeletal muscle, *FEBS Letters* **460**, 343–348 (1999).

137. P. C. Cheung, I. P. Salt, S. P. Davies, D. G. Hardie, D. Carling, Characterization of AMP-activated protein kinase gamma-subunit isoforms and their role in AMP binding, *Biochem. J.* **346 Pt 3**, 659–669 (2000).

138. H. Yu, N. Fujii, M. F. Hirshman, J. M. Pomerleau, L. J. Goodyear, Cloning and characterization of mouse 5'-AMP-activated protein kinase gamma3 subunit, *Am. J. Physiol., Cell Physiol.* **286**, C283–92 (2004).

139. M. Mahlapuu *et al.*, Expression profiling of the gamma-subunit isoforms of AMP-activated protein kinase suggests a major role for gamma3 in white skeletal muscle, *Am. J. Physiol. Endocrinol. Metab.* **286**, E194–200 (2004).

140. C. U. Niesler, K. H. Myburgh, F. Moore, The changing AMPK expression profile in differentiating mouse skeletal muscle myoblast cells helps confer increasing resistance to apoptosis, *Exp. Physiol.* **92**, 207–217 (2007).

141. H. M. O'Neill *et al.*, AMP-activated protein kinase (AMPK) beta1beta2 muscle null mice reveal an essential role for AMPK in maintaining mitochondrial content and glucose uptake during exercise, *Proceedings of the National Academy of Sciences* **108**, 16092–16097 (2011).

142. S. Jäger, C. Handschin, J. St-Pierre, B. M. Spiegelman, AMP-activated protein kinase (AMPK) action in skeletal muscle via direct phosphorylation of PGC-1alpha, *Proc. Natl. Acad. Sci. U.S.A.* **104**, 12017–12022 (2007).

143. I. Irrcher, V. Ljubicic, A. F. Kirwan, D. A. Hood, AMP-activated protein kinase-regulated activation of the PGC-1alpha promoter in skeletal muscle cells, *PLoS ONE* **3**, e3614 (2008).

144. C. Cantó *et al.*, Interdependence of AMPK and SIRT1 for metabolic adaptation to fasting and exercise in skeletal muscle, *Cell Metabolism* **11**, 213–219 (2010).

145. D. M. Gwinn *et al.*, AMPK phosphorylation of raptor mediates a metabolic checkpoint, *Molecular Cell* **30**, 214–226 (2008).

146. K. Inoki, T. Zhu, K.-L. Guan, TSC2 mediates cellular energy response to control cell growth and survival, *Cell* **115**, 577–590 (2003).

147. D. G. Hardie, R. W. Mackintosh, AMP-activated protein kinase - An archetypal protein kinase cascade? *Bioessays* **14**, 699–704 (1992).

148. G. Zhou *et al.*, Role of AMP-activated protein kinase in mechanism of metformin action, *Journal of Clinical Investigation* **108**, 1167–1174 (2001).

149. S. A. Hawley *et al.*, The ancient drug salicylate directly activates AMP-activated protein kinase, *Science* **336**, 918–922 (2012).

150. J. M. Corton, J. G. Gillespie, S. A. Hawley, D. G. Hardie, 5-aminoimidazole-4-carboxamide ribonucleoside. A specific method for activating AMP-activated protein kinase in intact cells? *Eur. J. Biochem.* **229**, 558–565 (1995).

151. A. D. Dam, A. S. Mitchell, J. Quadrilatero, Induction of mitochondrial biogenesis protects against caspase-dependent and caspase-independent apoptosis in L6 myoblasts, *Biochim. Biophys. Acta* (2013).

152. W. W. Winder *et al.*, Activation of AMP-activated protein kinase increases mitochondrial enzymes in skeletal muscle, *J. Appl. Physiol.* **88**, 2219–2226 (2000).

The Effects of AICAR Treatment During mtDNA Recovery in ρ⁻ C2C12 Cells

Alex E. Green and David A. Hood

Muscle Health Research Centre, School of Kinesiology and Health Science

York University, Toronto, Ontario, M3J 1P3, Canada

Keywords: C2C12, mitochondrial DNA, mitochondrial disease, AMPK, AICAR

Running title: AICAR and mtDNA Depletion

Address for correspondence:

Dr. David A Hood
School of Kinesiology and Health Science
York University, Toronto, ON
M3J 1P3, Canada
Tel: (416) 736-2100 ext. 66640
Fax: (416) 736-5698
Email: dhood@yorku.ca

Abstract

Mitochondria are the primary site of cellular energy production. The structure and function of mitochondria requires both the nuclear and the maternally-inherited mitochondrial genome. There are multiple copies of mitochondrial DNA (mtDNA) per cell and each mtDNA molecule contains the required information to produce 13 essential electron transport chain (ETC) proteins. When mtDNA is depleted, this results in mitochondrial DNA depletion syndrome (MDS). This is characterized by a decrease in ETC activity. It particularly affects cell types that depend on oxidative phosphorylation for energy production, such as skeletal muscle, heart and brain. AMP-activated protein kinase (AMPK) is an enzyme that can initiate mitochondrial biogenesis and mitophagy. We hypothesized that treating cells harbouring low numbers of mtDNA with an AMPK activator (5-Aminoimidazole-4-carboxamide ribonucleoside; AICAR) would ameliorate the mitochondrial dysfunction and improve mtDNA copy number. We developed murine myoblasts (C2C12 cells) with low levels of mtDNA by chronic treatment with ethidium bromide. We treated selected clones for 24 hours with 1 mM AICAR to activate AMPK. AICAR treatment decreased markers of mitochondrial biogenesis, mitochondrial function (e.g. maximal cellular respiration), and mitochondrial degradation. Furthermore, AICAR increased ROS production in the most depleted cells. We conclude that the activation of AMPK may have increased mitochondrial retrograde signaling to trigger nuclear compensatory adaptations leading to changes in the cellular phenotype toward ATP conservation, in the presence of mitochondrial dysfunction.

Introduction

Mitochondrial disorders are devastating diseases that affect cellular energy production and cause chronic morbidity. They originate from mutations in nuclear (nDNA) or mitochondrial DNA (mtDNA) genes that encode products essential for mitochondrial function and the maintenance of mtDNA. Because multiple copies of mtDNA exist and are randomly distributed during mitosis, symptoms of mitochondrial disease vary widely between patients and even between tissues within one patient. Hence, diagnosing the underlying disease is difficult and there is no cure. A partial or complete loss of mtDNA is termed mtDNA depletion syndrome (MDS). MDS is associated with at least 18% of respiratory chain deficiencies in childhood (*1*). Diseases from pathogenic mtDNA mutations have a diagnosed prevalence of 1 in 7,600 (*2*), but a minimum of 1 in 200 live births harbour pathogenic mtDNA mutations (*3*). Treatments generally consist of nutritional supplementation and attending to secondary symptoms that include ataxia, diabetes mellitus, and exercise intolerance. In these diseases, there is an accumulation of dysfunctional mitochondria and, consequently, a deficit in energy production. Theoretically, many resolutions exist, such as: 1) increasing the amount of mitochondria to a level that can sustain the energy demands of the cell, despite the dysfunctional nature of those mitochondria, 2) increasing the functional capacity of each mitochondrion, 3) reducing the number of dysfunctional mitochondria, or 4) a combination of 1, 2 or 3.

AMPK is a nutrient-sensing kinase that can phosphorylate PGC-1α (*4*) - the master regulator of mitochondrial biogenesis, and inactivate mTORC1 (*5*) - the major negative

regulator of autophagy. Thus, active AMPK both increases mitochondrial content by activating PGC-1α, and stimulates the degradation of malfunctioning organelles by inhibiting mTORC1. AMPK is triggered by metabolic stress, including exercise, but can also be stimulated pharmacologically by AICAR (5-Aminoimidazole-4-carboxamide ribonucleoside; *6*, *7*). Previous studies have investigated the triggering of the PGC-1α–AMPK pathway to treat mitochondrial disease. Viscomi et al. (*8*) demonstrated improved mitochondrial content and function when breeding mice deficient in a cytochrome c oxidase activity (COX) assembly factor (S*urf1*) with *PGC-1α* overexpressing animals. They also showed an improvement in the COX deficiency of mice not expressing *Surf1* or *Cox15* (another COX assembly factor) when treated with AICAR, and a similar improvement in mice expressing a mutant COX assembly factor (*Sco2*). Another group has identified AICAR as the most beneficial compound for improving mitochondrial function in cells with mutations in nuclear genes encoding electron transport chain (ETC) subunits (*9*, *10*). However, no research has demonstrated the use of AICAR to increase mitochondrial biogenesis, induce mitophagy or improve cellular function in cells without sufficient amounts of mtDNA.

The purpose of this study was to investigate the use of AMPK activation as a potential activator of mitophagy and therapy for treatment of mitochondrial disease. We hypothesized that activating AMPK would increase mitochondrial content and concurrently increase the quality of the mitochondrial pool by stimulating the degradation of dysfunctional organelles.

Methods

Cell Lines *– ρ^- Cell Generation:* Muscle is a highly metabolic tissue that is very reliant on mitochondria for ATP production. Thus, muscle is particularly affected by mitochondrial disease. We chose to use C2C12 murine myoblasts treated with ethidium bromide (EtBr) as a model of mtDNA depletion. C2C12 derived ρ^- cells were generated as previously described by our group (*11*). Briefly, murine myoblasts (C2C12, ATCC, Manassas, VA) were cultivated in DMEM medium containing 4.5 g/L glucose and 2 mM L-glutamine (Wisent, St-Bruno, QC, Canada), supplemented with 100 ng/mL EtBr, 50 μg/mL uridine, 1 mM sodium pyruvate, 10% fetal bovine serum (Thermo-Scientific, Waltham, MA), and 1% penicillin-streptomycin (Invitrogen, Carlsbad, CA). The medium was refreshed every day and cells were sub-cultured every 1 - 2 days for 6 weeks. Colony selection was performed by seeding cells at a concentration of ~4.5 cells/cm^2 and removing individual colonies using cloning cylinders. Colonies were grown for an additional 3 weeks in the presence of EtBr. DNA extracts were collected to assess mtDNA depletion. Clones containing 34% (moderate; MOD) and 13% (LOW) of control mtDNA levels were stocked. A subset of cells was selected to confirm that mtDNA remained depleted after stocking (Fig. 1B).

AICAR Treatment – For each experiment, a new stock of frozen cells was used. Cells were seeded and allowed to adhere for 24 hours before treatment. Because EtBr inhibits mitochondrial RNA and DNA synthesis (*12-15*), one hour before treatment with AICAR, cells were washed 3 times with complete medium to remove EtBr. Cells were

then either treated for 24 hours with 1 mM AICAR (Toronto Research Chemicals, Toronto, Ontario), or left untreated.

mtDNA to nDNA Quantification – To assess the mtDNA to nuclear DNA (nDNA) ratio, genomic DNA (gDNA) was isolated using a standard kit (Mammalian Genomic DNA Miniprep, Sigma-Aldrich, St. Louis, MS). A spectrophotometer was used to quantify the amount of gDNA isolated, and 5 ng of gDNA was used as the template for amplification reactions. A StepONE Plus PCR System (Applied Biosystems Inc., Foster City, CA, USA) was used to perform quantitative PCR with SYBR® Green technology. Primers were optimized using serial dilutions and melting point dissociation curves. The following genes were amplified: the nDNA gene Pecam1 (forward primer: 5'-ATGGAAAGCCTGCCATCATG-3', reverse primer: 5'-TCCTTGTTGTTCAGCATCAC-3') and the mtDNA gene ND1 (forward primer: 5'-CCTATCACCCTTGCCATCAT-3', reverse primer: 5'-GAGGCTGTTGCTTGTGTGAC-3') as described previously (*16*).

Cell Proliferation – Cells were harvested with 0.025% trypsin with EDTA (Invitrogen). The cell suspension was collected and the trypsin was inhibited by adding an equal volume of growth medium. A 15 µL aliquot was placed onto an hæmocytometer for counting. Values were expressed as the total amount of cells harvested over the original number plated.

Enzyme Extraction and Cytochrome C Oxidase (COX) Activity – COX enzyme activity was measured as per Uguccioni and Hood (*17*). Briefly, cells were harvested,

lysed and the supernatant fraction collected. Enzyme extracts were combined with a solution of reduced equine cytochrome c and absorbance at 550 nm was monitored on a plate reader (Bio-Tek Synergy HT, Winooski, VT). Results were then corrected for total protein concentration, as assessed by the Bradford method.

mRNA Quantification – To assess mRNA transcript levels, total RNA was isolated using TRIzol® (Invitrogen) and quantified with a UV spectrophotometer (Ultrospec 2100 Pro; Biochrom, Cambridge, United Kingdom). Complementary DNA (cDNA) was created from 4 μg of total RNA with Superscript III and Oligo$(dt)_{20}$ (Invitrogen) according to the manufacturer's instructions. Quantitative PCR was performed as described above. Primers were checked for C-G content and probability of primer-dimer formation. Final primers were as follows: *Cox1* (forward primer: 5'-CTAGCCGCAGGCATTACTAT-3', reverse primer: 5'-TGCCCAAAGAATCAGAACAG-3'), *Cox4* (forward primer: 5'-CTCCAACGAATGGAAGACAG-3', reverse primer: 5'-TGACAACCTTCTTAGGGAAC-3') and *β_2-Microglobulin* (forward primer: 5'-GGTCTTTCTGGTGCTTGTCT-3', reverse primer: 5'-TATGTTCGGCTTCCCATTCT-3'). With the exception of *Cox4* (50 ng), 5 ng of cDNA was used as a template for each reaction. All values were corrected for *β_2-Microglobulin* mRNA content and analyzed using the $\Delta\Delta^{Ct}$ method.

Flow Cytometric Analysis of mtΔΨ, Mitochondrial Mass, ROS, and Lysosomal Mass – To measure mtΔΨ, cells were incubated in complete growth media containing

100 nM tetratmethylrhodamine ethyl ester (TMRE; Invitrogen) for 45 minutes at 37ºC. To assess mitochondrial mass, cells were incubated with 100 nM MitoTracker Green FM (MTGFM; Invitrogen) for 45 minutes at 37ºC. ROS generation was measured using 2',7'-dichlorodihydrofluorescein diacetate (H_2DCFDA; Sigma-Aldrich, St. Louis, MO). Cells were incubated with 100 μM H_2DCFDA for 45 minutes at 37ºC. Lysosomal mass was evaluated by staining cells with 200 nM LysoTracker Red (LTR; Invitrogen) for 45 minutes at 37ºC.

Following incubation, cells were rinsed with PBS, trypsinized, and resuspended in complete growth media containing phenol red-free DMEM (Invitrogen). Fluorescence was assessed on the FL-1 channel (MTGFM and H_2DCFDA), and the FL-2 channel (TMRE and LTR) of a FACSCalibur flow cytometer (Becton Dickinson, Franklin Lakes, NJ). Unless otherwise stated, a total of at least 25,000 gated events were collected. Analyzed data were derived from the geometric mean fluorescence and corrected for autofluorescence from an unstained sample. To ascertain a measure of membrane potential per mitochondrion, TMRE fluorescence was corrected for mitochondrial mass by dividing by MTGFM fluorescence. Furthermore, mitochondria are significant sources of ROS (*18*) and thus we also corrected H_2DCFDA fluorescence with MTGFM fluorescence. Prior to treatment, with AICAR, subsets of cells were confirmed to have lower mitochondrial mass (Supp. Fig. 1).

Protein Extraction and Western Blotting – Cells were harvested via trypsinization and resuspended in Passive Lysis Buffer (Promega, Madison, WI)

supplemented with protease and phosphatase inhibitors (10 ng/mL Leupeptin, 1 ng/mL Pepstatin A, 10 ng/mL Aprotinin, 1 mM DTT, 0.5 mM PMSF, 2.5 mM $NaVO_3$, 50 mM NaF, and 50 mM β-Glycerolphosphate). Protein was then quantified via the Bradford method.

Following denaturation and disulfide bond reduction with SDS and β-mercaptoethanol, equal amounts of protein were separated by size on SDS-PAGE gels. Protein was then transferred to a nitrocellulose membrane and stained with Ponceau S. Membranes were then probed with antibodies diluted in 5% skim milk in TBST buffer. Antibody concentrations were as follows: LC3 – 1º, 1:250 (Cell Signaling, Danvers, MA), P-AMPK – 1º, 1:1000 (Cell Signaling) and T-AMPK 1º, 1:1000 (Cell Signaling). All secondary antibodies were diluted 1:1000 (Santa-Cruz Biotechnologies, Dallas, TX). Blots were incubated in enhanced chemiluminescence luminol (Santa-Cruz Biotechnologies) and exposures were collected on photographic film.

Oxygen Consumption **–** Whole-cell oxygen consumption rate (OCR) was assessed with a 96-well plate fluorescence assay (OxoPlates, Presens, Germany). Cells were inoculated 24 hours before treatment and treated with AICAR. Media was then replaced with complete growth media containing phenol red-free DMEM and respiration of each cell line was assessed in triplicate under the following treatments: 1) Vehicle Treatment – DMSO, 2) 1 μM Oligomycin, 3) 3 μM CCCP, and 4) 2 μM Rotenone and Antimycin A, as described by Nicholls et al. (*19*). Fluorescence was assessed every 3 minutes for 3 hours on a fluorescence plate reader (Bio-Tek Synergy HT, Winooski, VT).

Rates from 60 mins to 100 mins were averaged and corrected for cell number (CyQuant Cell Proliferation Assay, Invitrogen).

Lactate Production **–** Conditioned media was removed from cell culture plates. The media was spun at 1400 RPM, the supernatant fraction collected, and flash frozen. Media was deproteinized using perchloric acid, diluted 1:5 and analyzed using a colormetric lactate assay kit (Sigma-Aldrich).

Mitophagy Assessment **–** To assess autophagic flux, cells were simultaneously treated with 10 μM Chloroquine Diphosphate (CQ, Bioshop, Burlington, Ontario) and AICAR. Flux was measured by comparing the ratio of LC3-II to LC3-I protein content between conditions with CQ.

To estimate mitophagy, cells were inoculated on to custom-made glass bottom 6-well plates. Following treatment, cells were co-incubated with MTGFM and LTR (as described above). Media was replaced with complete growth media containing phenol red-free DMEM. Cells were then photographed under an inverted fluorescent microscope (Nikon TE2000-U, Melville, NY). For each experiment, a minimum of 20 cells from each condition was assessed. Discrete punctate mitochondria superimposed on individual lysosomes were counted and expressed as a percentage of the total number of lysosomes within the cell. Co-localization suggested that mitochondria were engulfed in lysosomes, and were undergoing mitophagy.

Statistical Analysis - All statistical analyses were completed with Graphpad Prism 5 (Graphpad, La Jolla, CA). Unless otherwise indicated, all results were analyzed

using a two-way ANOVA with Bonferonni *post-hoc* tests. Results were considered statistically significant when $P \leq 0.05$. All graph bars are means with error bars showing the S.E.M.

Results

mtDNA Content – EtBr treatment effectively reduced the mtDNA content of cell lines to 55% and 32% of control levels (Fig. 1B). We termed these cells with reduced mtDNA MOD and LOW, to indicate moderate and low levels of mtDNA, respectively. We then determined whether removing EtBr restored mtDNA levels during the subsequent 24 hours of treatment, with or without AICAR. We found that mtDNA levels were repleted back to control levels within this time frame (Fig. 1B), but that there was no additional increase in mtDNA with the provision of AICAR in the media (data not shown).

Cellular Proliferation – During the 48 hours following plating, cell number increased by 10-fold in the CON cells (Fig. 1C). In contrast, in MOD and LOW cells the rate of growth was attenuated, and increases of only 5- and 4-fold were observed, respectively. There was an overall effect of AICAR treatment, as CON, MOD and LOW cell proliferation rate were further reduced to increases of 9-, 3- and 2-fold, respectively. Thus, AICAR attenuated the growth rate of the cells.

AMPK Activation with mtDNA Depletion and AICAR Treatment – We sought to evaluate the basal activation of AMPK in MOD and LOW cell lines, along with the effectiveness of AICAR to stimulate AMPK. We assessed activation by measuring the

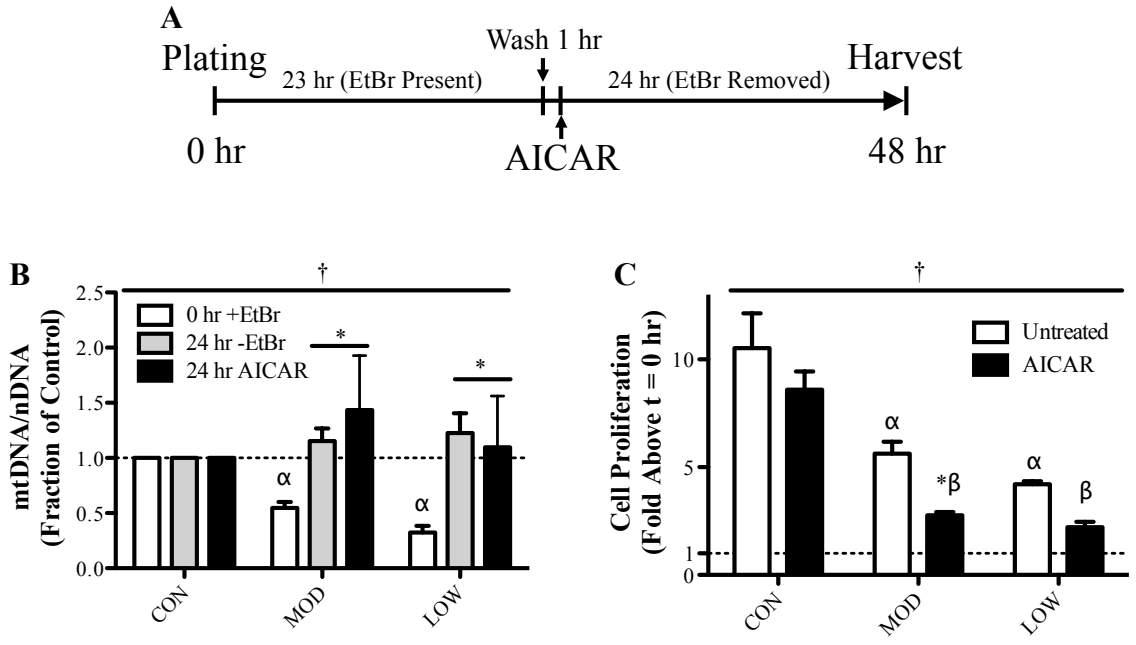

Figure 1. *Treatment plan, mtDNA content after EtBr removal and cell yield following treatment.* **A)** Cells were plated and treated as described in the methods. Treatment with AICAR occurred 24 hours prior to harvest, after EtBr had been removed. **B)** Relative quantities of mtDNA and nDNA were assessed. At 0 hours, MOD and LOW had less mtDNA than CON, but after removal of EtBr for 24 hours, mtDNA was restored to control levels. We observed no additional effect of AICAR. mtDNA/nDNA was assessed 24 hours before treatment and 24 hours after removal of EtBr (†, $P<0.01$, main effect of time and interaction effect; α, $P<0.05$ vs. 0 hour control; *, $P<0.05$ vs. matched untreated; N = 3-6 different cell stocks and experiments); **C)** Cells were counted following treatment (48 hours) and divided by the number of cells inoculated at 0 hours. AICAR and mtDNA depletion both decreased cell proliferation rate. (†, $P<0.0001$ main effect of prior depletion and $P<0.01$ main effect of treatment; α, $P<0.001$ vs. untreated CON; β, $P<0.001$ vs. AICAR treated CON; * $P<0.05$ vs. matched untreated; N = 7 experiments). Values are mean ± S.E.M.

levels of phosphorylated Thr172 on AMPK relative to the total amount of AMPK. AMPK phosphorylation was inversely related to the level of mtDNA observed during the depletion phase (Fig. 2). AICAR treatment caused an overall additional increase in the level of phosphorylated AMPK, and a concomitant augmentation in the expression of AMPK, except in control cells. Consequently, the ratio of phosphorylated to total AMPK remained unchanged (Supp. Fig. 2A and B).

Mitochondrial Content and COX Enzyme **–** To elucidate any changes in mitochondrial content with prior mtDNA depletion and AICAR treatment, we measured both mitochondrial mass and COX activity. A main effect of prior mtDNA depletion on mitochondrial mass was evident, but post-hoc analysis revealed that this was a result of the significant decline produced by AICAR treatment. No significant effect of mtDNA depletion in untreated cells was observed (Fig. 3A). COX activity was more dramatically reduced with prior mtDNA depletion, by 60% and 80% in MOD and LOW cells, respectively (Fig. 3B). Thus, the restoration of COX enzyme activity lagged behind that of mtDNA during the 24-hour repletion phase. AICAR was not effective in preventing this decline in MOD or LOW cells (Fig. 3B). Indeed, AICAR further decreased COX activity in all cell lines. The use of a longer AICAR treatment time (i.e. 72 hours) did not result in any further increase in COX activity, even in CON cells (Supp. Fig. 3).

To determine the possible reasons for the decline in COX activity, we assayed both the mtDNA-encoded *Cox1* mRNA transcript, and as well as the nuclear-encoded mRNA transcript *Cox4.* These represent subunits of the COX holoenzyme. In contrast to

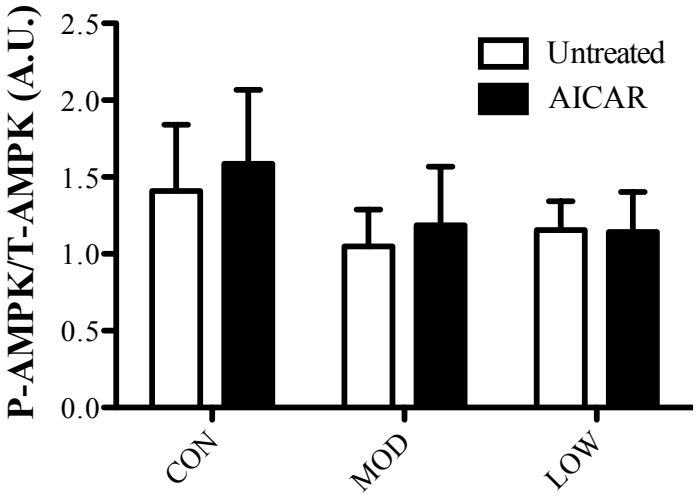

Figure 2. *Ratio of phosphorylated AMPK to total AMPK.* After 24 hours there was no increase in the ratio of phosphorylated AMPK to total AMPK (N = 7). Values are mean ± S.E.M.

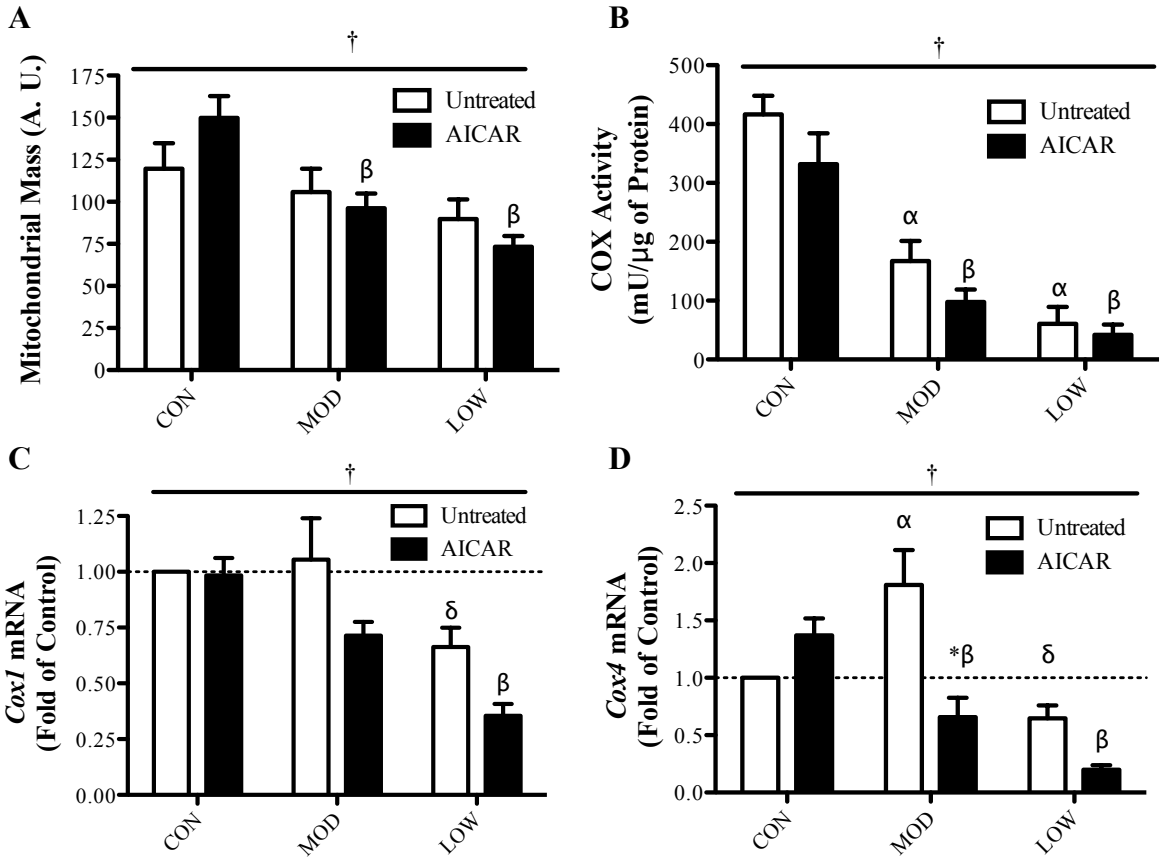

Figure 3. *Measures of mitochondrial content and COX subunit mRNA transcript expression.* **A)** Mitochondrial mass as assessed by MitoTracker Green FM staining and flow cytometry (†, P<0.001 main effect of prior depletion; β, P<0.01 vs. AICAR treated CON; N = 7 assays of ≥ 25,000 gated events); **B)** COX activity (†, P<0.0001 main effect of prior depletion and P<0.05 main effect of treatment; α, P<0.001 vs. untreated CON; β, P<0.001 vs. AICAR treated CON; N = 7 experiments); **C)** *Cox1* mRNA levels (†, P<0.05 main effect of treatment and P<0.001 main effect of prior depletion ; β, P<0.01 vs. AICAR treated CON; δ, P<0.05 vs. untreated MOD; N = 7 experiments); **D)** *Cox4* mRNA levels (†, P<0.01 main effect of treatment, P<0.0001 main effect of prior depletion, and P<0.001 interaction effect; α, P<0.001 vs. untreated CON; β, P<0.01 vs. AICAR treated CON; δ, P<0.001 vs. untreated MOD; * P<0.05 vs. matched untreated; N = 8 experiments). Values are mean ± S.E.M.

COX activity, *Cox1* mRNA was not decreased with prior mtDNA depletion in the MOD cells, but was reduced by 34% in LOW cells (Fig. 3C). AICAR treatment led to further decreases in *Cox1* mRNA, evident in MOD cells. Previously low levels of mtDNA also altered *Cox4* mRNA levels (Fig. 3D). Paradoxically, *Cox4* mRNA increased 1.8-fold in MOD cells, but decreased to 65% in LOW cells. Thus, the decline in COX activity observed in MOD cells could not be attributed to changes in *Cox1* or *Cox4* mRNA levels. Additionally, AICAR treatment did not enhance, but rather reduced *Cox4* mRNA in MOD and LOW cells to levels below those found in control cells.

Mitochondrial Membrane Potential and ROS Production – We determined the effect of prior mtDNA depletion and AICAR treatment on mitochondrial membrane potential using TMRE fluorescence. After correcting the measurements for mitochondrial mass, we found an overall reduction in membrane potential with prior mtDNA depletion, however this effect was only significant in AICAR treated cells (Fig. 4A). In addition, H_2DCFDA fluorescence was used to evaluate ROS production. ROS levels were reduced by 61% and 76% in MOD and LOW cells (Fig. 4B). The overall effect of AICAR depended on the prior level of mtDNA. In CON cells, ROS production was decreased by AICAR. In contrast, AICAR increased ROS levels in LOW cells that had the lowest prior mtDNA level.

Oxygen Consumption and Lactate Levels – ATP can be produced via mitochondrial and glycolytic pathways. To estimate the degree to which these pathways were used, along with overall mitochondrial functional capacity, we measured whole cell

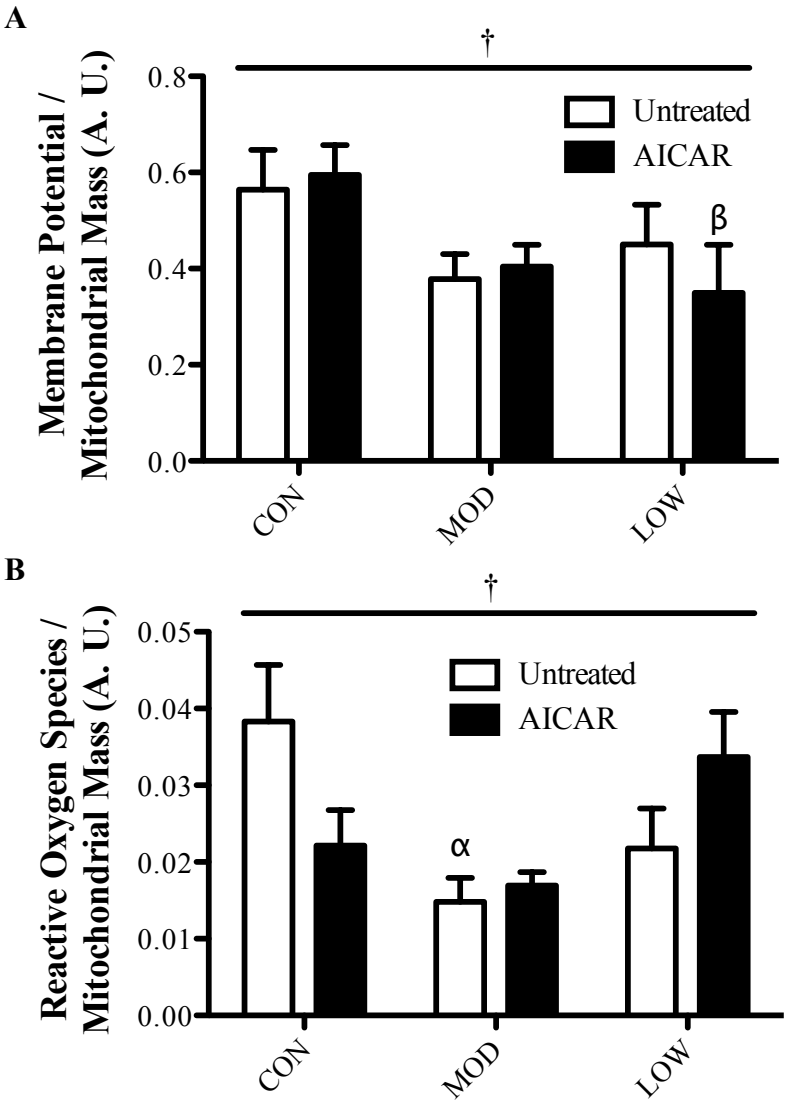

Figure 4. *Mitochondrial membrane potential and ROS production.* **A)** Mitochondrial membrane potential measured using TMRE fluorescence (†, $P<0.05$ main effect of prior depletion; β, $P<0.05$ vs. AICAR treated CON; N = 8 measurements of ≥ 25,000 gated events); **B)** Whole-cell ROS production measured using H_2DCFDA fluorescence (†, $P<0.05$ main effect of prior depletion and $P<0.05$ interaction effect; α, $P<0.01$ vs. untreated CON; N = 7-8 measurements of ≥ 25,000 gated events). Values are mean ± S.E.M.

respiration and culture medium lactate levels. Prior mtDNA depletion resulted in a progressive decline of both basal (vehicle) and maximal (CCCP) respiration in MOD and LOW cells, compared to control cells (Fig. 5A). AICAR treatment did not alter rates of respiration in either CON or LOW cells, but reduced respiration in MOD cells. We observed no differences in proton leak across the inner mitochondrial membrane, as measured by oligomycin-inhibited respiration, or in non-mitochondrial oxygen consumption following rotenone and antimycin A treatment (Supp. Fig. 5C and D). Lactate levels in the cell culture medium were low, and did not differ between CON, MOD, or LOW cell lines. However, lactate release increased significantly by 2-3 fold in the presence of AICAR, particularly in the CON and MOD cells (Fig. 5B).

Mitophagy – To estimate the degree of mitochondrial degradation produced by depletion and AICAR treatment, we measured indices of mitophagy, including autophagic flux, lysosomal content, and the degree of mitochondrial co-localization with lysosomes. To quantify autophagic flux, we treated cells with CQ, which inhibits autophagosome-lysosome fusion, and compared the LC3-II/LC3-I ratio. AICAR treatment elicited an overall reduction in autophagic flux with previous mtDNA depletion, but this effect was not present in untreated cells (Fig. 6A). Similarly, we observed a global decrease ($P \leq 0.05$) in lysosomal mass in MOD and LOW cells, but this main effect was largely a result of the significant effect produced by AICAR treatment (Fig. 6B). To evaluate the degradation of mitochondria through the autophagic machinery, we measured the co-localization of mitochondria with lysosomes by using fluorescence

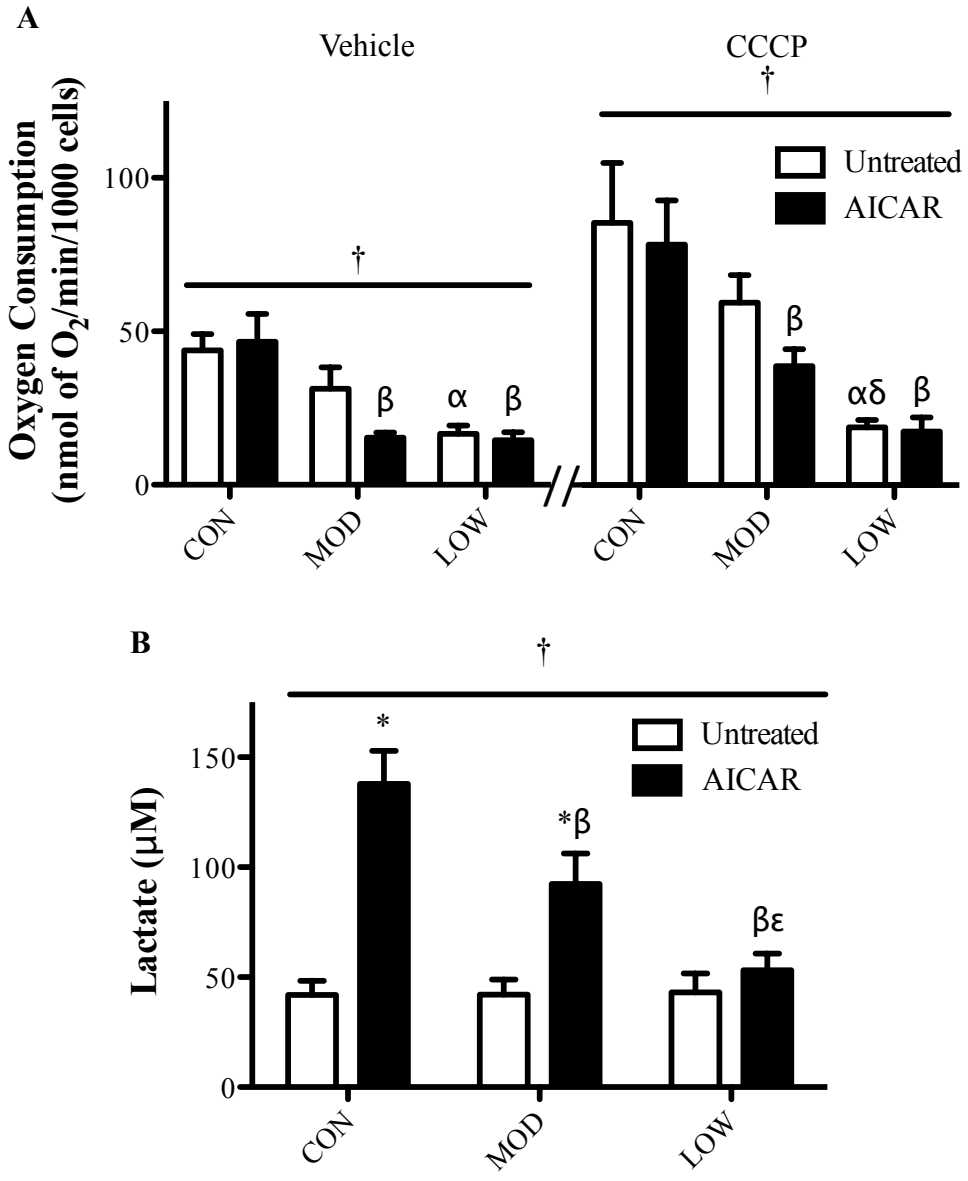

Figure 5. *Oxygen consumption and media lactate levels.* **A)** Oxygen consumption per 1000 cells (*Vehicle*: †, P<0.0001 main effect of prior depletion; α, P<0.01 vs. untreated CON; β, P<0.001 vs. AICAR treated CON; *CCCP*: †, P<0.0001 main effect of prior depletion; α, P<0.001 vs. untreated CON; β, P<0.05 vs. AICAR treated CON; δ, P<0.05 vs. untreated MOD; N = 8 experiments); **B)** Culture medium lactate content (†, P<0.0001 main effect of treatment, P<0.001 main effect of prior depletion, and P<0.001 interaction effect; β, P<0.001 vs. AICAR treated CON; ε, P<0.001 vs. AICAR treated MOD; * P<0.01 vs. matched untreated; N = 8 experiments). Values are mean ± S.E.M.

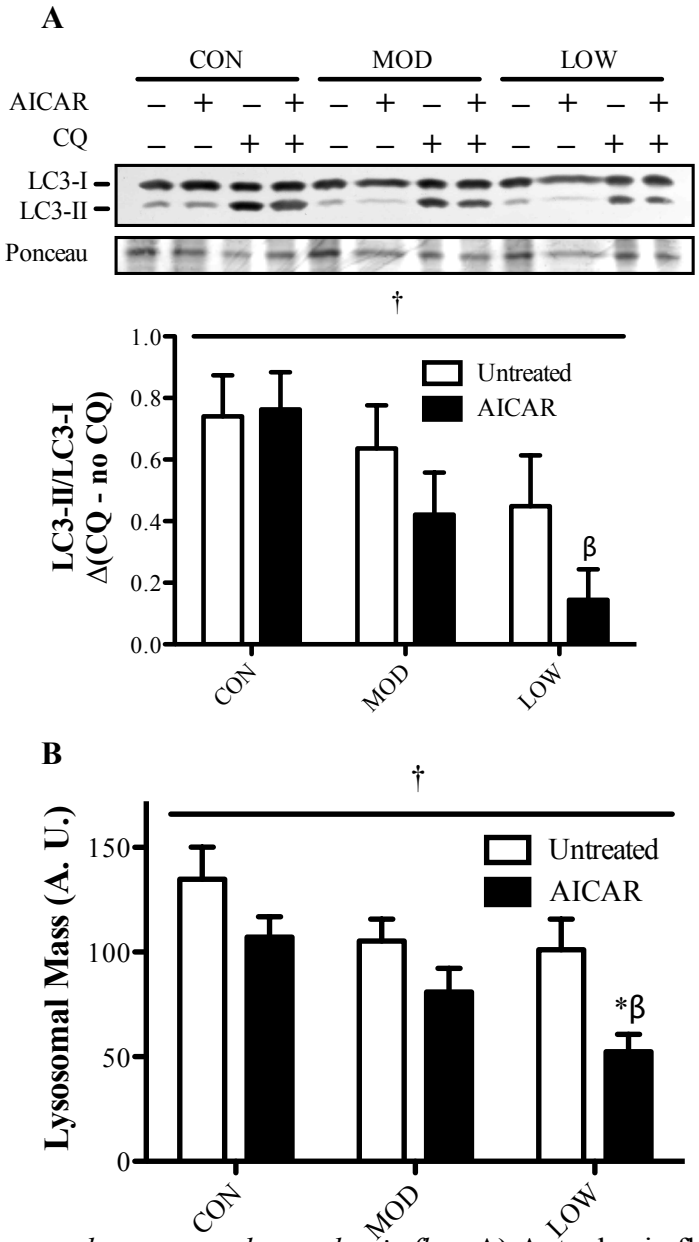

Figure 6. *Lysosomal content and autophagic flux.* **A)** Autophagic flux was measured with CQ treatment. The ratio of LC3-II to LC3-I protein was expressed compared with matched cells not treated with CQ (†, $P<0.01$ main effect of prior depletion; β, $P<0.01$ vs. AICAR treated CON; N = 6 experiments); **B)** Lysosomal Mass was measured by staining with LysoTracker Red and flow cytometry (†, $P<0.01$ main effect of treatment and $P<0.01$ main effect of prior depletion; β, $P<0.05$ vs. AICAR treated CON; *, $P<0.05$ significantly from matched untreated; N = 5-6 assays of ≥ 25,000 gated events). Values are mean ± S.E.M.

microscopy. When expressed as a percentage of the total number of lysosomes present, a significant overall effect of prior mitochondrial depletion on the number of mitochondria superimposed on lysosomes was observed (Figs. 7A and B). AICAR reduced this co-localization suggesting that fewer mitochondria were being engulfed by lysosomes, implying a decrease in mitophagy.

Discussion

The Effects of Prior mtDNA Depletion on Mitochondrial Composition and Function

Without mtDNA, energy production through oxidative phosphorylation is impaired due to a lack of mtDNA-encoded products. This results in an energy deficit and disease. As a model of mtDNA depletion, we chronically treated cells with EtBr, a known inhibitor of mtDNA synthesis. Our treatment successfully depleted mtDNA. Remarkably, in just 24 hours after EtBr removal, mtDNA content was restored back to control levels, thereby illustrating the reversibility of this treatment, as well as the speed at which myoblasts can replete mtDNA. In addition, mitochondrial mass was decreased by mtDNA depletion (Supp. Fig. 1A) and was rapidly restored to levels in untreated control cells. However, mitochondrial function remained perturbed. Thus, our experimental design serves as a useful model to investigate the kinetics of changes of both functional and structural components of mitochondria in muscle cells. We observed effects of mtDNA depletion on COX activity. Following 24 hours without EtBr, COX activity remained decreased, despite the complete restoration of mtDNA. *Cox1* mRNA, a

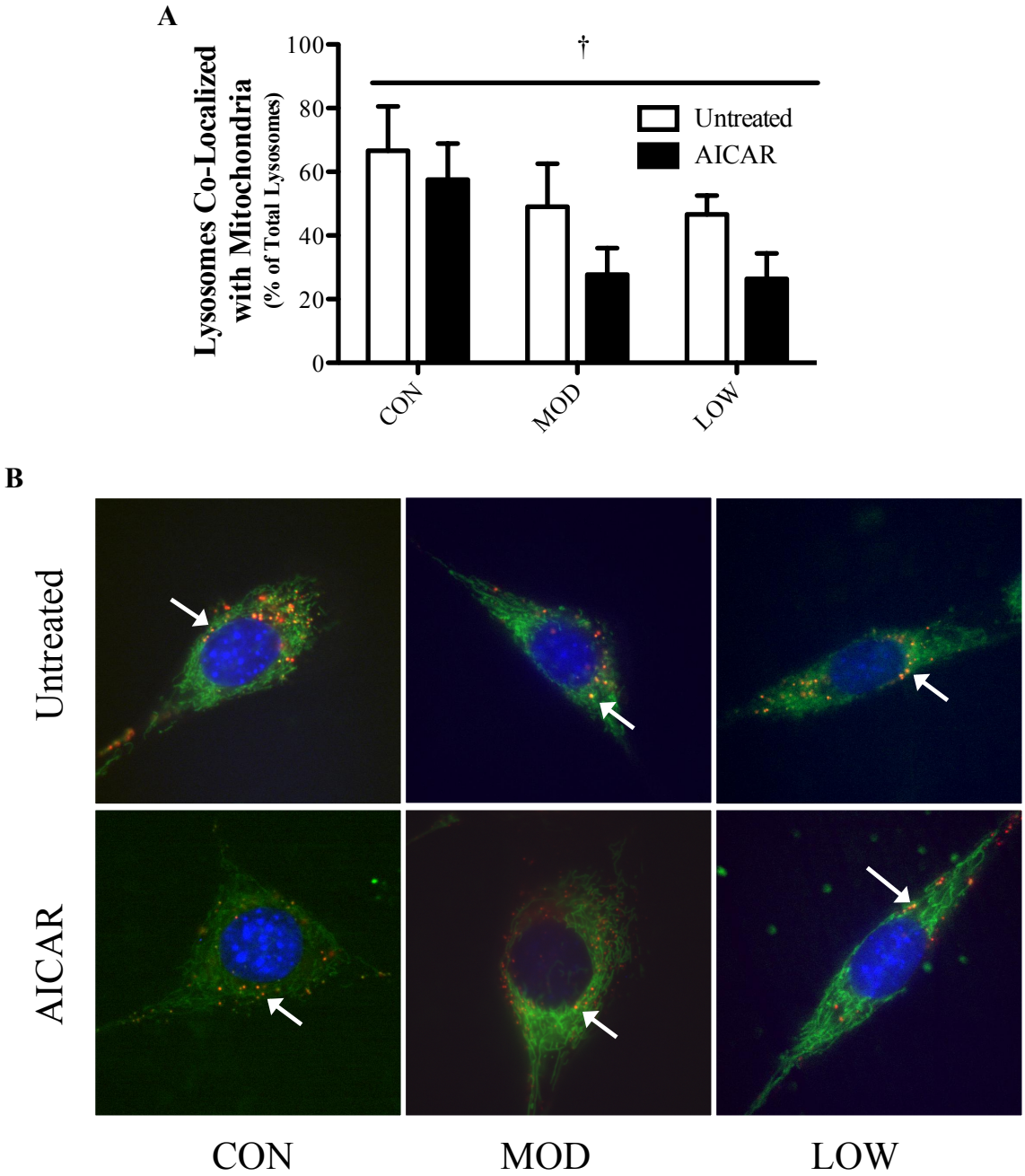

Figure 7. *Mitophagy*. **A)** Cells were stained with MitoTracker Green FM and LysoTracker Red. Mitochondria co-localized to lysosomes were counted and corrected for the total number of lysosomes per cell (†, $P<0.05$ main effect of prior depletion and main effect of treatment; N = 4-7 assessments. There were ≥ 20 cells per measurement); **B)** Representative images of cells quantified for mitophagy. White arrows indicate mitochondria co-localized with lysosomes. Values are mean ± S.E.M.

product of mtDNA, returned to control levels in MOD, but not LOW cells, while *Cox4,* a nuclear-encoded mRNA transcript encoding a subunit of the COX holoenzyme, was paradoxically elevated in MOD cells. If these changes in mRNA levels were reflected at the level of COXI and COXIV proteins, it is evident that normalization of these subunits cannot be a reason for the diminished level of COX holoenzyme activity in MOD cells. Thus, other subunits, likely involving the catalytic subunit COXII, or the mtDNA product COXIII, may be contributing to the reduced COX activity in MOD cells. The stark upregulation of the nuclear-encoded COX subunit IV in MOD cells may reflect a compensatory response of the nuclear genome to mtDNA depletion as described previously (*11*).

Our data reveal that mitochondrial membrane composition was altered in cells with prior mtDNA depletion, illustrated by the lack of change in mitochondrial mass, assessed by MitoTracker Green, relative to the large decrement in COX activity. Thus, we also investigated whether mtDNA depletion caused concomitant decrements in mitochondrial function that persisted following the 24-hour mtDNA repletion phase. The low COX activity, in MOD and LOW cells, along with reduced basal and maximal cellular respiration, are indicative of dysfunctional ETC activity. However this dysfunction did not result in a significant decline in mitochondrial membrane potential in untreated cells, a measurement that reflects the proton pumping activity of the ETC. Mitochondrial membrane potential is the driving force for ATP synthesis. Thus, despite the effect of prior mtDNA depletion on COX activity and respiration, aerobic ATP

production was likely sufficient to support resting metabolism in these quiescent myoblasts. This is reflected in the lack of change in lactate levels measured in the media of untreated CON, MOD and LOW cells. It is unlikely that this lack of difference would be maintained if the cells were confronted with an increase in energy demands, such as contractile activity.

Interestingly, ROS emission was reduced as a result of prior mtDNA depletion in MOD and LOW cells. This could be a result of a shift in the balance between ROS production by the ETC, and the anti-oxidant enzyme capacity of the MOD and LOW cells. It would be of interest to investigate whether the changes in MnSOD or GPx, known anti-oxidants, were components of the compensatory response to mtDNA depletion, as observed with *Cox4* mRNA and total AMPK activity.

Mitophagy is a process that degrades dysfunctional mitochondria with a reduced membrane potential. LOW and MOD cells had normal mitochondrial mass, but a disproportionately low COX activity, which suggests they contain dysfunctional mitochondria. However, this dysfunction did not result in a decrease in mitochondrial membrane potential. Thus, we conclude that despite the low COX activity, mitophagy is not activated in these cells, because they maintained a sufficient level of mitochondrial membrane potential.

We observed that during mtDNA repletion, phosphorylated AMPK and total AMPK protein expression increased simultaneously. This suggests an increase in whole cell AMPK activity MOD and LOW cells. Since, an ATP deficit has previously been

described in ρ^- cells (*11*, *20*), the increase in AMPK gene expression and consequently total AMPK activity may be a compensatory response to a prolonged ATP-deficit experienced when MOD and LOW cells were incubated in EtBr. Furthermore, upon glucose starvation, AMPK can activate p53 and consequently induce cell cycle arrest (*21*). Thus, the elevated amount of activated AMPK that we observed during mtDNA repletion may lead to the decreased cellular proliferation in MOD and LOW cells.

The Effect of AICAR Treatment

Situated at an intersection between the regulation of mitochondrial biogenesis and mitophagy, AMPK is a critical regulator of cellular metabolism and consequently an attractive therapeutic target for mitochondrial diseases. Active AMPK can phosphorylate downstream targets leading to the generation of new organelles, and/or the degradation of dysfunctional organelles. Thus, stimulated AMPK signaling could resolve mitochondrial disorders via: 1) the stimulation of mitochondrial biogenesis, 2) an increase the quality of the existing mitochondrial pool by degrading dysfunctional mitochondria, or 3) a combination of the two. Activation of AMPK can be achieved via pharmaceutical activators, like AICAR. Thus, we investigated whether stimulating AMPK activity through AICAR administration could improve mitochondrial content and function in C2C12 cells previously depleted of mtDNA.

In our experiments, AICAR treatment increased total AMPK activity and had a greater effect in cells previously depleted of mtDNA. Despite this, we did not observe a large increase in AMPK activity in control cells, or improvements in any of our

mitochondrial content or functional markers after 24 hours of AICAR treatment. Given that protein phosphorylation is a transient process, AMPK may have already been phosphorylated and dephosphorylated to normal levels within 24 hours in control cells, leading to an early ameliorative effect on mitochondrial content and function. Previous studies have shown that AICAR treatment increases phosphorylated AMPK in C2C12 myoblasts as early as 6 hours (*22*). Although we know that a longer, 72-hour treatment was not effective in further improving mitochondrial mass or COX activity in control cells, additional future work will be required to evaluate the benefits of shorter AICAR treatment times on mitochondrial function, because repeated, acute AICAR treatments have previously been shown to increase mitochondrial content in cultured myoblasts after 5 days (*23*, *24*). In contrast, in both MOD and LOW cells, AMPK activity and expression was increased, but the consequences was a worsened mitochondrial profile within these cell lines. Decreases in mitochondrial mass, COX activity, oxygen consumption, autophagy flux and mitophagy indices were evident. This likely contributed meaningfully to the reduced growth rate of the myoblasts in the presence of AICAR.

Although we did not measure downstream targets of AMPK, the decreases in COX subunit mRNA transcription, oxygen consumption and cell proliferation, may be a result of a change in AMPK and mTOR signaling. AMPK inhibits mTOR through TSC2 (*25*). This could attenuate COX activity and cellular respiration by preventing the transcriptional activity of the YY1–mTOR–PGC-1α transcription complex (*26*) and inhibiting mTORC1's positive regulation of protein synthesis via 4E-BP1 and p70S6K.

Additionally, AMPK can activate the p53–p21 pathway (*22*) and this could result in slower cellular proliferation.

The poor mitochondrial profile as a result of AICAR treatment may also be a result of defective mitochondrial clearance. We observed that AICAR reduced autophagic flux, lysosomal mass, and mitophagy in a manner that paralleled prior mtDNA depletion levels. This may be related to a possible decrease in global protein synthesis described above, or through a Bcl-2 dependent pathway. Previous studies have observed increased levels of Bcl-2 in ρ^- cells (*27*), which is known to inhibit Beclin-1 and the induction of autophagy (*28*). Previous studies have also shown that AICAR decreases autophagic flux through a Beclin-1 dependent mechanism (*29*). Thus AICAR may selectively inhibit autophagy in MOD and LOW cells because of their higher Bcl-2 content. AICAR treatment also induced a reduction of lysosomal mass and mitophagy indices. It is likely that the decreases in mitophagy resulting from AICAR treatment are secondary to decrements in autophagic flux, and to the reduction in lysosomal mass observed. It will also be interesting to investigate the underlying cause of these changes, possibly via changes in the expression of TFEB, a transcription factor which regulates lysosomal content (*30*).

Compensatory mechanisms may be upregulated with AICAR treatment in cells that previously had the least amount of mtDNA. AICAR treatment ameliorated ROS production in control cells, but caused greater ROS production in LOW cells. This may be an example of mitochondrial retrograde signaling, whereby the increased ROS

production may initiate a cytoplasmic signal cascade to invoke a nuclear genome response. Evidence for a similar induction of gene expression, particularly in LOW cells has been shown previously (*20*). mtDNA depletion resulted in increased mitochondrial Ca^{2+} release and an increase in *Cox5b* mRNA. Furthermore, we observed that culture medium lactate concentration was increased with AICAR treatment in control and MOD cells. AICAR is known to activate glucose oxidation in muscle, via an increase in glucose uptake (*31*). Other studies have shown a decrease in basal and insulin stimulated glucose uptake in L6 myoblasts depleted of mtDNA, because of a decrease in GLUT4 translocation to the plasma membrane (*32*). This may explain the increased lactate levels in control and MOD cells, and the absence of a response in LOW cells.

Conclusion

Following 24 hours of EtBr removal, mtDNA content rapidly repletes in cells depleted of mtDNA. However, other mitochondrial markers remain attenuated, such as COX activity and cellular respiration. In contrast, the transcription of nuclear genes encoding mitochondrial proteins (NUGEMPs) such as *Cox4* and other genes, may increase more rapidly as a compensatory response.

AICAR treatment for 24 hours did not improve mitochondrial content and function in myoblasts. Treatment with AICAR attenuated ATP consuming processes, such as cellular proliferation, and possibly protein synthesis, along with autophagy (Fig. 8). This may have served to induce an energy sparing mechanism within the cell to maintain ATP levels in the presence of declining mitochondrial function.

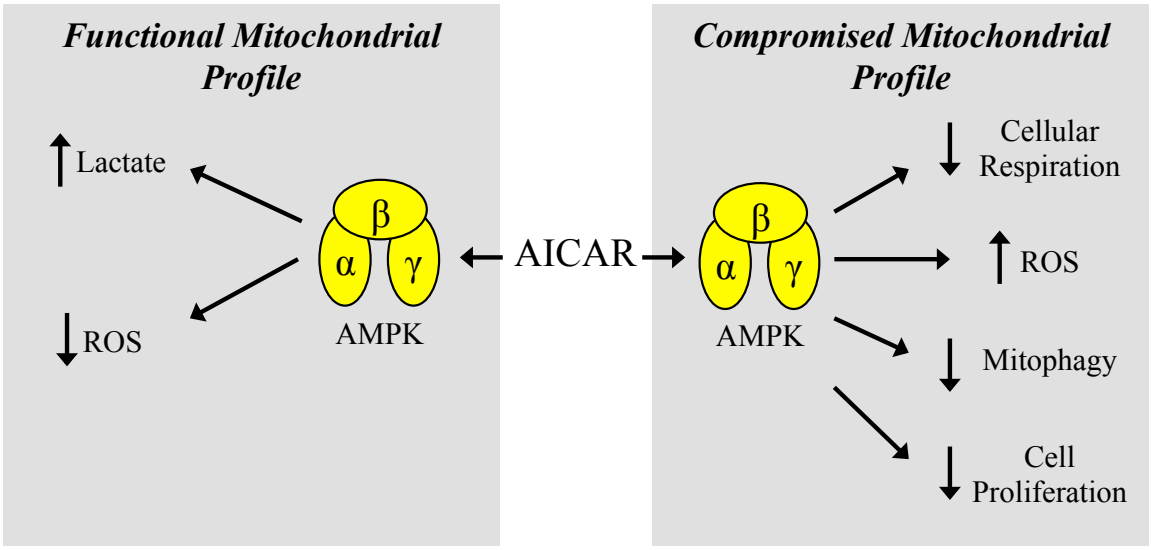

Figure 8. *Summary of AICAR induced effects.* In our control cells that have a functional mitochondrial profile, AICAR treatment for 24 hours led to increases in lactate and a decrease in ROS production. In contrast, MOD and LOW cells, with a compromised mitochondrial profile, contained more total cellular active AMPK. AICAR treatment resulted in a decrease in cellular respiration, an increase in ROS production, a decrease in mitophagy, and a reduction in cellular proliferation.

Manuscript References

1. E. Sarzi *et al.*, Mitochondrial DNA depletion is a prevalent cause of multiple respiratory chain deficiency in childhood, *J. Pediatr.* **150**, 531–4, 534.e1–6 (2007).

2. D. Skladal, J. Halliday, D. R. Thorburn, Minimum birth prevalence of mitochondrial respiratory chain disorders in children, *Brain* **126**, 1905–1912 (2003).

3. H. R. Elliott, D. C. Samuels, J. A. Eden, C. L. Relton, P. F. Chinnery, Pathogenic mitochondrial DNA mutations are common in the general population, *Am. J. Hum. Genet.* **83**, 254–260 (2008).

4. S. Jäger, C. Handschin, J. St-Pierre, B. M. Spiegelman, AMP-activated protein kinase (AMPK) action in skeletal muscle via direct phosphorylation of PGC-1alpha, *Proc. Natl. Acad. Sci. U.S.A.* **104**, 12017–12022 (2007).

5. J. Kim, M. Kundu, B. Viollet, K.-L. Guan, AMPK and mTOR regulate autophagy through direct phosphorylation of Ulk1, *Nature Cell Biology* **13**, 132–141 (2011).

6. J. E. Sullivan, F. Carey, D. Carling, R. K. Beri, Characterisation of 5“-AMP-activated protein kinase in human liver using specific peptide substrates and the effects of 5-”AMP analogues on enzyme activity, *Biochemical and Biophysical Research Communications* **200**, 1551–1556 (1994).

7. W. W. Winder *et al.*, Activation of AMP-activated protein kinase increases mitochondrial enzymes in skeletal muscle, *J. Appl. Physiol.* **88**, 2219–2226 (2000).

8. C. Viscomi *et al.*, In vivo correction of COX deficiency by activation of the AMPK/PGC-1α axis, *Cell Metabolism* **14**, 80–90 (2011).

9. A. Golubitzky *et al.*, O. S. Shirihai, Ed. Screening for Active Small Molecules in Mitochondrial Complex I Deficient Patient's Fibroblasts, Reveals AICAR as the Most Beneficial Compound, *PLoS ONE* **6**, e26883 (2011).

10. A. Saada, The use of individual patient's fibroblasts in the search for personalized treatment of nuclear encoded OXPHOS diseases, *Molecular Genetics and Metabolism* **104**, 39–47 (2011).

11. A.-M. Joseph, A. A. Rungi, B. H. Robinson, D. A. Hood, Compensatory responses of protein import and transcription factor expression in mitochondrial DNA defects, *Am. J. Physiol., Cell Physiol.* **286**, C867–75 (2004).

12. E. Zylber, C. Vesco, S. Penman, Selective inhibition of the synthesis of

mitochondria-associated RNA by ethidium bromide, *Journal of Molecular Biology* **44**, 195–204 (1969).

13. S. Perlman, S. Penman, Mitochondrial protein synthesis: Resistance to emetine and response to RNA synthesis inhibitors, *Biochemical and Biophysical Research Communications* **40**, 941–948 (1970).

14. E. Knight Jr, Mitochondria-associated ribonucleic acid of the HeLa cell. Effect of ethidium bromide on the synthesis of ribosomal and 4S ribonucleic acid, *Biochemistry* (1969).

15. M. M. Nass, Differential effects of ethidium bromide on mitochondrial and nuclear DNA synthesis in vivo in cultured mammalian cells, *Experimental Cell Research* **72**, 211–222 (1972).

16. H. Chen *et al.*, Mitochondrial fusion is required for mtDNA stability in skeletal muscle and tolerance of mtDNA mutations, *Cell* **141**, 280–289 (2010).

17. G. Uguccioni, D. A. Hood, The importance of PGC-1 in contractile activity-induced mitochondrial adaptations, *AJP: Endocrinology and Metabolism* **300**, E361–E371 (2011).

18. G. C. Brown, V. Borutaite, There is no evidence that mitochondria are the main source of reactive oxygen species in mammalian cells, *Mitochondrion* **12**, 1–4 (2012).

19. D. G. Nicholls *et al.*, Bioenergetic profile experiment using C2C12 myoblast cells, *J Vis Exp* (2010).

20. G. Biswas *et al.*, Retrograde Ca2+ signaling in C2C12 skeletal myocytes in response to mitochondrial genetic and metabolic stress: a novel mode of inter-organelle crosstalk, *EMBO J.* **18**, 522–533 (1999).

21. R. G. Jones *et al.*, AMP-activated protein kinase induces a p53-dependent metabolic checkpoint, *Molecular Cell* **18**, 283–293 (2005).

22. D. L. Williamson, D. C. Butler, S. E. Alway, AMPK inhibits myoblast differentiation through a PGC-1alpha-dependent mechanism, *AJP: Endocrinology and Metabolism* **297**, E304–14 (2009).

23. G. K. McConell *et al.*, Central role of nitric oxide synthase in AICAR and caffeine-induced mitochondrial biogenesis in L6 myocytes, *Journal of Applied Physiology* **108**, 589–595 (2010).

24. A. D. Dam, A. S. Mitchell, J. Quadrilatero, Induction of mitochondrial biogenesis

protects against caspase-dependent and caspase-independent apoptosis in L6 myoblasts, *Biochim. Biophys. Acta* (2013).

25. K. Inoki, T. Zhu, K.-L. Guan, TSC2 mediates cellular energy response to control cell growth and survival, *Cell* **115**, 577–590 (2003).

26. J. T. Cunningham *et al.*, mTOR controls mitochondrial oxidative function through a YY1-PGC-1alpha transcriptional complex, *Nature* **450**, 736–740 (2007).

27. G. Biswas, M. Guha, N. G. Avadhani, Mitochondria-to-nucleus stress signaling in mammalian cells: nature of nuclear gene targets, transcription regulation, and induced resistance to apoptosis, *Gene* **354**, 132–139 (2005).

28. M. C. Maiuri *et al.*, Functional and physical interaction between Bcl-X(L) and a BH3-like domain in Beclin-1, *EMBO J.* **26**, 2527–2539 (2007).

29. R. Viana *et al.*, Role of AMP-activated protein kinase in autophagy and proteasome function, *Biochemical and Biophysical Research Communications* **369**, 964–968 (2008).

30. M. Sardiello *et al.*, A gene network regulating lysosomal biogenesis and function, *Science* **325**, 473–477 (2009).

31. A. C. Smith, C. R. Bruce, D. J. Dyck, AMP kinase activation with AICAR simultaneously increases fatty acid and glucose oxidation in resting rat soleus muscle, *The Journal of Physiology* **565**, 537–546 (2005).

32. S. Y. Park *et al.*, Depletion of mitochondrial DNA causes impaired glucose utilization and insulin resistance in L6 GLUT4myc myocytes, *J. Biol. Chem.* **280**, 9855–9864 (2005).

Future Work

Our results demonstrate that AICAR treatment induced a mitochondrial-preservation program in cells previously depleted of mtDNA. In our experiments, the underlying mechanisms responsible are thus far largely unidentified and to elucidate these pathways we could perform the following experiments.

1. AICAR has been shown to have AMPK-independent effects. To reveal the role of AMPK in the results we observed, we should complete treatments with AMPK inhibitors, such as Compound C, or alternatively, transfect cells with a dominant negative AMPK α, or siRNA against AMPK α. We can then assess markers of mitochondrial content, such as COX activity or mitochondrial mass. Other AMPK agonists, such as A-769662, could also be employed to confirm the role of AMPK in our results.
2. To confirm if AMPK activation with AICAR is indeed a transient process in our control cells, we should treat cells for 1, 6, 12 and 24 hours with AICAR and immunoblot for the phosphorylation status of AMPK.
3. To elucidate the mechanisms responsible for our results, we could perform an experiment to infer the role of transcription factors, such as mTOR, TFEB, and p53, and determine the content and activation of anti-oxidants, autophagy inhibitors, protein synthesis markers and cell cycle arrest markers. Following 24 hours of treatment with AICAR, we could perform cell subfractionation followed by immunoblotting of the nuclear and cytosolic fractions to determine if mTOR,

TFEB and p53 translocate to the nucleus. This would suggest an increase in their transcriptional activity. Furthermore, immunoblotting on entire cell fractions would elucidate the amount of anti-oxidants, such as GPx and MnSOD, the content of autophagy inhibitors, such as Bcl-2, the phosphorylation status of protein synthesis regulators and mTORC1 targets, such as 4E-BP1 and p70S6K, and cell cycle inhibitors and p53 transcriptional activity products, such as p21.

These additional studies may provide a better insight into the role of AMPK in regulating mitochondrial content in cells with compromised mitochondrial profiles.

Appendix A: Data and Statistical Analyses

Table 1A. mt/nDNA ΔΔCt values and statistical analysis before and after removal of EtBr

	Raw Values					
	CON		MOD		LOW	
	0 H	48 H	0 H	48 H	0 H	48 H
N						
1	572319	793446	358134	777998	190848	852338
2	404478	509173	174254	655230	161595	777265
3	654870	683923	378419	753626	123453	788614
4		460534		700757		781851
5		771702		676887		527535
Mean	543889	643756	303602	712899	158632	745520
S.E.M.	73667	67850	64939	23094	19512	56175

2-Way ANOVA		
	P-Value	Significant
Interaction	0.0019	Yes
Time	< 0.0001	Yes
Depletion	0.0727	No

Bonferroni Post-Hoc Tests						
Cell Line	Treatment		Cell Line	Treatment	P-Value	Significant
CON	0 H	vs.	CON	48 H	P > 0.05	No
CON	0 H	vs.	MOD	0 H	P < 0.05	Yes
CON	0 H	vs.	LOW	0 H	P < 0.01	Yes
CON	48 H	vs.	MOD	48 H	P > 0.05	No
CON	48 H	vs.	LOW	48 H	P > 0.05	No
MOD	0 H	vs.	MOD	48 H	P < 0.001	Yes
LOW	0 H	vs.	LOW	48 H	P < 0.001	Yes
MOD	0 H	vs.	LOW	0 H	P > 0.05	No
MOD	48 H	vs.	LOW	48 H	P > 0.05	No

Table 1B. Individual values for cell proliferation and statistical analysis

	Raw Values					
	CON		MOD		LOW	
	Untreated	AICAR	Untreated	AICAR	Untreated	AICAR
N						
1	9.74	7.38	6.92	2.65	3.90	1.00
2	9.91	8.94	6.79	2.62	3.97	1.94
3	13.83	9.24	5.94	2.99	4.87	2.14
4	5.88	6.78	6.14	2.62	4.39	2.56
5	11.18	12.29	4.00	2.13	4.26	3.17
6	17.61	9.98	4.52	3.17	3.76	2.68
7	5.54	5.54	3.75	2.58	4.04	2.17
Mean	10.53	8.59	5.44	2.68	4.17	2.24
S.E.M.	1.61	0.85	0.50	0.13	0.14	0.26

2-Way ANOVA		
	P-Value	**Significant**
Interaction	0.8311	No
Depletion	< 0.0001	Yes
Treatment	0.0014	Yes

Bonferroni Post-Hoc Tests						
Cell Line	**Treatment**		**Cell Line**	**Treatment**	**P-Value**	**Significant**
CON	UT	vs.	CON	AICAR	P > 0.05	No
CON	UT	vs.	MOD	UT	P < 0.001	Yes
CON	UT	vs.	LOW	UT	P < 0.001	Yes
CON	AICAR	vs.	MOD	AICAR	P < 0.001	Yes
CON	AICAR	vs.	LOW	AICAR	P < 0.001	Yes
MOD	UT	vs.	MOD	AICAR	P < 0.05	Yes
LOW	UT	vs.	LOW	AICAR	P > 0.05	No
MOD	UT	vs.	LOW	UT	P > 0.05	No
MOD	AICAR	vs.	LOW	AICAR	P > 0.05	No

Table 2A. Individual values of phosphorylated AMPK protein levels and statistical analysis

	Raw Values					
	CON		MOD		LOW	
	Untreated	AICAR	Untreated	AICAR	Untreated	AICAR
N						
1	1.359	1.569	2.132	5.457	2.883	10.684
2	0.000	1.814	1.323	2.682	1.606	1.194
3	0.000	2.049	1.077	1.628	2.592	5.288
4	3.432	6.090	1.795	0.431	2.656	3.060
5	2.761	0.349	2.865	6.287	3.542	3.018
6	1.439	1.730	1.812	4.497	2.728	2.916
7	1.489	1.648	0.353	3.425	4.019	7.862
Mean	1.497	2.178	1.623	3.487	2.861	4.860
S.E.M.	0.484	0.684	0.303	0.790	0.289	1.263

2-Way ANOVA		
	P-Value	Significant
Interaction	0.6052	No
Depletion	0.0140	Yes
Treatment	0.0254	Yes

Bonferroni Post-Hoc Tests						
Cell Line	Treatment		Cell Line	Treatment	P-Value	Significant
CON	UT	vs.	CON	AICAR	P > 0.05	No
CON	UT	vs.	MOD	UT	P > 0.05	No
CON	UT	vs.	LOW	UT	P > 0.05	No
CON	AICAR	vs.	MOD	AICAR	P > 0.05	No
CON	AICAR	vs.	LOW	AICAR	P < 0.05	Yes
MOD	UT	vs.	MOD	AICAR	P > 0.05	No
LOW	UT	vs.	LOW	AICAR	P > 0.05	No
MOD	UT	vs.	LOW	UT	P > 0.05	No
MOD	AICAR	vs.	LOW	AICAR	P > 0.05	No

Table 2B. Individual values of total AMPK protein levels and statistical analysis

	Raw Values					
	CON		MOD		LOW	
	Untreated	AICAR	Untreated	AICAR	Untreated	AICAR
N						
1	1.375	1.283	1.449	3.061	1.969	4.411
2	0.000	1.240	1.473	1.948	2.545	3.833
3	1.875	2.195	2.128	5.407	3.104	6.568
4	1.220	1.505	1.803	2.975	3.373	4.335
5	2.204	1.440	2.259	2.401	2.833	3.240
6	0.459	0.721	0.876	0.286	1.321	1.901
7	2.207	2.065	2.582	3.850	3.799	6.083
Mean	1.334	1.493	1.796	2.847	2.706	4.339
S.E.M.	0.323	0.191	0.219	0.601	0.320	0.606

2-Way ANOVA		
	P-Value	**Significant**
Interaction	0.2117	No
Depletion	< 0.0001	Yes
Treatment	0.0079	Yes

Bonferroni Post-Hoc Tests						
Cell Line	**Treatment**		**Cell Line**	**Treatment**	**P-Value**	**Significant**
CON	UT	vs.	CON	AICAR	P > 0.05	No
CON	UT	vs.	MOD	UT	P > 0.05	No
CON	UT	vs.	LOW	UT	P < 0.05	Yes
CON	AICAR	vs.	MOD	AICAR	P > 0.05	No
CON	AICAR	vs.	LOW	AICAR	P < 0.001	Yes
MOD	UT	vs.	MOD	AICAR	P > 0.05	No
LOW	UT	vs.	LOW	AICAR	P < 0.05	Yes
MOD	UT	vs.	LOW	UT	P > 0.05	No
MOD	AICAR	vs.	LOW	AICAR	P < 0.05	Yes

Table 3A. Mitochondrial mass values and statistical analysis

	Raw Values					
	CON		MOD		LOW	
	Untreated	AICAR	Untreated	AICAR	Untreated	AICAR
N						
1	74.17	102.30	72.52	84.18	86.62	65.47
2	184.93	208.33	147.79	122.89	102.88	81.32
3	88.93	126.83	97.50	87.59	90.66	45.65
4	112.42	118.69	96.14	118.07	62.44	52.91
5	142.07	152.99	81.67	84.34	57.39	59.86
6	40.12	104.81	40.46	79.19	30.99	67.40
7	161.10	164.15	181.26	49.21	146.75	91.61
8	140.37	194.12	115.71	106.92	112.72	100.15
9	133.38	176.54	118.78	132.69	117.06	94.93
Mean	119.72	149.86	105.76	96.12	89.72	73.26
S.E.M.	15.13	12.96	13.87	8.74	11.76	6.50

2-Way ANOVA		
	P-Value	**Significant**
Interaction	0.1168	No
Depletion	0.0002	Yes
Treatment	0.8903	No

Bonferroni Post-Hoc Tests						
Cell Line	**Treatment**		**Cell Line**	**Treatment**	**P-Value**	**Significant**
CON	UT	vs.	CON	AICAR	P > 0.05	No
CON	UT	vs.	MOD	UT	P > 0.05	No
CON	UT	vs.	LOW	UT	P > 0.05	No
CON	AICAR	vs.	MOD	AICAR	P < 0.01	Yes
CON	AICAR	vs.	LOW	AICAR	P < 0.001	Yes
MOD	UT	vs.	MOD	AICAR	P > 0.05	No
LOW	UT	vs.	LOW	AICAR	P > 0.05	No
MOD	UT	vs.	LOW	UT	P > 0.05	No
MOD	AICAR	vs.	LOW	AICAR	P > 0.05	No

Table 3B. Raw COX activity values and statistical analysis

	Raw Values					
	CON		MOD		LOW	
	Untreated	AICAR	Untreated	AICAR	Untreated	AICAR
N						
1	362.18	175.58	110.62	63.21	37.91	4.77
2	506.11	399.27	273.95	165.39	55.43	24.38
3	480.45	248.79	78.81	59.05	1.22	
4	364.02	465.60	177.36	70.57	168.80	83.21
5	369.74	369.58	196.54	130.72	40.79	55.47
Mean	416.50	331.76	167.46	97.79	60.83	41.96
S.E.M.	31.63	52.53	34.19	21.32	28.43	17.26

2-Way ANOVA		
	P-Value	**Significant**
Interaction	0.6140	No
Depletion	< 0.0001	Yes
Treatment	0.0486	Yes

Bonferroni Post-Hoc Tests						
Cell Line	**Treatment**		**Cell Line**	**Treatment**	**P-Value**	**Significant**
CON	UT	vs.	CON	AICAR	P > 0.05	No
CON	UT	vs.	MOD	UT	P < 0.001	Yes
CON	UT	vs.	LOW	UT	P < 0.001	Yes
CON	AICAR	vs.	MOD	AICAR	P < 0.001	Yes
CON	AICAR	vs.	LOW	AICAR	P < 0.001	Yes
MOD	UT	vs.	MOD	AICAR	P > 0.05	No
LOW	UT	vs.	LOW	AICAR	P > 0.05	No
MOD	UT	vs.	LOW	UT	P > 0.05	No
MOD	AICAR	vs.	LOW	AICAR	P > 0.05	No

Table 3C. Raw $\Delta\Delta^{Ct}$ values of COXI mRNA levels and statistical analysis

	Raw Values					
	CON		MOD		LOW	
	Untreated	AICAR	Untreated	AICAR	Untreated	AICAR
N						
1	19817.77	21945.77	11545.79	13798.75	13186.33	5039.82
2	19980.02	20555.92	15441.28	14333.85	9951.28	3653.42
3	14893.99	17230.35	15712.33	15828.77	13937.95	6813.12
4	23085.77	22838.37	48175.59	12379.88	18329.68	12919.82
5	24282.52	26847.25	20460.31	16498.00	9931.28	5412.00
6	19969.93	18825.46	22888.79	13086.39	8217.50	9061.36
7	14618.58	8082.69	13174.16	9373.10	13508.00	5245.87
Mean	19521.22	19475.12	21056.89	13614.11	12437.43	6877.92
S.E.M.	1391.50	2226.36	4760.54	893.92	1281.25	1193.88

2-Way ANOVA		
	P-Value	**Significant**
Interaction	0.2781	No
Depletion	0.0005	Yes
Treatment	0.0302	Yes

Bonferroni Post-Hoc Tests						
Cell Line	**Treatment**		**Cell Line**	**Treatment**	**P-Value**	**Significant**
CON	UT	vs.	CON	AICAR	P > 0.05	No
CON	UT	vs.	MOD	UT	P > 0.05	No
CON	UT	vs.	LOW	UT	P > 0.05	No
CON	AICAR	vs.	MOD	AICAR	P > 0.05	No
CON	AICAR	vs.	LOW	AICAR	P < 0.01	Yes
MOD	UT	vs.	MOD	AICAR	P > 0.05	No
LOW	UT	vs.	LOW	AICAR	P > 0.05	No
MOD	UT	vs.	LOW	UT	P < 0.05	Yes
MOD	AICAR	vs.	LOW	AICAR	P > 0.05	No

Table 3D. Raw $\Delta\Delta^{Ct}$ values for COXIV mRNA levels and statistical analysis

	Raw Values					
	CON		MOD		LOW	
	Untreated	AICAR	Untreated	AICAR	Untreated	AICAR
N						
1	2.343	4.514	3.815	4.047	3.164	0.286
2	2.674	4.417	5.610	1.176	2.201	1.217
3	4.467	3.699	2.937	1.456	2.061	0.506
4	3.247	4.512	7.038	1.449	1.158	0.788
5	3.187	2.837	5.476	0.604	1.695	0.511
6	3.661	4.417	12.933	3.077	1.577	0.646
7	2.634	3.150	4.269	1.486	1.749	0.487
8	2.750	5.107	2.892	1.961	1.571	0.383
Mean	3.120	4.081	5.621	1.907	1.897	0.603
S.E.M.	0.243	0.274	1.159	0.396	0.213	0.103

2-Way ANOVA		
	P-Value	**Significant**
Interaction	0.0003	Yes
Depletion	< 0.0001	Yes
Treatment	0.0033	Yes

Bonferroni Post-Hoc Tests						
Cell Line	**Treatment**		**Cell Line**	**Treatment**	**P-Value**	**Significant**
CON	UT	vs.	CON	AICAR	P > 0.05	No
CON	UT	vs.	MOD	UT	P < 0.01	Yes
CON	UT	vs.	LOW	UT	P > 0.05	No
CON	AICAR	vs.	MOD	AICAR	P < 0.05	Yes
CON	AICAR	vs.	LOW	AICAR	P < 0.001	Yes
MOD	UT	vs.	MOD	AICAR	P < 0.001	Yes
LOW	UT	vs.	LOW	AICAR	P > 0.05	No
MOD	UT	vs.	LOW	UT	P < 0.001	Yes
MOD	AICAR	vs.	LOW	AICAR	P > 0.05	No

Table 4A. Individual values for mitochondrial membrane potential after correction for mitochondrial mass and statistical analysis

	Raw Values					
	CON		MOD		LOW	
	Untreated	AICAR	Untreated	AICAR	Untreated	AICAR
N						
1	0.837	0.741	0.625	0.611	0.335	0.254
2	0.293	0.407	0.223	0.232	0.292	0.212
3	0.459	0.515	0.387	0.366	0.409	0.221
4	0.945	0.914	0.388	0.415	0.765	0.663
5	0.675	0.664	0.468	0.495	0.762	0.794
6	0.342	0.403				
7	0.538	0.620	0.287	0.359	0.271	0.149
8	0.424	0.496	0.272	0.351	0.320	0.153
Mean	0.564	0.595	0.379	0.404	0.450	0.350
S.E.M.	0.083	0.062	0.052	0.046	0.082	0.100

2-Way ANOVA		
	P-Value	Significant
Interaction	0.6079	No
Depletion	0.0201	Yes
Treatment	0.8075	No

Bonferroni Post-Hoc Tests						
Cell Line	Treatment		Cell Line	Treatment	P-Value	Significant
CON	UT	vs.	CON	AICAR	P > 0.05	No
CON	UT	vs.	MOD	UT	P > 0.05	No
CON	UT	vs.	LOW	UT	P > 0.05	No
CON	AICAR	vs.	MOD	AICAR	P > 0.05	No
CON	AICAR	vs.	LOW	AICAR	P < 0.05	Yes
MOD	UT	vs.	MOD	AICAR	P > 0.05	No
LOW	UT	vs.	LOW	AICAR	P > 0.05	No
MOD	UT	vs.	LOW	UT	P > 0.05	No
MOD	AICAR	vs.	LOW	AICAR	P > 0.05	No

Table 4B. Individual values for reactive oxygen species after correcting for mitochondrial mass and statistical analysis

	Raw Values					
	CON		MOD		LOW	
	Untreated	AICAR	Untreated	AICAR	Untreated	AICAR
N						
1	0.026	0.007	0.004	0.012	0.014	0.036
2	0.054	0.035	0.015	0.018	0.014	0.034
3	0.036	0.028	0.011	0.018	0.019	0.015
4	0.075	0.044	0.021		0.052	0.062
5	0.032	0.022	0.015	0.02	0.021	0.019
6	0.020	0.017				
7	0.053	0.018	0.029	0.021	0.021	0.028
8	0.011	0.006	0.009	0.011	0.010	0.042
Mean	0.038	0.022	0.015	0.017	0.022	0.034
S.E.M.	0.007	0.005	0.003	0.002	0.005	0.006

2-Way ANOVA		
	P-Value	Significant
Interaction	0.0299	Yes
Depletion	0.0253	Yes
Treatment	0.8684	No

Bonferroni Post-Hoc Tests						
Cell Line	Treatment		Cell Line	Treatment	P-Value	Significant
CON	UT	vs.	CON	AICAR	P > 0.05	No
CON	UT	vs.	MOD	UT	P > 0.05	No
CON	UT	vs.	LOW	UT	P > 0.05	No
CON	AICAR	vs.	MOD	AICAR	P > 0.05	No
CON	AICAR	vs.	LOW	AICAR	P > 0.05	No
MOD	UT	vs.	MOD	AICAR	P > 0.05	No
LOW	UT	vs.	LOW	AICAR	P > 0.05	No
MOD	UT	vs.	LOW	UT	P > 0.05	No
MOD	AICAR	vs.	LOW	AICAR	P > 0.05	No

Table 5A-I. Raw oxygen consumption values after vehicle treatment and statistical analysis

	Raw Values					
	CON		MOD		LOW	
	Untreated	AICAR	Untreated	AICAR	Untreated	AICAR
N						
1	28.04	23.67	33.73	8.94	14.95	7.47
2	59.06	82.83	74.48	13.35	31.98	17.43
3	54.60	69.27	26.00	11.86	19.33	11.51
4	59.06	25.89	13.5	13.84	16.37	11.08
5	57.84	75.96	18.21	23.27	21.60	25.63
6	30.66	33.60	26.48	13.85	7.58	8.34
7	34.69	42.54	41.38	17.73	11.17	9.24
8	26.13	19.22	16.35	19.97	9.73	25.43
Mean	43.76	46.62	31.27	15.35	16.59	14.52
S.E.M.	5.34	9.04	6.99	1.64	2.77	2.63

2-Way ANOVA		
	P-Value	**Significant**
Interaction	0.2118	No
Depletion	< 0.0001	Yes
Treatment	0.2612	Yes

Bonferroni Post-Hoc Tests						
Cell Line	**Treatment**		**Cell Line**	**Treatment**	**P-Value**	**Significant**
CON	UT	vs.	CON	AICAR	P > 0.05	No
CON	UT	vs.	MOD	UT	P > 0.05	No
CON	UT	vs.	LOW	UT	P < 0.01	Yes
CON	AICAR	vs.	MOD	AICAR	P < 0.001	Yes
CON	AICAR	vs.	LOW	AICAR	P < 0.001	Yes
MOD	UT	vs.	MOD	AICAR	P > 0.05	No
LOW	UT	vs.	LOW	AICAR	P > 0.05	No
MOD	UT	vs.	LOW	UT	P > 0.05	No
MOD	AICAR	vs.	LOW	AICAR	P > 0.05	No

Table 5A-II. Raw oxygen consumption values after CCCP treatment and statistical analysis

	Raw Values					
	CON		MOD		LOW	
	Untreated	AICAR	Untreated	AICAR	Untreated	AICAR
N						
1	31.47	23.20	20.55	14.96	8.21	7.56
2	156.45	99.33	92.86	40.82	19.48	12.79
3	172.42	121.49	94.86	65.75	30.18	14.24
4	58.79	65.69	48.06	47.21	14.58	16.28
5	112.53	141.41	69.73	47.51	21.48	47.79
6	40.22	44.31	46.14	22.74	14.59	7.39
7	45.08	48.66	55.41	37.22	22.74	17.10
8	65.53	81.72	47.34	33.39	19.48	16.62
Mean	85.31	78.23	59.37	38.70	18.84	17.47
S.E.M.	19.38	14.35	8.92	5.57	2.32	4.54

2-Way ANOVA		
	P-Value	**Significant**
Interaction	0.6660	No
Depletion	< 0.0001	Yes
Treatment	0.2833	No

Bonferroni Post-Hoc Tests						
Cell Line	**Treatment**		**Cell Line**	**Treatment**	**P-Value**	**Significant**
CON	UT	vs.	CON	AICAR	P > 0.05	No
CON	UT	vs.	MOD	UT	P > 0.05	No
CON	UT	vs.	LOW	UT	P < 0.001	Yes
CON	AICAR	vs.	MOD	AICAR	P > 0.05	Yes
CON	AICAR	vs.	LOW	AICAR	P < 0.001	Yes
MOD	UT	vs.	MOD	AICAR	P > 0.05	No
LOW	UT	vs.	LOW	AICAR	P > 0.05	No
MOD	UT	vs.	LOW	UT	P < 0.05	Yes
MOD	AICAR	vs.	LOW	AICAR	P > 0.05	No

Table 5B. Individual lactate concentration values and statistical analysis

	Raw Values					
	CON		MOD		LOW	
	Untreated	AICAR	Untreated	AICAR	Untreated	AICAR
N						
1	19.05	90.75	27.31	114.36	30.85	43.84
2	22.29	118.49	70.39	145.64	22.59	36.75
3	60.66	182.82	61.25	60.95	23.47	40.59
4	73.64	199.64	26.13	66.85	28.20	34.10
5	32.03	83.08	19.05	147.41	30.26	56.82
6	41.50	134.01	61.09	63.27	76.60	99.18
7	40.96	169.11	33.34	92.11	82.86	66.81
8	44.77	125.03	38.24	48.31	50.21	47.49
Mean	41.86	137.87	42.10	92.36	43.13	53.20
S.E.M.	6.51	14.99	6.85	13.87	8.55	7.59

2-Way ANOVA		
	P-Value	Significant
Interaction	0.0007	Yes
Depletion	0.0010	Yes
Treatment	< 0.0001	Yes

Bonferroni Post-Hoc Tests						
Cell Line	Treatment		Cell Line	Treatment	P-Value	Significant
CON	UT	vs.	CON	AICAR	P > 0.001	Yes
CON	UT	vs.	MOD	UT	P > 0.05	No
CON	UT	vs.	LOW	UT	P > 0.05	No
CON	AICAR	vs.	MOD	AICAR	P < 0.01	Yes
CON	AICAR	vs.	LOW	AICAR	P < 0.001	Yes
MOD	UT	vs.	MOD	AICAR	P < 0.01	Yes
LOW	UT	vs.	LOW	AICAR	P > 0.05	No
MOD	UT	vs.	LOW	UT	P > 0.05	No
MOD	AICAR	vs.	LOW	AICAR	P < 0.05	Yes

Table 6A. Ratio of LC3-II to LC3-I protein and statistical analysis

	Raw Values					
	CON		MOD		LOW	
	Untreated	AICAR	Untreated	AICAR	Untreated	AICAR
N						
1	1.110	0.963	0.750	0.773	0.893	0.233
2	0.557	0.435	0.253	0.000	0.109	0.000
3	0.638	0.622	0.569	0.438	0.380	0.355
4	0.579	0.574	0.378	0.774	0.437	0.048
5	1.183	0.739	0.635	0.479	-0.060	-0.210
6	0.378	1.247	1.232	0.067	0.937	0.440
Mean	0.741	0.763	0.636	0.422	0.449	0.144
S.E.M.	0.133	0.121	0.14	0.136	0.165	0.099

2-Way ANOVA		
	P-Value	**Significant**
Interaction	0.4591	No
Depletion	0.0075	Yes
Treatment	0.1400	No

Bonferroni Post-Hoc Tests						
Cell Line	**Treatment**		**Cell Line**	**Treatment**	**P-Value**	**Significant**
CON	UT	vs.	CON	AICAR	$P > 0.05$	No
CON	UT	vs.	MOD	UT	$P > 0.05$	No
CON	UT	vs.	LOW	UT	$P > 0.05$	No
CON	AICAR	vs.	MOD	AICAR	$P > 0.05$	No
CON	AICAR	vs.	LOW	AICAR	$P < 0.01$	Yes
MOD	UT	vs.	MOD	AICAR	$P > 0.05$	No
LOW	UT	vs.	LOW	AICAR	$P > 0.05$	No
MOD	UT	vs.	LOW	UT	$P > 0.05$	No
MOD	AICAR	vs.	LOW	AICAR	$P > 0.05$	No

Table 6B. Raw values of lysosomal mass and statistical analysis.

	Raw Values					
	CON		MOD		LOW	
	Untreated	AICAR	Untreated	AICAR	Untreated	AICAR
N						
1	21.12	20.38	18.07	10.69	27.20	13.71
2	33.30	27.80	26.11	15.58	23.93	14.41
3	36.18	24.89	20.31	14.40	11.15	8.26
4	31.66	22.98		27.12	27.34	13.13
5	26.06	21.32	26.66	17.37	22.03	10.86
6	16.22	13.42	15.91	13.58	11.77	3.56
Mean	27.42	21.80	21.41	16.46	20.57	10.66
S.E.M.	3.14	2.00	2.15	2.32	3.00	1.69

2-Way ANOVA		
	P-Value	Significant
Interaction	0.5548	No
Depletion	0.0033	Yes
Treatment	0.0020	Yes

Bonferroni Post-Hoc Tests						
Cell Line	Treatment		Cell Line	Treatment	P-Value	Significant
CON	UT	vs.	CON	AICAR	P > 0.05	No
CON	UT	vs.	MOD	UT	P > 0.05	No
CON	UT	vs.	LOW	UT	P > 0.05	No
CON	AICAR	vs.	MOD	AICAR	P > 0.05	No
CON	AICAR	vs.	LOW	AICAR	P < 0.01	Yes
MOD	UT	vs.	MOD	AICAR	P > 0.05	No
LOW	UT	vs.	LOW	AICAR	P > 0.05	Yes
MOD	UT	vs.	LOW	UT	P > 0.05	No
MOD	AICAR	vs.	LOW	AICAR	P > 0.05	No

Table 7. Percentages of lysosomes co-localized with mitochondria and statistical analysis

	Raw Values					
	CON		MOD		LOW	
	Untreated	AICAR	Untreated	AICAR	Untreated	AICAR
N						
1	65.51	58.16	67.25	45.40	48.35	35.22
2	104.08	62.72	72.80	50.36	55.70	53.75
3	89.75	96.72				
4				14.11	48.83	15.93
5					66.85	
6	27.89	31.51	13.93	9.74	28.32	15.27
7	45.73	38.40	42.19	18.74	31.75	11.54
Mean	66.59	57.50	49.04	27.67	46.63	26.34
S.E.M.	13.92	11.42	13.47	8.41	5.93	8.00

2-Way ANOVA		
	P-Value	Significant
Interaction	0.8034	No
Depletion	0.0331	Yes
Treatment	0.0543	No

Bonferroni Post-Hoc Tests						
Cell Line	Treatment		Cell Line	Treatment	P-Value	Significant
CON	UT	vs.	CON	AICAR	P > 0.05	No
CON	UT	vs.	MOD	UT	P > 0.05	No
CON	UT	vs.	LOW	UT	P > 0.05	No
CON	AICAR	vs.	MOD	AICAR	P > 0.05	No
CON	AICAR	vs.	LOW	AICAR	P > 0.05	No
MOD	UT	vs.	MOD	AICAR	P > 0.05	No
LOW	UT	vs.	LOW	AICAR	P > 0.05	No
MOD	UT	vs.	LOW	UT	P > 0.05	No
MOD	AICAR	vs.	LOW	AICAR	P > 0.05	No

Appendix B: Additional Data

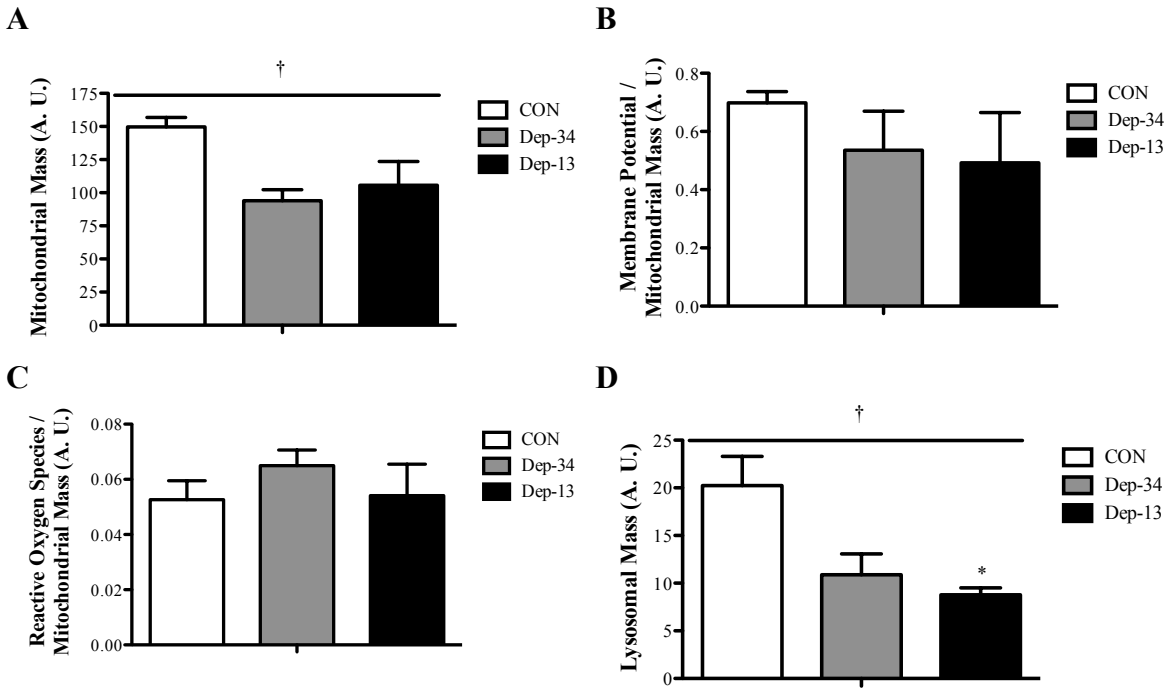

Supplementary Figure 1. *Pre-treatment mitochondrial content and quality, and lysosomal content.* Mitochondrial mass (**A)**, membrane potential (**B)**, reactive oxygen species (**C**), and lysosomal mass (**D**) were measured on a flow cytometry (1-way ANOVA; † indicates significant main effect of prior depletion $P<0.05$; * indicates vs. control; N = 3 measurements of ≥ 10,000 gated events).

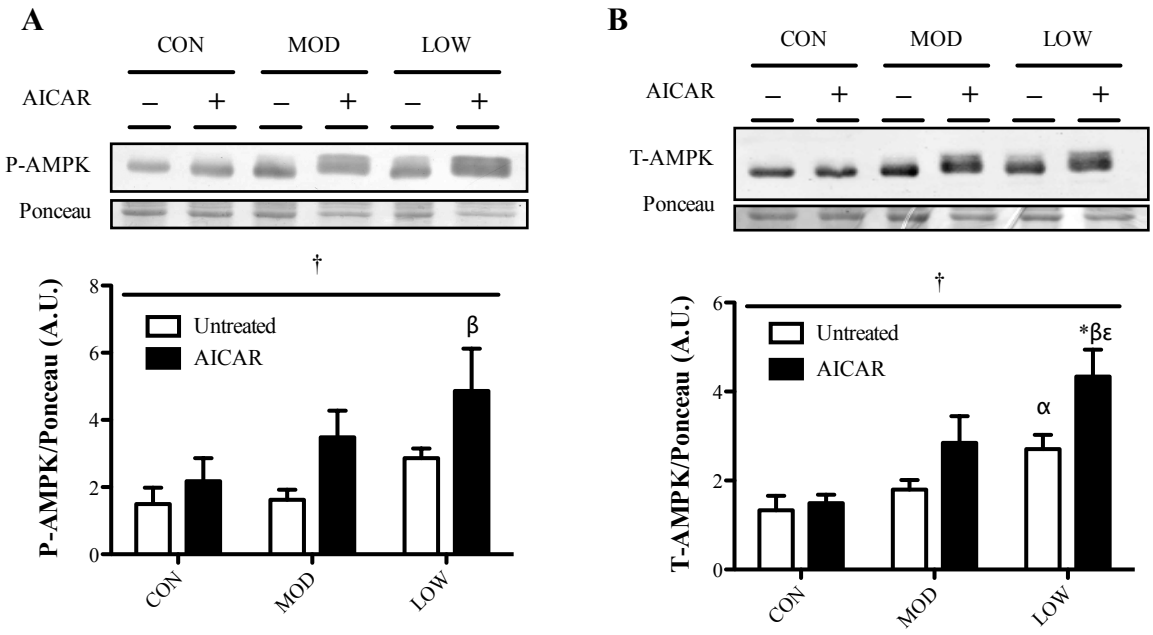

Supplementary Figure 2. *AMPK phosphorylation and expression after AICAR treatment.* **A)** P-AMPK protein levels relative to Ponceau S staining (†, $P<0.05$ main effect of prior depletion and treatment; β, $P<0.05$ vs. AICAR CON; N=7 experiments); **B)** T-AMPK protein levels relative to Ponceau S staining (†, $P<0.0001$ main effect of treatment and $P<0.01$ main effect of prior depletion; α, $P<0.05$ vs. untreated CON; β, $P<0.001$ vs. AICAR treated CON; ε, $P<0.05$ vs. AICAR treated MOD; * $P<0.05$ vs. matched untreated; N = 7 experiments). Values are mean ± S.E.M.

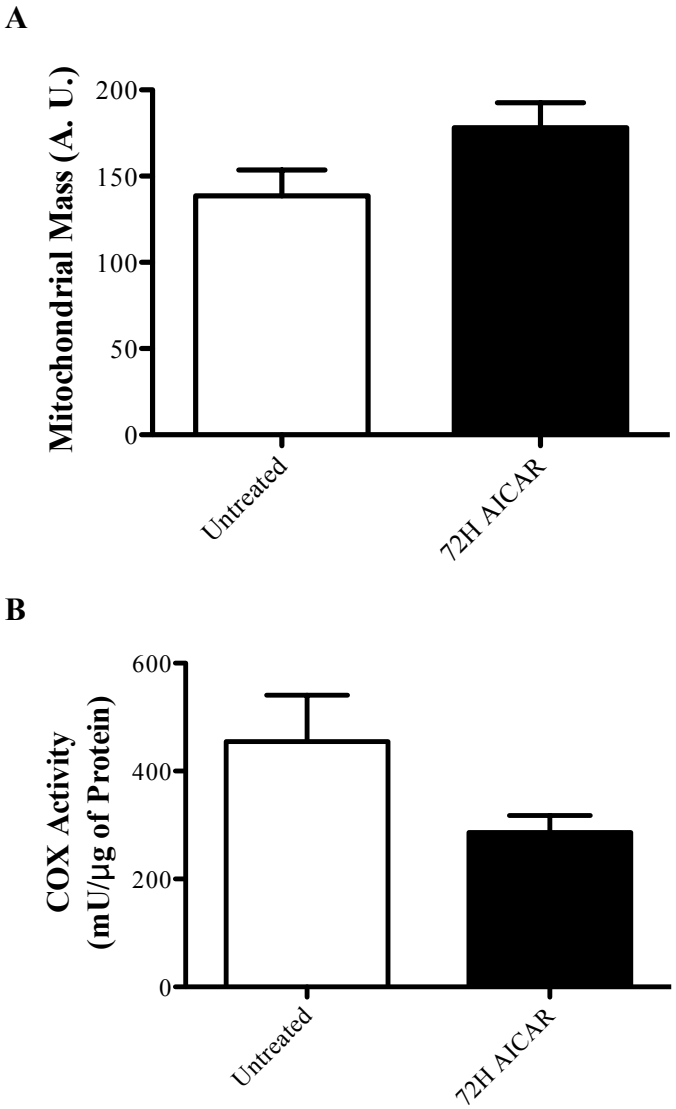

Supplementary Figure 3. *Mitochondrial mass and COX activity.* After 72 hours, mitochondrial mass and mitochondrial content were not significantly increased with AICAR treatment in control cells (N = 4).

A

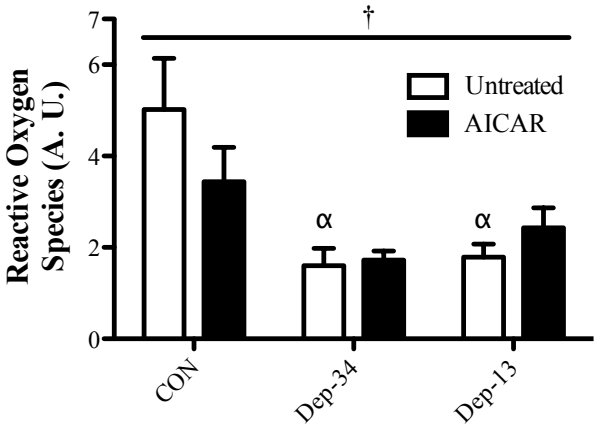

B

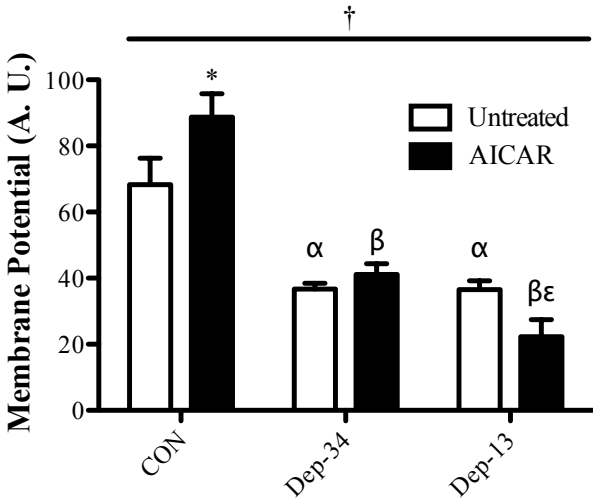

Supplementary Figure 4. *Uncorrected values for mitochondrial membrane potential and reactive oxygen species.* **A)** An overall main effect of prior depletion was observed for reactive oxygen species generation (†, $P<0.05$ main effect of prior depletion; α, $P<0.05$ vs. untreated CON; N = 7-8); **B)** There was an overall decrease in mitochondrial membrane potential (†, $P<0.05$ effect of interaction and $P<0.05$ main effect of prior depletion; α, $P<0.001$ vs. untreated CON; β, $P<0.001$, vs. AICAR treated CON; ε, $P<0.05$ vs. AICAR treated MOD; *, $P<0.05$ vs. matched untreated; N = 7-8).

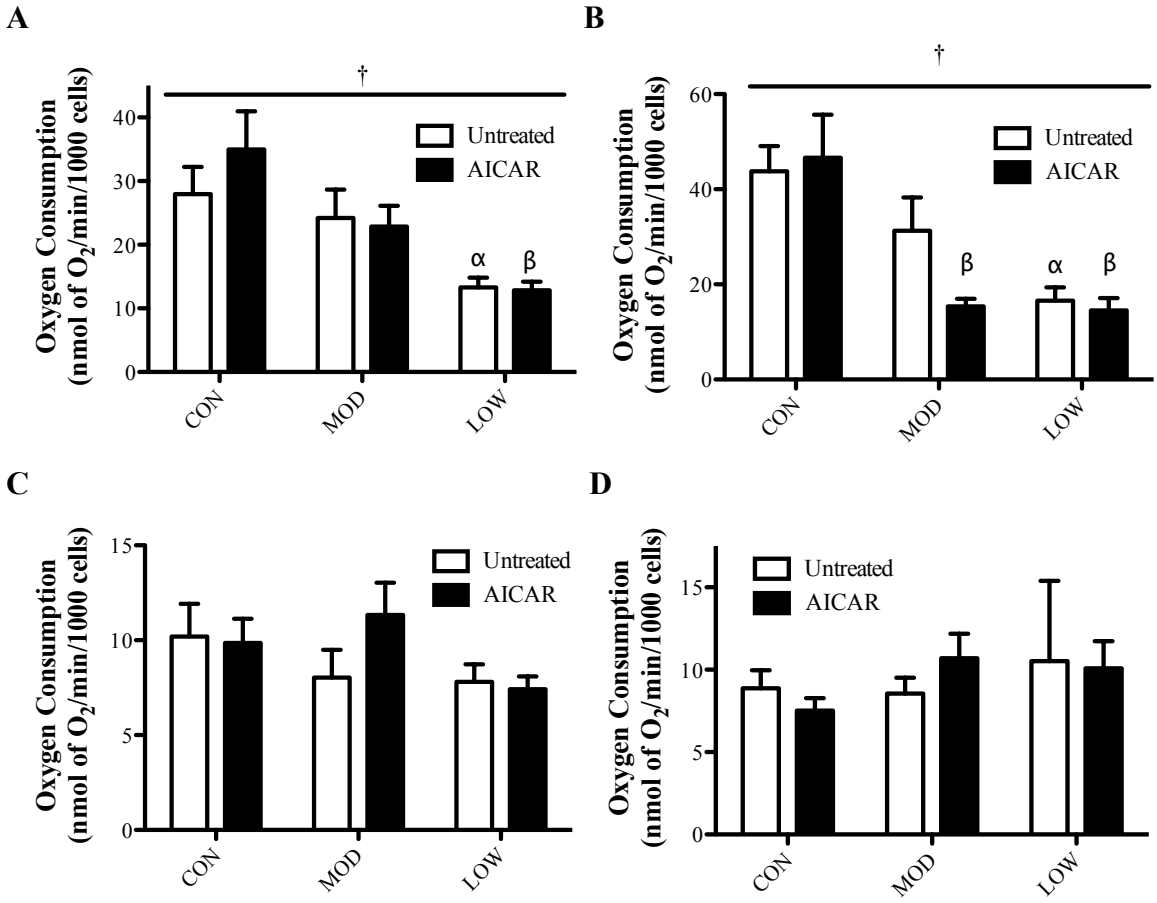

Supplementary Figure 5. *Respiration in growth media or growth media containing the vehicle (DMSO) for respiration reagents.* Oligomycin, CCCP, rotenone and antimycin A are dissolved in DMSO. We found that respiration decreases with mtDNA depletion and respiration is slightly increased with DMSO treatment. Furthermore, we found no defects in mitochondrial membrane leak or non-mitochondrial oxygen consumption. A) Respiration in growth media (†, $P<0.05$ main effect of prior depletion; α, $P<0.05$ vs. untreated CON; β, $P<0.05$, vs. AICAR treated; N = 8 experiments) B) Respiration in cells treated with vehicle (†, $P<0.05$ main effect of prior depletion; α, $P<0.05$ vs. untreated CON; β, $P<0.05$, vs. AICAR treated; N = 8 experiments). C) Respiration cells treated with oligomycin. D) Respiration in cells treated with rotenone and antimycin A.

Appendix C: Laboratory Methods and Protocols

C2C12 ρ^- Generation

Reagents:

- 100 ng/mL Ethidium bromide (EtBr)
- Complete Growth Medium
    - DMEM
        - 4.5 g/L Glucose
        - With Glutamine
    - 1 mM Sodium Pyruvate
    - 50 μg/mL Uridine
- Cloning Cylinders
- Autoclaved Vacuum Grease in a glass 60 cm^2 petri dish
- DPBS
- Trypsin

Procedure:

1. Obtain a low passage of C2C12 cells.
2. Stock a minimum of 2 cryovials for the generation of ρ^- cells and passage-matched controls.
3. Start growing 1 cryovial in Complete Growth Medium with 100 ng/mL EtBr. Add EtBr fresh each time because it is light sensitive.
4. Refresh medium every day and split cells 1:3 as necessary (typically every 2-3 days).
5. After a few weeks of growth start the second vial and growth in the presence of just Complete Growth Medium. Passage these as necessary 1:3 and change medium daily. These cells will serve as the passage matched controls. They are started later because they replicate at a faster rate than ρ^- cells.
6. After 6-weeks of growth in the presence of EtBr, seed 100 cells on 60 cm^2 tissue culture treated dishes. Seed a few plates to ensure success.
7. After 1-3 days, use Cloning Cylinders to isolate colonies.
    a. Remove growth medium and secure the lid of the dish with tape.
    b. Invert the dish and place under inverted light microscope.
    c. With an alcohol resistant marker circle groups of cells.
    d. Wash plate with DPBS.
    e. Dip the cloning cylinders by into the petri dish of vacuum grease, to evenly coat the rim of the cylinders.

f. Place the cylinders firmly over the circled colonies.
g. Add 200 – 500 µL of Trypsin to the middle of the cylinders and incubate at 37ºC for 5 minutes.
h. Remove trypsin and place into wells of a 96-well plate.
i. Allow colonies to grow and transfer to a 24-well plate, 25 cm^2 flask, and 175 cm^2 flask as necessary.
j. Stock colonies and freeze aliquot as described for genomic DNA isolation.
k. Isolate gDNA and perform qPCR to assess mtDNA to nDNA ratio. Name colonies respectively and stock desired colonies for future experiments. From start to finish cells are maintained in EtBr for 10.5 weeks.

Cytochrome C Oxidase (COX) Activity Assay

Part A: Enzyme Extraction

Reagents:

- Dulbecco's Phosphate Buffered Saline (DPBS)

Procedure:

1. Grow cells up 175 cm^2 flask.
2. Pour off the medium. Wash each plate with 5 ml Dulbecco's Phosphate Buffered Saline (DPBS) without Ca^{2+} and Mg^{2+}. Remove all of the DPBS.
3. Add 5 ml of Trypsin with EDTA and incubate at 37C for 5 minutes.
4. Tap flask and inhibit trypsin with 5 mL of complete media.
5. Spin the cells at 1400 RPM for 3 minutes. Remove all supernate. Resuspend in 2 mLs DPBS. Count cells and aliquot 2 x 10^6 cells for enzyme extraction.
6. Spin the cells at for 3 min at 1400 RPM in a microcentrifuge. Discard the supernate with a Pasteur pipette.
7. Add 150 µl enzyme extraction buffer and vortex vigorously to disperse the pellet.
8. Vortex and flash freeze. Store at -80 until ready.
9. Freeze in liq N_2 and thaw at 37 ^oC. Vortex vigorously for 5 sec.
10. Repeat step 9 three times.
11. Sonicate 3 x 3 sec on ice. Make sure that the sonicator is set to 30.
12. Spin in microcentrifuge at 4 ^oC for 5 min at 13.0 rcf.
13. Remove the supernate and add it to a new, labelled eppendorf tube.
14. Run COX activity below. Use 25 uL of sample 75 uL of test solution. Perform 4 times.
15. Measure the total protein concentration using a Bradford protein assay.

Part B: Cytochrome C Oxidase (COX) Assay with Microplate Reader

Theory:

Cell extract containing cytochrome c oxidase is added to the test solution containing fully reduced cytochrome c. The rate of cytochrome c oxidation is measured over time as a reduction in absorbance at 550 nm. The reaction is carried out at 30^{o} C.

Reagents:

- Horse Heart Cytochrome c (Sigma C-2506)
- Sodium Dithionite
- 100mM K-Phosphate Buffer (KPO_4 pH 7.0)
- Make and mix equal proportions of 0.1M KH_2PO_4 and 0.1M $K_2HPO_4.3H_20$
- 10mM K-Phosphate Buffer (KPO_4)
- Dilute 100mM K-Phosphate Buffer 1:10 with ddH_20

Procedure:

1. Immediately following the completion of the enzyme extraction protocol from cells proceed to making Test Solution. Add the following to a scintillation vial:
    a. Weigh out 10mg of horse heart cytochrome c;
    b. Add 500 uL of 10mM KPO_4 buffer and fully dissolve cytochrome c.
2. Make up a small volume of 10mg/ml sodium dithionite-10mM KPO_4 stock solution (make fresh each experiment for immediate use within 20mins).
3. Add 20µl of dithionite solution to the Test Solution and observe a colour change from red to orange.
4. Add 4ml of ddH_20.
5. Add 500 uL of 100mM KPO4 buffer and wrap vial in aluminium foil as Test Solution becomes light sensitive at this step.
6. Add ≥ 300µl of Test Solution into 7 wells of a 96-well microplate and incubate at 30°C for 10 minutes to stabilize the temperature of absorbance.
7. Open KC4 plate reader program. Select CONTROL icon, then PRE-HEATING tab, enter 30°C and select ON. (Do not run assay until KC4 temperature has reached 30°C.)
8. Setup COX activity protocol on the KC4 program.
    a. Select WIZARD icon, then READING PARAMETERS icon.
        i. Select *Kinetic* for Reading Type.
        ii. Select *Absorbance* for Reader and *550nm* for wavelength (drop-down menu).

iii. Select *Sweep* for Read Mode.
iv. Select *96 Well Plate* (default) for Plate Type.
v. Enter A1 – A7
vi. Select *Yes* and Pre-heating and enter *30* for Temperature Control.
vii. For Shaking enter *4* for intensity and 1 sec for duration.
viii. Do not select either of the two options for Pre-reading.
ix. Click on the *KINETIC…* rectangular tile to open the Kinetic window.
x. Enter run time (*1 minute* is recommended) and select *MINIMUM* for Interval time (under these conditions the minimum Interval time should be 3 seconds).
xi. Select *Allow Well Zoom During Read* to see data in real time (optional).
xii. Under Scales, checkmarks should appear for both Auto check boxes. Do not select Individual Well Auto Scaling.
xiii. Press *OK* to return to Reading Parameters window. Press *OK* to return to Wizard window. Press *OK*. Do not save the protocol.

9. Set the multipipette to 75 µl and secure 7 tips on the white projections (make sure they are on tight and all at the same height).
10. In a clean 96 well plate, pipette 25 µL of enzyme extraction buffer into A1 and 25 µL of samples into the next 6 empty wells (start with A1). At all times, minimize the formation of bubbles.
11. Confirm the microplate reader has reached the desired 30ºC.
12. Remove the microplate with Test Solution from the incubator. Place this plate beside the plate with the sample extracts in it.
13. Using the multipipette transfer 75 µL of test solution to the wells containing the relevant samples. Make sure the volume is equal in all the pipette tips and gently remove the multipipette tips prior to the final expulsion to minimize the formation of bubbles.
14. Immediately, begin reading the plate using the microplate reader.
15. Generate a report with an overlay of the "Well-Zoom" for each relevant well. On this report a delta absorbance will be given.
16. The delta absorbance will appear in units of mOD/min and the number given will be negative. Convert this to OD/min by dividing by 1000 and omit the negative sign in the calculation. (eg. if Mean V: -394.8 mOD/min, then use 0.395 OD/min)

Calculation:

$$COX\ Activity = \frac{\frac{mean\ delta\ absorbance}{minute} \times total\ volume\ (mL) \times 1000}{18.5\ \left(\frac{\mu mole}{mL} extinction\ coeffcient\right) \times sample\ volume\ (mL) \times \frac{total\ \mu g\ of\ protein}{well}}$$

Example Calculation:

Sample Volume	25 µL
Test Solution Volume	75 µL
Mean Delta Absorbance	0.5843 OD/min
Sample Protein Concentration	3.2023 µg/µL

$$COX\ Activity = \frac{0.5843\ \frac{OD}{minute} \times 0.1\ mL \times 1000}{\left(18.5\ \frac{\mu mole}{mL} extinction\ coeffcient\right) \times 0.025\ mL \times \left(3.2023\ \frac{\mu g}{\mu L} \times 0.025\ mL\right)}$$

$$COX\ Activity = 1579.2\ \frac{Units}{\mu g\ of\ protein}$$

DNA and RNA Assessment Procedure

Part A: Genomic DNA Isolation

Reagents:

- Mammalian Genomic DNA Miniprep Kit (Sigma-Aldrich G1N70)
    - Resuspension Solution
    - RNase A Solution
    - 20 mg/mL Proteinase K Solution
    - Lysis Solution C
    - Column Preparation Solution
    - Wash Solution
    - Elution Solution
- 100% Ethanol (EtOH)
- DEPC ddH_2O
- Complete Growth Medium
    - DMEM
        - With Glutamine
        - With 1 mM Sodium Pyruvate
        - With 50 μg/mL Uridine
    - 10% FBS
    - 1% Penicillin – Streptomycin
- DPBS without Ca^{2+} or Mg^{2+}

Procedure:

1. Cell Culture:
    a. Grow cells up 175 cm^2 flask.
    b. Pour off the medium. Wash each plate with 5 ml Dulbecco's. Phosphate Buffered Saline (DPBS) without Ca^{2+} and Mg^{2+}. Remove all of the DPBS.
    c. Add 5 ml of Trypsin with EDTA and incubate at 37ºC for 5 minutes.
    d. Tap flask and inhibit trypsin with 5 mL of Complete Growth Media.
    e. Spin the cells at 1400 RPM for 3 minutes. Remove all supernate. Resuspend in 2 mLs DPBS. Count cells and aliquot 2 x 10^6 cells for DNA extraction.
    f. Spin the cells at for 3 min at 1400 RPM in a microcentrifuge. Discard the supernate with a Pasteur pipette.
    g. Flash freeze and store at -80 until ready to continue
2. DNA Isolation

a. Follow the directions of the Mammalian Genomic DNA Miniprep Kit as briefly described below.
b. Allow pellet to thaw slightly and then resuspend the pellet in 200 µL of Resuspension Solution.
c. Treat cell suspension with 20 µL of RNAse A Solution for 2 minutes at room temperature.
d. Add 20 µL of 20 mg/mL Proteinase K and 200 µL of Lysis Solution C. Vortex vigorously and incubate at 70ºC for 10 minutes.
e. Prepare Binding Columns
    i. Add 500 µL of Column Preparation Solution.
    ii. Centrifuge at 12000 g for 1 minute.
f. Add 200 µL of EtOH to sample lysates and vortex vigorously.
g. Load lysate into Binding Columns and centrifuge at 6500 g for 1 minute.
h. Empty collection tube and add 500 µL of Wash Solution. Centrifuge for 1 minute at 6500 g
i. Empty collection tube and add 500 µL of Wash Solution. Centrifuge for 3 minutes at 16000 g.
j. Replace collection tube and add 200 µL of Elution Solution for 5 minutes.
k. Centrifuge for 1 minute at 6500 g and store at -20ºC.

3. Quantify DNA
    a. Use a spectrophotometer to measure the absorbance at 260 nm.

Part B: Total RNA Isolation

Reagents:

- TRIZol® Reagent
- 24:1 Chloroform:Isoamylalcohol
    - 24 parts Chlorofom
    - 1 part Isoamylalcohol
- 100% Isopropanol
- 75% Ethanol
- DEPC ddH_2O

Procedure:

1. Cell Culture:
    a. Grow cells up 175 cm^2 flask.

b. Pour off the medium. Wash each plate with 5 ml Dulbecco's. Phosphate Buffered Saline (DPBS) without Ca^{2+} and Mg^{2+}. Remove all of the DPBS.
c. Add 5 ml of Trypsin with EDTA and incubate at 37ºC for 5 minutes.
d. Tap flask and inhibit trypsin with 5 mL of Complete Growth Media.
e. Spin the cells at 1400 RPM for 3 minutes. Remove all supernate. Resuspend in 2 mLs DPBS.
f. Spin the cells at for 3 min at 1400 RPM in a microcentrifuge. Discard the supernate with a Pasteur pipette.
g. Flash freeze and store at -80 until ready to continue

2. RNA Isolation
    a. Thaw pellet slightly and add 1ml TRIZOL. Vortex thoroughly until pellet is completely disrupted.
    b. Add 200 µL of 24:1 chloroform:isoamlyalcohol.
    c. Shake vigorously for 15 seconds and leave @ room temperature for 5 minutes.
    d. Spin at 14000 g for 15 minutes at 4°C.
    e. Transfer the upper phase carefully to a new eppendorf tube. Add 500 µL of 100% isopropanol and briefly shake.
    f. Incubate at room temperature for 30 minutes.
    g. Spin at 14000 g for 10 minutes at 4°C.
    h. Remove supernatant. Add 500 µL of 75% EtOH and wash the RNA pellet with gentle pipetting.
    i. Spin at 14000 g for 1 minute at 4°C.
    j. Carefully, remove supernatant and air dry the RNA pellet.
    k. Resuspend the pellet in 50 µL of DEPC ddH_2O.
    l. Heat RNA samples at 65°C for 10 minutes.
3. Quantify RNA
    a. Use a spectrophotometer to measure the absorbance at 260 nm.
    b. Freeze and store at -80°C.

Part C: Reverse Transcriptase

Reagents:

- Oligo(dt) 20
- 10 mM dNTP
    - asd
- DEPC ddH_2O
- Master Mix (per sample)
    - 8 µL of 5x Buffer
    - 2 µL of 0.1 M Dithiothreitol (DTT)

    - 2 µL of RNAse Out
- Superscript III

Procedure:

1. Combine 2 µL of Oligo(dt) 20, 2 µL of 10 mM dNTP, and 4 µg of Sample RNA in a sterile 0.5 mL sterile eppendorf. Bring the volume to 26 µL with DEPC ddH_2O.
2. Heat the eppendorf at 65ºC for 5 minutes, followed by 1 minute at 4ºC in a thermocycler.
3. Make the Master Mix.
4. After the eppendorfs have been heated, add 12 µL of the Master Mix and 2 µL of Supercript III RT.
5. Incubate the eppendorf for 50 minutes at 55ºC, followed by 15 minutes at 70ºC.
6. Store samples at -20ºC.

Part D: Quantitative Polymerase Chain Reaction (qPCR) Procedure

Reagents:

- DEPC ddtH2O
- Master Mix (per sample and per gene of interest)
    - Table 1 (COX I, β_2-Microglobulin, ND1 and Pecam1):
        - 12.5 µL of PerfeCTa® SYBR® Green SuperMix with ROX™
        - 2.5 µL of 20 µM Forward Primer
        - 2.5 µL of 20 µM Reverse Primer
        - 5.5 µL of DEPC ddH_2O
    - Table 2 (COX IV)
        - 12.5 µL of PerfeCTa® SYBR® Green SuperMix with ROX™
        - 0.625 µL of 20 µM Forward Primer
        - 0.625 µL of 20 µM Reverse Primer
        - 9.25 µL of DEPC ddH_2O

Procedure:

1. Biochemical Assay
    a. Autoclave qPCR microtube strips and pipette tips. Sterilize pipettes with EtOH for use.
    b. Dilute gDNA or cDNA Samples appropriately with DEPC ddH_2O for the gene of interest:

i. cDNA for COXI and β_2-Microglobulin assessments are diluted 1:40 to obtain a 2.5 ng/µL stock.
ii. gDNA is diluted to a 50 ng/µL stock and then 1:20 to obtain a 2.5 ng/µL stock.
iii. cDNA for COXIV assessment is diluted 1:4 to obtain a 25 ng/µL stock.

c. Create appropriate Master Mixes as determined during optimization. Always use a housekeeping gene to correct for difference in total cDNA amount.
d. Add 2 µL of each diluted cDNA sample in triplicate to microtube strips.
e. Add 23 µL of Master Mix to all wells.
f. Close wells and place in Applied Biosystems StepOne Plus qPCR machine.
g. Set the StepOne Plus application for a reaction volume of 25 µL, SYBR® Green Technology, Normal (~2.5 hour) Reaction Speed, and Include a Melt Curve Analysis.

2. ΔΔCt Analysis
   a. After the run is complete. Confirm that the automatically determined thresholds are in the exponential amplification phase for each gene of interest. Export all data to an Excel spread sheet.
   b. Obtain the cycle number where the sample's amplification plot crosses the defined threshold (i.e. the Ct value).
   c. Average the two closest Ct values.
   d. To determine the ΔCt take the difference between the Ct value of the gene of interest and the Ct value of your housekeeping gene. Raise this to the power of two (i.e. $2^{\Delta Ct}$) and use this to compare differences in gene expression.
   e. To determine find the fold change in the gene expression from your control samples take the ΔCt of each sample and subtract the ΔCt of the control sample. Use these values (ΔΔCt) to generate a graph of gene expression relative to your control condition.

Flow Cytometry

Reagents:

- 100 nM Tetramethylrhodamine Ethyl Ester (TMRE)
- 100 μM Dichlorodihydrofluorescein Diacetate (H_2DCFDA)
- 100 nM MitoTracker Green FM (MTGFM)
- 200 nM LysoTracker Red (LTR)
- Phenol Red Free Complete Growth Medium
    - DMEM – Phenol Red Free
    - 10% FBS
    - 1% Penicillin-Streptomycin
- Complete Growth Medium
    - DMEM
    - 10% FBS
    - 1% Penicillin-Streptomycin
- 5 mL polystyrene round-bottom tube with cell strainer
  BD Falcon – REF 352235
- 5 mL polystyrene round-bottom tube
  BD Falcon – REF 352052
- Sheath Fluid
  BDFACS Flow - 342003

Procedure:

1. Preparation
    a. Plate cells in 5 - 75 cm^2 tissue culture treated flasks.
    b. Allow a minimum of 24 hours for cells to adhere to the flask.
2. Analysis
    a. Prepare all reagents.
    b. Aspirate all media from each flask
    c. Apply 5 mL of the staining solutions above to separate flasks for 45 minutes. Include an unstained control.
    d. After staining, remove media and rinse flasks with DPBS.
    e. Incubate flasks for 5 minutes with trypsin.
    f. Triturate cell suspensions with Complete Growth Medium and place in previously labelled screw top plastic tubes.
    g. Centrifuge tubes at 1400 RPM for 3 minutes.
    h. Aspirate supernatant fraction without disturbing the pellet.
    i. Aliquot 400 μL of Phenol Red Free Complete Growth Medium to each tube.

3. Flow Cytometry
    a. Clean the BD FACSCalibur as per standard laboratory practices.
    b. Apply the following settings to the BD FACSCalibur.
    c. Immediately before reading each sample, gently resuspend each pellet and filter through a cell strainer capped 5 mL polysterene round-bottom tube.
    d. Place the 5 mL tube on the SIP of the BD FACSCalibur. Wait until the sample voltage has reached 6.25V and start collection. Collect a minimum of 25,000 events for each sample.
    e. Remove sample and place a 5 mL tube containing pure sheath fluid on the SIP.
    f. Repeat steps c and d for each sample.
    g. Clean BD FACSCalibur as per standard laboratory practices.

Fluorescence Microscopy

Reagents:

- 100 nM MitoTracker Green FM (MTGFM)
- 200 nM LysoTracker Red (LTR)
- 2.5 μg/mL DAPI
- Phenol Red Free Complete Growth Medium
    - DMEM – Phenol Red Free
    - 10% FBS
    - 1% Penicillin-Streptomycin

Procedure:

1. Staining
    a. Following treatment, remove medium.
    b. Apply 1.5 mL of Staining Solution for 40 minutes under normal cell growth conditions.
    c. Following 40 minutes at 15 μL of DAPI staining solution for 5 minutes.
    d. Remove Staining Solution and incubate cells with 2 mL of Phenol Red Free Complete Growth Medium
2. Microscopy
    a. Warm incubator to 37ºC and open valve from gas cylinder to obtain a gas flow of 100 mL/min.
    b. Change to the 100x objective and apply 1-3 drops of immersion oil.
    c. Open SimplyPCI.
    d. Change Profile to "Alex MTG-LTR-DAPI"
    e. Change to "Three Color Image" in the Capture window.
    f. Open "Filter Setup…" and confirm that there will be a pause following each exposure to allow you to manually change the emission filters.
    g. Change the settings to those below

Channel	Filter	Offset	Gain	Exposure (s)
Red	TRITC	0	255	0.4
Green	FITC	0	255	0.1
Blue	DAPI	0	255	0.05

    h. Move the FITC emission filter into place.

i. Select “Focus” in the Capture window. Raise the objective into place and bring the cell into focus. Do this rapidly to avoid photobleaching.
j. Select “Cancel.”
k. Move the TRITC emission filter into place.
l. Then select “Capture 1.”
m. When the prompt appears, select “OK.”
n. When the following prompt appears, move the “FITC” excitation into place and select “OK.”
o. When the following prompt appears, move the “DAPI” excitation into place and select “OK.”
p. Save the multicolour photo and record the settings used.
q. Obtain a minimum of 40 photos per condition. Try to obtain pictures of only cells that are not touching.

3. Analysis
    a. Use ImageJ to turn off the Blue channel.
    b. Increase the Green or Red channels as required.
    c. Count the distinct Red punctae and any Green punctae that are co-localized with Red punctae. Record the counts.

Lactate Analysis

Part A: Preparation of Deproteinized Samples

Reagents:

- 70% $HClO_4$ (Perchloric Acid)
- 2 N KOH
- Cold PBS

Procedure:

1. Remove ~ 1000 µL of cell culture medium and place in a prelabeled eppendorf.
2. Centrifuge eppendorf at 1.4 RPM for 3 minutes.
3. Transfer 500 µL of the supernatant fraction to a new eppendorf and flash freeze in liquid nitrogen. Store at -80ºC until ready for further processing.
4. Thaw samples quickly and transfer 100 µL of cell culture medium to a new eppendorf and refreeze remaining medium.
5. Add 16.3 µL of cold 70% $HClO_4$ to the 100 µL of cell culture medium. Immediately, add 80 µL of PBS and vigorously vortex.
6. Incubate sample on ice for 10 minutes.
7. Centrifuge samples for 5 minutes at max speed (14,000g) at 4ºC.
8. Add 110.4 µL of cold 2 N KOH and vortex vigorously.
9. Incubate on ice for 3 minutes and repeat step 7.
10. Carefully, transfer the supernatant fraction to a new eppendorf and store the deproteinized samples at -20ºC for future analysis.

Part B: Lactate Assay

Reagents:

- Lactate Assay Kit I – Sigma Aldrich (MAK064-1KT)
  - 100 nmole/µL Lactate Standard
  - Lactate Assay Buffer
  - Lactate Enzyme Mix
  - Lactate Probe
- Clear bottom, black walled 96-well plate

Procedure:

1. Bring all reagents to room temperature.
2. Dilute Lactate Probe 1:10 in warm Lactate Assay Buffer to reduce background.
3. Reconstitute Lactate Enzyme Mix by adding 220 µL of Lactate Assay Buffer and vigorous pipetting.
4. Dilute 1 nmole/µL Lactate Standard 100x in Lactate Assay Buffer to make a 1 nmole/µL Lactate Standard. Dilute 1 nmole/µL 10x in Lactate Assay buffer to make a 0.1 nmole/µL Standard.
5. Create reaction Master Mix (50 µL required per well).

Master Mix	1x
Lactate Assay Buffer	46
Lactate Enzyme Mix	2
Lactate Probe	2

6. Add 0.1 nmole/µL Lactate Standard and Lactate Assay Buffer in duplicate to wells as outlined below.

Lactate Standard	0.1 nmole/µL Lactate Standard	Lactate Assay Buffer
0	0	50
0.2	2	48
0.4	4	46
0.6	6	44
0.8	8	42
1	10	40

7. For deproteinized cell culture medium, add 5 µL of deproteinized sample and 45 µL of Lactate Assay Buffer in duplicate for each sample.
8. Apply 50 µL of Master Mix to each well and mix thoroughly using a pipette and with an orbital shaker.
9. Protect reaction plate from light and incubate for 30 minutes at room temperature.
10. Use a microplate reader to assess absorbance at 570 nm for each well. Use the standard curve to assay the amount of lactate in each well. To ascertain the concentration of lactate in each sample, divide by the volume of sample in each well (for cell culture medium: 5 µL).

Western Blot Procedure

Part A: Protein Extraction

Reagents:

- Complete Growth Medium
  - DMEM
    - With Glutamine
    - With 1 mM Sodium Pyruvate
    - With 50 µg/mL Uridine
  - 10% FBS
  - 1% Penicillin – Streptomycin
- DPBS without Ca^{2+} or Mg^{2+}
- Passive Lysis Buffer (PLB; for 1 mL):
  - 200 µL 5x Passive Lysis Buffer
  - 427.5 µL of ddH_2O
  - Protease Inhibitors:
    - 2 µL of 5 mg/mL Leupeptin
    - 1 µL of 1 mg/mL Pepstatin A
    - 1 µL of 10 mg/mL Aprotinin
    - 1 µL of 1 M Dithiothreitol (DTT)
    - 5 µL of 100 mM Phenylmethylsulfonyl fluoride (PMSF)
      - Made in isopropanol.
      - Add fresh each time because extremely unstable in aqueous solution.
  - Phosphatase Inhibitors
    - 12.5 µL of 200mM Sodium Orthovanadate ($Na3VO_4$)
    - 100 µL of 500 mM Sodium Fluoride (NaF)
    - 250 µL of 200 mM ß-Glycerolphosphate (ß-GP)

Procedure:

1. Grow cells in one 175 cm^2 tissue culture flask.
2. Pour off media. Wash with 5 mL DPBS. Aspirate DPBS. Add 5 mL of 0.25% Trypsin with EDTA and incubate at 37ºC for 5 minutes.
3. Tap flask to disturb any adherent cells. Confirm detachment with a light microscope.
4. Add 5 mL of complete growth media to inhibit trypsin. Use cell suspension to rinse the culture surface to remove any additional cells.

5. Transfer the cell suspension to a 15 mL conical tube and spin for 3 minutes at 1400 RPM.
6. Aspirate the supernatant fraction and resuspend the pellet in 1 mL of DPBS.
7. Transfer the cell suspension to an eppendorf and spin the cells for another 3 minutes at 1400 RPM.
8. Aspirate the DPBS and add 100 μL of PLB.
9. Vigorously vortex and flash freeze eppendorf in liquid nitrogen. Store at -80ºC until ready for analysis
10. To continue, remove the eppendorf and thaw at 37ºC. Immediately, vortex vigorously for 5 seconds. Freeze in liquid nitrogen and repeat 3 times. Thaw the cells one last time and vortex vigorously.
11. Spin in microcentrifuge at 4 ^{o}C for 5 min at 13.0 rpm.
12. Remove the supernate and add it to a new-labelled eppendorf tube.
13. Freeze samples at -80ºC for protein quantification using the Bradford assay.

Part B: SDS Polyacrylamide Gel Electrophoresis (SDS-PAGE) – Bio-Rad Mini Protein System

Reagents:

- Acrylamide/Bis-Acrylamide, 30% Solution 37.5:1 (BioShop 10.502)
  - Store at 4°C
- Under Tris Buffer
  - 1M Tris-HCl, pH 8.8 (60.5g/500ml)
  - Store at 4°C
- Over Tris Buffer
  - 1M Tris-HCl, pH 6.8 (12.1g/100ml)
  - Bromophenol Blue (for colour)
  - Store at 4°C
- Ammonium Persulfate (APS)
  - 10% (w/v) APS in ddH_20 (1g/10ml)
  - Store at 4°C
- Sodium Dodecyl Sulfate (SDS)
  - 10% (w/v) in ddH_20 (1g/10ml)
  - Store at room temperature
- TEMED (Sigma T-9281)
- Electrophoresis Buffer, pH 8.3 (10L)
  - 25mM Tris 30.34g, 192mM Glycine 144g, 0.1% SDS 10g
  - Volume to 10L with ddH_20
  - Store at room temperature
- 2 x Lysis Buffer
- *tert*-Amyl alcohol ReagentPlus, 99% (Sigma 152463)

Procedure:

1. Prepare Mini-Protean gel caster system:
   a. Assemble glass plates as shown below:

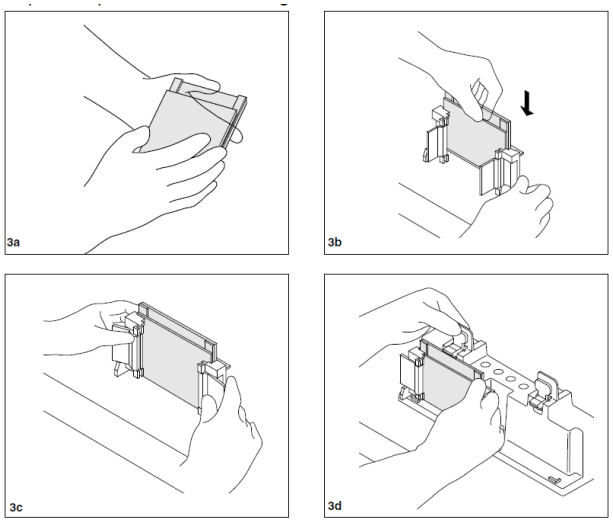

2. Check the seal by adding a small volume of ddH_20 then pour off and let dry.
3. Make a mark 2 cm below the top edge of the short plate. This will indicate how high to fill the separating gel.
4. Prepare separating gels:

Mini Protean 3 Bio-Rad System volumes

Separating Gel	**8 %**	**10 %**	**12 %**	**15 %**	**18 %**
Acrylamide	2.7 ml	3.3 ml	4.0 ml	5.0 ml	6.0 ml
Water	4.1 ml	3.5 ml	2.8 mL	1.8 ml	0.8 ml
Under Tris	3.0 ml	3.0 ml	3.0 ml	3.0 ml	3.0 ml
SDS	100 µl	100 µl	100 µl	100 µl	100 µl
APS	100 µl	100 µl	100 µl	100 µl	100 µl
TEMED	10 µl	10 µl	10 µl	10 µl	10 µl

   a. Mix the contents of the separating gel without TEMED.
   b. Add TEMED. Briefly stir. Immediately, pour the contents between the short and spacing plates until the volume reaches 2 cm from the top edge of the short plate
   c. Coat the top surface of the gel solution with *tert*-Amyl alcohol to remove any bubbles.
   d. Allow 10 - 30 minutes for gel polymerization.
   e. Remove *tert*-Amyl alcohol by pouring it off and remove any remainder with a scrap piece of Whatman paper.
5. Prepare stacking gel:
   a. For a single mini gel use the following volumes:

Stacking Gel (3% Acrylamide)	1 Mini Gel
Acrylamide	250 µL
Water	1.875 mL
Above Tris buffer	312.5 µL
SDS	25 µL
APS	25 µL
TEMED	10 µL

   b. Mix the contents of the stacking gel without adding TEMED. Stir.
   c. Add TEMED. Stir and pour the stacking gel on top of the polymerized separating gel.
   d. Immediately, add the appropriate comb for desired number of wells and thickness of spacer plate.
   e. Allow 10 - 30 minutes for gel polymerization.
   f. Gels may be used immediately or stored in a wet sealed container at 4ºC.

6. Prepare samples:
   a. Warm block heater to 95ºC.
   b. Pipette the appropriate volume of each sample into a new eppendorf. *This volume is determined by the protein concentration assessed using the Bradford assay and the required amount of protein required for the detection of the desired protein.*
   c. Add an equal amount of 2X Lysis Buffer supplemented with 5% B-Mercaptoethanol. Add 5 µL of Sample Dye to each sample.
   d. Briefly spin each sample to bring volume to the bottom of the eppendorf.
   e. Incubate each sample at 95ºC for 5 minutes in the heating block to denature the proteins.
   f. Briefly spin again to return volume to the bottom of the eppendorf.

7. Assemble Mini-Protean electrophoresis rack:
   a. See images below:

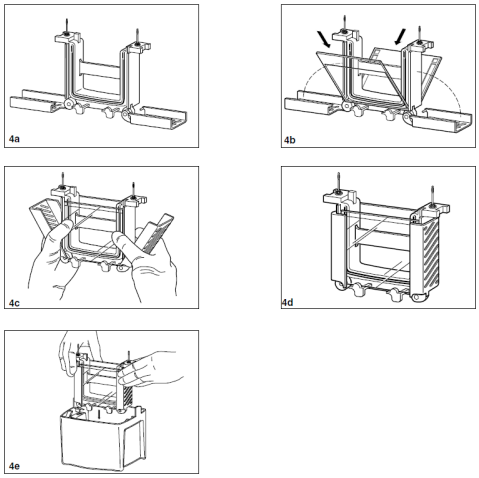

b. If you are only running one gel a plastic rectangular pseudo plate must be clamped on the other side of the caster.
c. Fill the middle chamber of the electrophoresis apparatus with Electrophoresis Buffer. Fill the outer chamber with Electrophoresis Buffer, until the level is approximately 2 cm above the bottom of the gels.
d. Slowly remove the comb using both hands (one on each side) by pulling the comb straight upwards.
e. Fix any wells that are deformed using a pipette tip.
f. Clean out the wells using a pipette tip and Electrophoresis Buffer.
g. Apply 10 μL of protein ladder to the first well.
h. Withdraw the entire volume of the sample using a gel-loading tip. Inject the solution slowly into the bottom of the well.

8. Gel Electrophoresis:
    a. After all samples are loaded, immediately, place the lid on the gel chamber.
    b. Place the positive and negative leads into the power supply.
    c. Use a power supply to apply a constant voltage of 90V across the gel. After the bromophenol blue has passed the border between the stacking and separating gel, increase the voltage to 120V for 60 – 120 minutes until sufficient separation has been achieved as indicated by the protein ladder.
    d. Prepare for electrotransfer of proteins from the gel to nitrocellulose membrane.

Part C: Western Blotting and Immunodetection

Reagents:

- Transfer Buffer
  - 0.025M Tris-HCl pH 8.3 12.14g
  - 0.15M Glycine 45.05g
  - 20% Methanol 800ml
  - Make 4L with ddH_20
  - Store at 4°C
- Ponceau S stain
  - 0.1% (w/v) Ponceau S
  - 0.5% (v/v) Acetic Acid
  - Store at room temperature
- Wash Buffer
  - Tris-HCl pH 7.5 12g
  - NaCl 58.5g
  - 0.1% Tween 10ml
  - Store at room temperature
- Blocking Buffer
  - 5% (w/v) skim milk power in Wash Buffer
- Enhanced Chemiluminescence Fluid (ECL; Santa Cruz - SC-2048)
- Film Developer and Fixer

Procedure:

1. Transfer Procedure
   a. Using a paper cutter cut 6 pieces of Whatman paper per gel. Each piece should measure 8.5 cm x 6 cm. Wearing gloves cut an 8.5cm x 6 cm piece of nitrocellulose membrane (GE Healthcare RPN303D). Soak Whatman paper and nitrocellulose membrane in Transfer Buffer until use.
   b. Remove electrophoresis plates from chamber and separate the plates.
   c. Remove stacking gel
   d. Assemble Whatman paper, nitrocellulose membrane and gel as shown below, ensuring that the gel and membrane are orientated so that the gel is closer to the black surface and the membrane closer to the white plastic clamp.

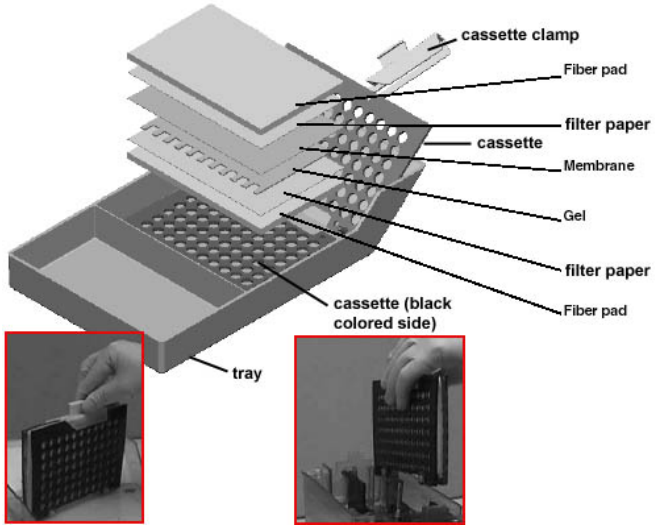

e. Close the cassette and place in the transfer chamber with the black side of the cassette facing the negative electrode (black side) of the chamber.
f. Place an ice pack and magnetic stir bar in the chamber.
g. Place the chamber in a Tupperware container. Place the container on top of a magnetic stir plate. Turn on the stir plate and ensure the magnetic stir bar is spinning.
h. Fill the chamber completely with cold Transfer Buffer. Place lid on the chamber and connect the leads to a power supply.
i. Turn on the power supply and apply a constant voltage of 120V for 1.5 hours. This can vary depending on the size of the protein of interest.

2. Removal of nitrocellulose membrane:
   a. Turn off the power supply and disconnect leads from the power supply.
   b. Remove the cassette from the chamber.
   c. While wearing gloves, carefully dispose of the Whatman paper and gel.
   d. Gently place the nitrocellulose membrane in a plastic dish and apply Ponceau S stain for 5 minutes.
   e. Drain off the remaining Ponceau S and save for reuse.
   f. Rinse the membrane 3-5x with ddH_2O to reduce the red background. Wrap membrane in saran wrap and scan.
   g. Cut the membrane while protein bands are still visible at the desired molecular weight.
   h. Rotate membrane at room temperature in Wash Buffer until remaining Ponceau S stain has been removed (~5 minutes).
   i. Incubate membrane for 1 hour with rotation in Blocking Buffer at room temperature.

3. Immunodetection
    a. Primary Antibody Incubation
        i. Wrap a flat piece of glass in parafilm. Place the glass in a Pyrex dish. Arrange balls of wet tissue around the dish and cover the entire dish with saran wrap.
        ii. Place the dish in a 4ºC fridge and level.
        iii. Place nitrocellulose membrane strips face up on the flat parafilm surface.
        iv. Dilute the primary antibody raised against the protein of interest in Blocking Buffer. Gently apply ~1-1.5 mL of diluted antibody overtop of the appropriate membrane strip.
        v. Specific antibody dilutions used in this study are listed at the end of this protocol.
    b. Secondary Antibody Incubation
        i. Wash the blots in Wash Buffer with gentle rotation for 5 minutes 3X.
        ii. Incubate the blots as described in step 3.a with the following changes. Incubate the blots for 1 hour with a secondary antibody raised against the species and specific immunoglobulin molecule of the primary antibody. Incubate at room temperature.
    c. Following the incubation, wash the membrane 3X for 5 minutes with Wash Buffer.
4. Enhanced Chemiluminescence Detection

    Note: Complete the following steps in a dark room sufficient for photographic film developing.

    a. Mix ECL fluids "A" and "B" in a 1:1 ratio in a small plastic box.
    b. Place blots facedown in the small plastic box and place on a level surface. Some swirling may be required to ensure equal coverage.
    c. Following 2 minutes, remove blots and place face down on clean Kim wipes to remove excess ECL fluid.
    d. Place membrane strips on clean overhead transparency film and remove any bubbles.
    e. Turn off any lights.
    f. Place membrane strips face up in a film cassette.
    g. Momentarily cover the strips with cardboard while cutting pieces of film to the approximate size of the membrane strips.
    h. Remove the film and apply film overtop of the membrane strips. Do not move the film once it has been placed on top of the membrane.
    i. Close the cassette and expose the film for the desired time.
    j. After the exposure time, remove the film and place the cassette aside.

k. Attach the film to a film hanger and dip 5-6x in film developing solution.
l. Hold the film up to a red light. When bands become apparent, immediately submerge the film in water and then in the film fixing solution for 5 minutes.
m. Following 5 minutes in the fixing solution, the film can then be submerged in water and attached to butterfly binder clips to dry. They are no longer light sensitive.

Protein of Interest	% Gel	Loaded Protein Mass	Protein Mass	Primary Antibody	Primary Antibody Dilution	Secondary Antibody	Secondary Antibody Dilution	Exposure Time
P-AMPK	12	25 µg	62 kDa	Cell Signalling	1:1000 in 5% BSA	Santa Cruz anti-Rabbit IgG	1:1000 in 5% Skim Milk	~ 30 s
T-AMPK	12	25 µg	62 kDa	Cell Signalling	1:1000 in 5% Skim Milk	Santa Cruz anti-Rabbit IgG	1:1000 in 5% Skim Milk	~ 60 s
LC3	15	50 µg	12 and 18 kDa	Cell Signalling	1:250 in 5% Skim Milk	Santa Cruz anti-Rabbit IgG	1:1000 in 5% Skim Milk	~ 15 s

Whole Cell Respiration Procedure

Part A: OxoPlate Respiration

Adapted from OxoPlate Manual and Nicholls

Reagents and Disposables Required:

- 96-well Flat Bottomed OxoPlate – OP96C
  Manufacturer – PreSens (http://www.presens.de/)
  North American Distributor – Innovative Instruments Inc.
  (http://www.3i-usa.com/)
- 0% O_2 Standard
  - Add 150mg of sodium sulfite (Na_2SO_3) to a 15 mL screw top tube.
  - Add 15 mL of ddH_2O and seal tube
  - Vortex and allow >1 minute for oxygen to be depleted from solution
    Notes:
    - Must use a screw top lid and use enough ddH_2O to almost entirely fill container. This will minimize any dissolving of O_2 from the air in the tube.
    - DO NOT REPLACE ddH_2O with Growth Media
    - Shelf life is ~24 hours
- 100% O_2 Standard
  - Aliquot 7.5 mL of Phenol Red Free Growth Media into a 15 mL screw top tube.
  - Shake vigorously for 2 minutes.
  - Loosen screw top and gently rotate tube to decrease foaming and prevent oversaturation of solution.
    Notes:
    - Shelf life is ~24 hours
- Grow Medium
  - DMEM – Phenol Red Free
  - 10% FBS
  - 1% Penicillin-Streptomycin
- Oligomycin
  Sigma O4876
  Mixture 65% Oligomycin A – MW: 791
  Remainder:
  - Oligomycin B – MW 805.1
  - Oligomycin C – MW: 775.1

  Average MW: 790.685

- Final Concentration: 1 µM
- Stock Solution: 300 µM in DMSO
- Serial Dilutions:
  - 1 mg in 1 mL DMSO = 1.265 mM
  - 237.15 µL of 1.265 mM in 762.85 µL DMSO = 300 µM
- Working Solution:
  - Aliquot 12 mL Phenol Red Free Growth Medium
  - Remove 40 µL
  - Add 40 µL of 300 µM Oligomycin

- Carbonyl Cyanide 3-Chlorophenylhydrazone (CCCP)
  Sigma C2759
  MW: 204.62
  - Final Concentration: 3 µM
  - Stock Solution: 900 µM in DMSO
  - Serial Dilutions:
    - 2.0462 mg in 1 mL DMSO = 10 mM
    - 90 µL of 10 mM in 910 µL DMSO = 900 µM
  - Working Solution:
    - Aliquot 12 mL Phenol Red Free Growth Medium
    - Remove 40 µL
    - Add 40 µL of 900 µM CCCP
- Rotenone
  Sigma R8875
  MW: 394.42
  - Final Concentration: 2 µM
  - Stock Solution: 600 µM in DMSO
  - Serial Dilutions:
    - 3.9442 mg in 1 mL DMSO = 10 mM
    - 60 µL of 10 mM in 940 µL DMSO = 600 µM
- Antimycin A
  Sigma A8674
  MW: 548.63
  - Final Concentration: 2 µM
  - Stock Solution: 600 µM in DMSO
  - Serial Dilutions:
    - 5.4963 mg in 1 mL DMSO = 10 mM
    - 60 µL of 10 mM in 940 µL DMSO = 600 uM
- Rotenone and Antimycin A Working Solution
  - Working Solution:
    - Aliquot 12 mL Phenol Red Free Growth Medium
    - Remove 80 µL

        - Add:
            - 40 µL of 600 µM Rotenone
            - 40 µL of 600 µM Antimycin A
- Dimethyl Sulfoxide (DMSO)
    - Working Solution:
        - Aliquot 12 mL Phenol Red Free Growth Medium
        - Remove 40 µL
        - Add 40 µL of DMSO

Procedure:

1. Initial Day:
    a. All conditions must be performed in triplicate.
    b. Perform all work in darkness and protect the OxoPlate from light at all times.
    c. Plate a sufficient number of cells to acquire a minimum of 8,000 cells/well when measuring oxygen consumption.
        i. DO NOT PLATE CELLS IN WELLS FOR STANDARDS.
        ii. A sample seeding plan is included below.
    d. Cover plate, protect from light, and incubate.
    e. Incubate long enough for cells to adhere (recommended 24 hours).
2. Respiration Day:
    a. Prepare standards (0% O_2 Standard and 100% O_2 Standard).
    b. Warm all cell culture media and drugs.
    c. Make working solutions.
    d. Aliquot 400 µL of each solution into the relevant wells of a second sterile 96-well plate.
    e. Place the plate containing the experimental media in an incubator close to plate reader and warm to 37ºC.
    f. Make 0% and 100% solutions and warm to 37ºC.
    g. Prepare another plate with > 75 µL of mineral oil and warm to 37ºC.
    h. Gently aspirate all media from the OxoPlate
    i. Add 350 µL of the 0% standard in triplicate to the appropriate OxoPlate wells.
    j. Add 250 µL of the 100% standards in triplicate to the OxoPlate wells.
    k. Rapidly, use a multichannel pipette to transfer 350 µL of warm media from the warmed plate to the OxoPlate.
    l. Rapidly, use a multichannel pipette to overlay the OxoPlate wells with 50 µL of warm mineral oil.
    m. Further seal the plate with clear transparent PCR plate sealing film.
    n. Immediately read on fluorescent plate reader with the parameters listed below.

3. If required, correct for differences in cell number (part B)

Fluorescence Plate Reader Settings:

- Reading Type: Kinetic
- Reader: Synergy HT-I on: Fluorescence
- Filer Set: 2
- Excitation: 530/25 (for both)
- Emission: 645/40 and 590/35
- Optics Position: Bottom (for both)
- Sensitivity: 50 (for both)
- Click Options (same for both)
    - Nb Samples per Well: 20 – *Can decrease reading time by reducing this number*
    - Delay before Sampling: 300 msec – *Can decrease reading time by reducing this number*
    - Delay between samples: 1 msec
- Select: Kinetic…
    - Run Time: 03:00:00
    - Click Minimum
    - Interval should be 00:02:51 with above settings
    - Check Allow Well Zoom during read
- Temperature Control: Yes
- Check Pre-Heating
- Temperature: 37ºC
- Lag time: 00:00:00

Sample Plate Layout

	1	2	3	4	5	6	7	8	9	10	11	12
A	0	0	0	100	100	100	CON 8000 DMSO	CON 8000 DMSO	CON 8000 DMSO	CON-AR DMSO	CON-AR DMSO	CON-AR DMSO
B	CON 8000 Basal	CON 8000 Basal	CON 8000 Basal	CON 8000 Oligo	CON 8000 Oligo	CON 8000 Oligo	CON 8000 CCCP	CON 8000 CCCP	CON 8000 CCCP	CON 8000 ROT + AA	CON 8000 ROT + AA	CON 8000 ROT + AA
C	CON-AR 8000 Basal	CON-AR 8000 Basal	CON-AR 8000 Basal	CON-AR 8000 Oligo	CON-AR 8000 Oligo	CON-AR 8000 Oligo	CON-AR 8000 CCCP	CON-AR 8000 CCCP	CON-AR 8000 CCCP	CON-AR 8000 ROT + AA	CON-AR 8000 ROT + AA	CON-AR 8000 ROT + AA
D	D34 8000 Basal	D34 8000 Basal	D34 8000 Basal	D34 8000 Oligo	D34 8000 Oligo	D34 8000 Oligo	D34 8000 CCCP	D34 8000 CCCP	D34 8000 CCCP	D34 8000 ROT + AA	D34 8000 ROT + AA	D34 8000 ROT + AA
E	D34-AR 8000 Basal	D34-AR 8000 Basal	D34-AR 8000 Basal	D34-AR 8000 Oligo	D34-AR 8000 Oligo	D34-AR 8000 Oligo	D34-AR 8000 CCCP	D34-AR 8000 CCCP	D34-AR 8000 CCCP	D34-AR 8000 ROT + AA	D34-AR 8000 ROT + AA	D34-AR 8000 ROT + AA
F	D13 8000 Basal	D13 8000 Basal	D13 8000 Basal	D13 8000 Oligo	D13 8000 Oligo	D13 8000 Oligo	D13 8000 CCCP	D13 8000 CCCP	D13 8000 CCCP	D13 8000 ROT + AA	D13 8000 ROT + AA	D13 8000 ROT + AA
G	D13-AR 8000 Basal	D13-AR 8000 Basal	D13-AR 8000 Basal	D13-AR 8000 Oligo	D13-AR 8000 Oligo	D13-AR 8000 Oligo	D13-AR 8000 CCCP	D13-AR 8000 CCCP	D13-AR 8000 CCCP	D13-AR 8000 ROT + AA	D13-AR 8000 ROT + AA	D13-AR 8000 ROT + AA
H	D34 8000 DMSO	D34 8000 DMSO	D34 8000 DMSO	D34-AR 8000 DMSO	D34-AR 8000 DMSO	D34-AR 8000 DMSO	D13 8000 DMSO	D13 8000 DMSO	D13 8000 DMSO	D13-AR 8000 DMSO	D13-AR 8000 DMSO	D13-AR 8000 DMSO

Part B: Cell Quantification

Adapted from CyQuant Manual

Reagents:

- Life Technologies CyQuant Assay
  - 20x Cell-Lysis Buffer
  - CyQuant GR Dye
- DEPC ddH_2O
- CyQuant Assay Buffer (for 25 mL)
  - 1250 µL of 20x Cell-Lysis Buffer
  - 23687.5 µL of DEPC ddH_2O
  - 62.5 µL of CyQyant GR Dye

Procedure:

1. Generate Cell Number Standard
   a. Grow control cells under normal conditions.
   b. Rinse cells with DPBS without Calcium and Phosphorus
   c. Apply Trypsin with 0.25% EDTA for 5 minutes at 37ºC
   d. Triturate cell suspension with equal volumes of complete growth medium.
   e. Centrifuge the cell suspension in a screw cap tube at 1400 RPM for 3 minutes.
   f. Remove the supernate and triturate the pellet in 1-1.5 mL of DPBS.
   g. Carefully determine the cell concentration with a hæmocytometer.
   h. Aliquot 1 mL of the cell suspension in a sterile eppendorf and centrifuge the eppendorf at 1400 RPM for 3 minutes.
   i. Remove the supernate and freeze at -80ºC.
   j. Add a volume of CyQuant Assay Buffer to generate a solution with a cell concentration of 1×10^6 cells/mL.
2. Prepare OxoPlate
   a. Gently remove media from the OxoPlate by inverting the plate and/or careful aspiration of the media.
   b. Freeze the OxoPlate at -80ºC
3. Analyze OxoPlate
   a. Add the following amount of the standard and CyQuant Assay Buffer to the standard wells (A1-A6) of the OxoPlate.

Cell Number	Volume of Standard	Volume of Buffer
0	0	200
10000	10	190
20000	20	180
30000	30	170
40000	40	160
50000	50	150

b. Apply 200 µL of CyQuant Assay Buffer to each well.
c. Mix vigorously with an orbital shaker. Protect from light and allow to react for 5 minutes.
d. Read assay on microplate reader with the settings below.

Fluorescence Plate Reader Settings:

- Reading Type: Kinetic
- Reader: Synergy HT-I on: Fluorescence
- Filer Set: 1
- Excitation: 530/25
- Emission: 645/40 and 590/35
- Optics Position: Bottom
- Sensitivity: 50
- Click Options
    - Nb Samples per Well: 20
    - Delay before Sampling: 300 msec
    - Delay between samples: 1 msec

Appendix D: Other Contributions to the Literature

Published Abstracts

1. **A. E. Green**, D. A. Hood, Effects of AMPK Activation on C2C12 cells depleted of mtDNA, *Proc. Muscle Health Awareness Day* **4**, 16 (2013).

2. **A.E. Green**, K. J. Menzies, D. A. Hood. Thyroid hormone (T_3) as a potential mediator of mitophagy in cells containing mtDNA mutations, *Proc. Ontario Exercise Physiology* 11 (2012).

Oral Presentations

1. **A. E. Green**, D. A. Hood, Autophagy and Mitochondrial Disease, *KAHS Graduate Student Seminar, York University, Toronto, ON*, (February 15, 2013).